Possible mechanisms of the protective effects of anti-LOX-1 antibody against ischemia-reperfusion injury

Our findings suggest that activation of the LOX-1 pathway occurs after ischemia-reperfusion and that activation of the LOX-1 pathway plays a significant role in determining the extent of myocardial ischemia-reperfusion injury. The question then arises, what is the mechanism by which anti-LOX-1 antibody reduces myocardial infarction size? First, it has been shown that myocardial cell apoptosis by oxidant stress is associated with reperfusion injury [8]. Recent reports suggest that activation of the LOX-1 pathway is involved in the induction of apoptosis [5–7]. Furthermore, the present study demonstrates that anti-LOX-1 antibody blocks myocardial cell apoptosis induced by hydrogen peroxide, a representative oxidant stress. Thus, one mechanism may be that blockage of the LOX-1 pathway inhibits the apoptosis associated with reperfusion injury. Second, binding of activated platelets to endothelial LOX-1 after reperfusion will plug small vessels, resulting in the no reflow phenomenon. Thus, blockage of the LOX-1 pathway might improve myocardial perfusion. However, further studies will be necessary to elucidate the precise mechanisms of the protective effects of anti-LOX-1 antibody.

While LOX-1 expression in cardiac myocytes is induced following ischemia-reperfusion, the physiological ligands that activate LOX-1 have not yet been identified. Since oxidized LDL cannot readily pass through endothelium, cardiac myocytes may not encounter oxidized LDL. However, LOX-1 can actively bind apoptotic cells and activated platelets [12,13], which are frequently observed in ischemia-reperfused myocardium. These findings suggest that the LOX-1 pathway could be activated during ischemia-reperfusion even in the absence of oxidized LDL. In contrast to the situation in this experimental model in rats, the majority of patients with acute myocardial infarction have diseased coronary arteries as a result of atherosclerosis. In such patients, oxidized LDL levels are usually high. Thus, it would be particularly interesting to pursue the possibility that blockage of the LOX-1 pathway would provide a novel strategy for treatment of acute myocardial infarction in humans.

References

[1] D.J. Hearse, R. Bolli, Reperfusion induced injury: manifestations, mechanisms, and clinical relevance, Cardiovasc. Res. 26 (1992) 101–108.

[2] M.L. Entman, C.W. Smith, Postreperfusion inflammation: a model for reaction to injury in cardiovascular disease, Cardiovasc. Res. 28 (1994) 1301–1311.

[3] R.A. Kloner, K. Przyklenk, P. Whittaker, Deleterious effects of oxygen radicals in ischemia/reperfusion. Resolved and unresolved issues, Circulation 80 (1989) 1115–1127.

[4] T. Sawamura, N. Kume, T. Aoyama, H. Moriwaki, H. Hoshikawa, Y. Aiba, T. Tanaka, S. Miwa, Y. Katsura, T. Kita, T. Masaki, An endothelial receptor for oxidized low-density lipoprotein, Nature 386 (1997) 73–77.

[5] D. Li, J.L. Mehta, Upregulation of endothelial receptor for oxidized LDL (LOX-1) by oxidized LDL and implications in apoptosis of human coronary artery endothelial cells, Arterioscler. Thromb. Vasc. Biol. 20 (2000) 1116–1122.

[6] H. Kataoka, N. Kume, S. Miyamoto, M. Minami, M. Morimoto, K. Hayashida, N. Hashimoto, T. Kita, Oxidized LDL modulates bax/bcl-2 trough the lectinlike ox-LDL receptor-1 in vascular smooth muscle cells, Arterioscler. Thromb. Vasc. Biol. 21 (2001) 955–960.

[7] E. Iwai-Kanai, K. Hasegawa, T. Sawamura, M. Fujita, T. Yanazume, S. Toyokuni, S. Adachi, Y. Kihara, S. Sasayama, Activation of lectin-like oxidized low-density lipoprotein receptor-1 induces apoptosis in cultured neonatal rat cardiac myocytes, Circulation 104 (2001) 2948–2954.

[8] R.A. Gottlieb, K.O. Burleson, R.A. Kloner, B.M. Babior, R.L. Engler, Reperfusion injury induces apoptosis in rabbit cardiomyocytes, J. Clin. Invest. 94 (1994) 1621–1628.

[9] M. Chen, S. Narumiya, T. Masaki, T. Sawamura, Conserved C-terminal residues within the lectin-like domain of LOX-1 are essential for oxidized low-density-lipoprotein binding, Biochem. J. 355 (2001) 289–296.

[10] T. Kakita, K. Hasegawa, E. Iwai-Kanai, S. Adachi, T. Morimoto, H. Wada, T. Kawamura, T. Yanazume, S. Sasayama, Calcineurin pathway is required for endothelin-1-mediated protection against oxidant stress-induced apoptosis in cardiac myocytes, Circ. Res. 88 (2001) 1239–1246.

[11] H. Selye, E. Bajusz, S. Grasso, S. Mendell, Simple techniques for the surgical occlusion of coronary vessels in the rat, Angiology 11 (1960) 398–407.

[12] K. Oka, T. Sawamura, K. Kikuta, S. Itokawa, N. Kume, T. Kita, T. Masaki, Lectin-like oxidized low-density lipoprotein receptor 1 mediates phagocytosis of aged/apoptotic cells in endothelial cells, Proc. Natl. Acad. Sci. USA 95 (1998) 9535–9540.

[13] M. Kakutani, T. Masaki, T. Sawamura, A platelet-endothelium interaction mediated by lectin-like oxidized low-density lipoprotein receptor-1, Proc. Natl. Acad. Sci. USA. 97 (2000) 360–364.

THE JOURNAL OF BIOLOGICAL CHEMISTRY
© 2003 by The American Society for Biochemistry and Molecular Biology, Inc.

Vol. 278, No. 11, Issue of March 14, pp. 9327–9331, 2003
Printed in U.S.A.

Vortex-mediated Mechanical Stress Induces Integrin-dependent Cell Adhesion Mediated by Inositol 1,4,5-Trisphosphate-sensitive Ca^{2+} Release in THP-1 Cells*

Received for publication, December 4, 2002, and in revised form, January 7, 2003
Published, JBC Papers in Press, January 7, 2003, DOI 10.1074/jbc.M212316200

Noboru Ashida‡, Hajime Takechi‡, Toru Kita§, and Hidenori Arai‡¶

From the Department of ‡Geriatric and §Cardiovascular Medicine, Kyoto University Graduate School of Medicine, Kyoto, 606-8507, Japan

In the downstream regions of stenotic vessels, cells are subjected to a vortex motion under low shear forces, and atherosclerotic plaques tend to be localized. It has been reported that such a change of shear force on endothelial cells has an atherogenic effect by inducing the expression of adhesion molecules. However, the effect of vortex-induced mechanical stress on leukocytes has not been investigated. In this study, to elucidate whether vortex flow can affect the cell adhesive property, we have examined the effect of vortex-mediated mechanical stress on integrin activation in THP-1 cells, a monocytic cell line, and its signaling mechanisms. When cells are subjected to vortex flow at 400–2,000 rpm, integrin-dependent cell adhesion to vascular cell adhesion molecule-1 or fibronectin increased in a speed- and time-dependent manner. Next, to examine the role of Ca^{2+} in this integrin activation, various pharmacological inhibitors involved in Ca^{2+} signaling were tested to inhibit the cell adhesion. Pretreatment of cells with BAPTA-AM, thapsigargin +$NiCl_2$, or U-73122 (a phospholipase C inhibitor) inhibited cell adhesion induced by vortex-mediated mechanical stress. We also found that W7 (a calmodulin inhibitor) blocked the cell adhesion. However, pretreatment of cells with $GdCl_3$, $NiCl_2$, or ryanodine did not affect the cell adhesion. These data indicate that vortex-mediated mechanical stress induces integrin activation through calmodulin and inositol 1,4,5-trisphosphate-mediated Ca^{2+} releases from intracellular Ca^{2+} stores in THP-1 cells.

The nature of blood flow patterns and shear forces within blood vessels may be very variable depending upon vessel size, shape, branching, and partial obstructions (1). Biomechanical forces induced within the cardiovascular system affect gene expression in cells of blood vessel walls (2, 3) and functions of the cells in the vessel wall and in the fluid phase (4–8). Changes of shear forces occur in bifurcated or stenotic regions where atherosclerotic regions are prone to develop.

According to the multistep theory in cell transmigration, monocytes roll on the endothelial cells, interact with selectins, adhere to the endothelial cells by firm adhesion to ICAM-1[1] and vascular cell adhesion molecule-1 (VCAM-1), and then migrate into the subendothelium (9). Rolling of monocytes on endothelial cells is dependent on the binding of E-selectin and sialyl Lewis X, and adhesion to the endothelium is dependent on the interaction between integrins on monocytes and adhesion molecules on the endothelial cells, such as VCAM-1 and ICAM-1. Integrins consist of several subtypes, and each subtype is specific for each ligand. For example, $\alpha4\beta1$ integrin, VLA-4, binds to VCAM-1, and $\beta2$ integrins bind to ICAM-1. Fibronectin, one of the extracellular matrix proteins, is also known to bind to $\beta1$ integrins, mainly to $\alpha5\beta1$ integrin. Thus activation of adhesion molecules in endothelial cells and leukocytes is important for the cell migration process.

In this study, we hypothesized that leukocyte adhesion might be increased at bifurcations and in the downstream of the restricted vessels. In normal laminar flow, it has been reported that human leukocytes respond to fluid shear stress by retracting pseudopods and down-regulation of integrins (10, 11), which is a requirement for normal passage of circulating leukocytes through the microcirculation. In the downstream of the region where the vessel lumen is partially occluded, however, a backward vortex can be observed where cells in the fluid phase are subjected to a vortex motion under low shear forces (1, 12–14). Although such a change of shear force on endothelial cells can regulate the expression of adhesion molecules resulting in the progression of atherosclerosis (15, 16), the effect of vortex-mediated mechanical stress on leukocytes has not yet been determined. If vortex-induced mechanical stress can induce cell adhesion in leukocytes, leukocytes would be more prone to attach to the endothelial lining in the turbulent flow because the residence time of leukocytes in the regions with nonlaminar flow is longer than in those with laminar flow (12, 13).

A variety of signaling systems are induced by a mechanosensor in endothelial cells. As a mechanosensor, stretch-activated channels have been reported to regulate Ca^{2+} influx induced by flow stress in cells such as endothelial cells or smooth muscle cells (17). There is much evidence that stretch increases intracellular Ca^{2+} levels (4, 17). Thus the importance of Ca^{2+} signaling in endothelial mechanotransduction has been established. However, the role of Ca^{2+} in cell response to the mechanical stress in leukocytes has not been examined so far. Therefore, the aim of this study was to examine the effect of mechanical stress on integrin-dependent cell adhesion in human monocytic THP-1 cells and to elucidate the role of Ca^{2+} signaling involved in this process.

* This study was supported by Grants-in-aid 13307034 and 14570657 and Center of Excellence Grant 12CE2006 from the Japanese Ministry of Education, Science, Sports, and Culture (12CE2006) and a research grant for health sciences from the Japanese Ministry of Health and Welfare. The costs of publication of this article were defrayed in part by the payment of page charges. This article must therefore be hereby marked "*advertisement*" in accordance with 18 U.S.C. Section 1734 solely to indicate this fact.

¶ To whom correspondence should be addressed: Dept. of Geriatric Medicine, Kyoto University Graduate School of Medicine, 54 Kawahara-cho, Shogoin, Sakyo-ku, Kyoto, 606-8507, Japan. Tel.: 81-75-751-3463; Fax: 81-75-751-3463; E-mail: harai@kuhp.kyoto-u.ac.jp.

[1] The abbreviations used are: ICAM-1, intercellular adhesion molecule-1; VCAM-1, vascular cell adhesion molecule-1; MES, 4-morpholineethanesulfonic acid; VLA-4, very late antigen-4; PLC, phospholipase C.

EXPERIMENTAL PROCEDURES

Reagents—RPMI medium was obtained from Nissui Pharmaceuticals Co. Ltd. (Tokyo, Japan). Fetal calf serum was purchased from Grand Cayman (British West Indies). L-glutamine and penicillin/streptomycin were obtained from Bio Whittaker (Walkersville, MD). Recombinant human soluble VCAM-1 and ICAM-1 were from Genzyme/Techne (Minneapolis, MN). Fibronectin, thapsigargin, W-7, ryanodine, U-73122, bovine serum albumin, RGDS peptides, and RGES peptides were from Sigma. Anti-human $\alpha4$ (VLA-4) antibody was from Upstate Biotechnology (Lake Placid, NY). $GdCl_3{\cdot}6H_2O$ and $NiCl_2{\cdot}6H_2O$ were from Wako Pure Chemical Industries, Ltd. (Osaka, Japan). BAPTA-AM was from Dojindo (Kumamoto, Japan).

Cell Lines—The monocytic cell line THP-1 was a generous gift from Dr. K. Nishida (Daiichi Pharmaceuticals Co. Ltd., Tokyo) and was cultured in RPMI supplemented with L-glutamine and penicillin/streptomycin plus 10% fetal calf serum in an atmosphere of 95% air and 5% CO_2 at 37 °C.

Cell Adhesion Assay—Cell adhesion assays were carried out essentially as described (18). Briefly, polystyrene 96-well flat-bottomed microtiter plates (Costar 3595, Corning Inc., Corning, NY) were coated with 50 μl of soluble VCAM-1 (2.5 μg/ml), soluble ICAM-1 (2.5 μg/ml), or fibronectin (10 μg/ml) for 1 h at room temperature. After incubation, wells were blocked by incubation with 200 μl of 10 mg/ml heat-denatured bovine serum albumin for 30 min at room temperature. Control wells were filled with 10 mg/ml heat-denatured bovine serum albumin. One hundred μl of THP-1 cells suspended at a concentration of 10^6/ml in 10% fetal calf serum-RPMI were incubated for the indicated times in a CO_2 incubator at 37 °C after exposure to vortex flow by vortex machine (MS1 minishaker from IKA Works, Wilmington, NC). After incubation, nonadherent cells were removed by centrifugation (top side down) at 48 × *g* for 5 min. The plates were then centrifuged inversely at 80 × *g* for 5 min. Attached cells were fixed with 5% glutaraldehyde for 30 min at room temperature. Cells were washed three times with water, and 100 μl of 0.1% crystal violet in 200 mM MES (pH 6.0) was added to each well and incubated at room temperature for 20 min. Excess dye was removed by washing with water three times, and the bound dye was solubilized with 100 μl of 10% acetic acid. The absorbance of each well at 595 nm was then measured using a multiscan enzyme-linked immunosorbent assay reader (SPECTRA classic, Tecan, Maennedorf, Austria). Each sample was assayed in triplicate. The absorbance was linear to the cell number up to OD of 1.9 (data not shown). For example, 0.05 of OD. represents adhesion of about 2,000 cells, and 0.5 of OD represents adhesion of about 25,000 cells.

RESULTS

Vortex-mediated Mechanical Stress Increased Adhesion of THP-1 Cells to VCAM-1 and Fibronectin—To determine the regulation of integrin avidity or affinity by mechanical stress mediated by vortex flow, we studied adhesion of THP-1 cells to purified adhesion molecules. Cell adhesion to soluble VCAM-1, soluble ICAM-1, and fibronectin was determined after cells were exposed to vortex flow for 5 s at 1,500 rpm to mimic vortices that may occur in the cardiovascular system (12, 13, 19). Vortex-mediated mechanical stress increased adhesion of THP-1 cells to VCAM-1 and fibronectin by approximately five-fold but not to ICAM-1 (Fig. 1).

Vortex-mediated cell adhesion to VCAM-1 and fibronectin increased in a speed-dependent manner (Fig. 2). To show that this cell adhesion is dependent on $\alpha4\beta1$ and $\alpha5\beta1$ integrins, we preincubated the cells with anti-$\alpha4$ antibody and RGDS peptides. Preincubation of the cells with anti-$\alpha4$ antibody inhibited vortex-mediated cell adhesion to VCAM-1 by about 80%, but not with control IgG (Fig. 3*A*). Preincubation with RGDS, but not with REDS peptides, inhibited vortex-mediated cell adhesion to fibronectin (Fig. 3*B*). We also studied the change of $\beta1$ integrin expression on THP-1 cells induced by vortex-mediated mechanical stress, but we could not find any change of the expression by flow cytometry (data not shown). These data indicate that cell adhesion in our assay depends on the interaction between integrins and their ligands and that vortex-mediated mechanical stress increased the avidity or affinity of both $\alpha4\beta1$ and $\alpha5\beta1$ integrins in THP-1 cells.

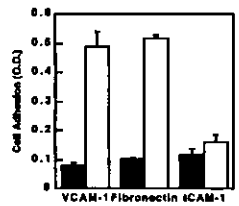

FIG. 1. **Vortex flow stimulates cell adhesion to VCAM-1 and fibronectin, but not ICAM-1, in THP-1 cells.** THP-1 cells were subjected to adhesion assays on ICAM-1, VCAM-1, or fibronectin for 5 min (*VCAM-1*, *fibronectin*) or 10 min (*ICAM-1*) with (*open bar*) or without (*filled bar*) vortexing at 1,500 rpm for 5 s. Data represent the mean ± S.D. of triplicate measurements from three independent experiments.

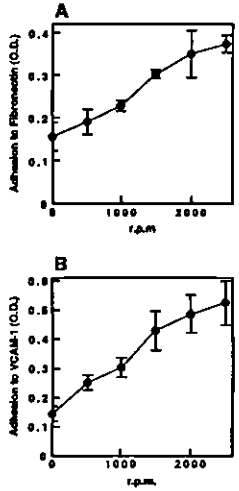

FIG. 2. **Speed-dependence of vortex-induced adhesion of THP-1 cells to VCAM-1 and fibronectin.** THP-1 cells were subjected to adhesion assays on VCAM-1 or fibronectin for 5 min after vortexing at the indicated speeds for 5 s. Data represent the mean ± S.D. of triplicate measurements from three independent experiments.

Transient Integrin Activation after Vortex-mediated Mechanical Stress—Next, we studied the time-dependent effect of vortex flow on cell adhesion to VCAM-1 and fibronectin. We found that vortex-mediated mechanical stress increased cell adhesion to both VCAM-1 and fibronectin quite rapidly, reaching a peak at 2–5 s of stimulation, indicating that such a brief vortex stimulation is enough to activate $\beta1$ integrin (Fig. 4). To examine reversibility of this integrin activation, cells were vortexed at 1,500 rpm for 5 s and left static for the indicated minutes. Cell adhesion to VCAM-1 or fibronectin was then determined. After the cells were left static for only 4 min, the cell adhesion induced by vortex flow was rapidly reduced to ~50% (Fig. 5), showing that this integrin activation induced by vortex-mediated mechanical stress is quite transient and reversible.

FIG. 3. **Time-dependent increase of vortex-induced adhesion of THP-1 cells to VCAM-1 and fibronectin.** THP-1 cells were subjected to adhesion assays on VCAM-1 or fibronectin for 5 min after vortexing at 1,500 rpm for the indicated seconds. Data represent the mean ± S.D. of triplicate measurements from three independent experiments.

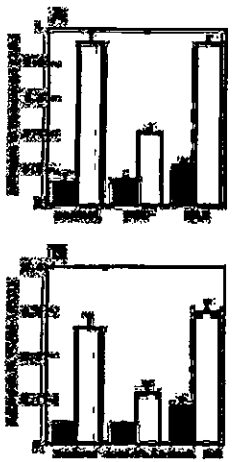

FIG. 4. **Cell adhesion depends on β1 integrin.** THP-1 cells were preincubated with 10 μg/ml anti-α4 antibody or control IgG (for VCAM-1) and 2 mM RGDS or RGES peptide (for fibronectin) for 1 h in an atmosphere of 95% air and 5% CO_2 at 37 °C. After the incubation, cells were subjected to adhesion assays on VCAM-1 or fibronectin with (*open bar*) or without (*filled bar*) vortexing at 1,500 rpm for 5 s. Data represent the mean ± S.D. of triplicate measurements from three independent experiments.

Integrin Activation Induced by Vortex-mediated Mechanical Stress Depends on IP_3-sensitive Ca^{2+} Release from Intracellular Stores—Calcium signals are reported to be important for various cell responses such as integrin activation leading to cell adhesion (20). To determine whether Ca^{2+} is involved in integrin activation induced by vortex-mediated mechanical stress, we next pretreated the cells with BAPTA-AM, an intracellular Ca^{2+}chelator. Pretreatment of the cells with BAPTA-AM inhibited vortex-mediated cell adhesion to fibronectin (Fig. 6*A*) and VCAM-1 (data not shown), indicating that intracellular Ca^{2+} is necessary for this integrin activation. To determine whether a stretch-activated Ca^{2+} channel, a well known sensing system for mechanical stress (17), or Ca^{2+} influx from the extracellular space is involved in integrin activation induced by vortex-mediated mechanical stress, we next pretreated the cells with $GdCl_3$-$6H_2O$, a specific stretch-activated channel inhibitor, or $NiCl_2$-$6H_2O$, a nonspecific Ca^{2+} influx inhibitor. Pretreatment of cells with these inhibitors did not affect vortex-mediated cell adhesion to fibronectin (Fig. 6*B*) or VCAM-1 (data not shown), indicating that this integrin activation does not depend on stretch-activated channels or Ca^{2+} influx from outside of the cells. These data indicate that Ca^{2+} release from intracellular Ca^{2+} stores such as endoplasmic reticulum may play a key role for this phenomenon.

Ca^{2+} is released from the intracellular Ca^{2+} stores via two known channels, one sensitive to inositol 1,4,5-trisphosphate (IP_3) and the other sensitive to ryanodine. Therefore, to determine the mechanism of Ca^{2+} release from intracellular Ca^{2+} stores, we pretreated the cells with thapsigargin, an inhibitor of Ca^{2+}-ATPase that inhibits IP_3-dependent Ca^{2+} release from intracellular stores (21, 22). Because thapsigargin itself induces sustained elevation of intracellular calcium mediated by capacitative Ca^{2+} influx (23, 24), we added $NiCl_2$ to block this Ca^{2+} influx. Pretreatment of THP-1 cells with thapsigargin and $NiCl_2$ inhibited vortex-mediated mechanical stress-induced cell adhesion to fibronectin (Fig. 6*B*) and VCAM-1 (data not shown). We also pretreated the cells with U-73122, a specific PLC inhibitor, because mechanical stimulation of a single cell can activate PLC to elevate IP_3 (25). Pretreatment of the cells with U-73122 inhibited vortex-mediated cell adhesion to fibronectin and VCAM-1 (data not shown) in a dose-dependent manner (Fig. 6*C*).

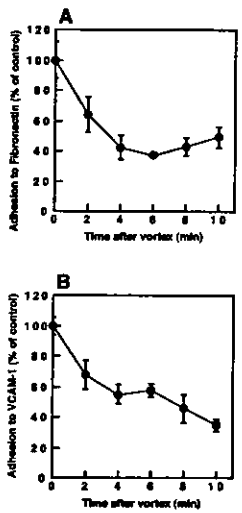

FIG. 5. **Vortex-induced integrin activation is transient and reversible.** THP-1 cells were subjected to adhesion assays on VCAM-1 or fibronectin for 5 min after left static for the indicated minutes after vortexing at 1,500 rpm for 5 s. Data represent the mean ± S.D. of triplicate measurements from three experiments. The value at the baseline was expressed as 100%.

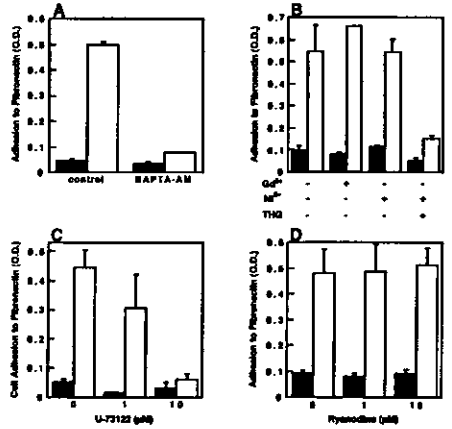

FIG. 6. **Integrin activation induced by vortex-mediated mechanical stress depends on IP_3-sensitive Ca^{2+} release from intracellular stores.** *A*, THP-1 cells were preincubated with 50 μM BAPTA-AM for 1 h in an atmosphere of 95% air and 5% CO_2 at 37 °C. After incubation, cells were subjected to adhesion assays on fibronectin for 5 min with (*open bar*) or without (*filled bar*) vortexing at 1,500 rpm for 5 s. Data represent the mean ± S.D. of triplicate measurements from three independent experiments. *B*, THP-1 cells were preincubated with 50 μM $GdCl_3$-$6H_2O$ for 1 h or 1 mM $NiCl_2$-$6H_2O$ for 1 h followed by treatment with or without 1 μM thapsigargin (*THG*) for 3 h in an atmosphere of 95% air and 5% CO_2 at 37 °C. After incubation, cells were subjected to adhesion assays on fibronectin for 5 min with (*open bar*) or without (*filled bar*) vortexing at 1,500 rpm for 5 s. Data represent the mean ± S.D. of triplicate measurements from three independent experiments. *C* and *D*, THP-1 cells were preincubated with the indicated concentrations of U-73122 (*C*) or ryanodine (*D*) for 1 h in an atmosphere of 95% air and 5% CO_2 at 37 °C. After incubation, cells were subjected to adhesion assays on VCAM-1 for 5 min with (*open bar*) or without (*filled bar*) vortexing at 1,500 rpm for 5 s. Data represent the mean ± S.D. of triplicate measurements from three independent experiments.

To examine the role of ryanodine-sensitive Ca^{2+} release from intracellular Ca^{2+} stores, we next pretreated the cells with ryanodine, which can inhibit ryanodine-sensitive Ca^{2+} release (26). Pretreatment of THP-1 cells with ryanodine up to 10 μM did not affect vortex-mediated cell adhesion to fibronectin (Fig. 6*D*). These data indicate that IP_3-dependent Ca^{2+} release from intracellular Ca^{2+} stores plays a key role in this phenomenon.

Calmodulin Is Also Necessary for Integrin Activation Induced by Vortex-mediated Mechanical Stress—We also examined the potential role of Ca^{2+}-calmodulin in integrin activation induced by vortex-mediated mechanical stress. To determine the involvement of calmodulin in integrin activation induced by vortex-mediated mechanical stress, we pretreated the cells with W-7, a calmodulin inhibitor, before vortexing the cells. Pretreatment of cells with W-7 inhibited vortex-mediated cell adhesion to VCAM-1 and fibronectin in a dose-dependent manner (Fig. 7), indicating that calmodulin is also involved in integrin activation induced by vortex-mediated mechanical stress.

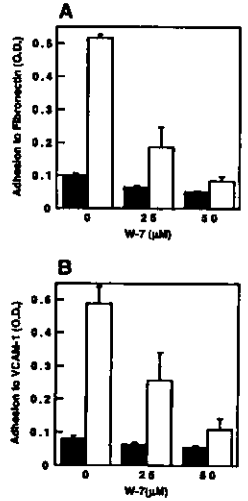

FIG. 7. **Calmodulin inhibitor inhibits vortex-induced adhesion to VCAM-1 and fibronectin in a dose-dependent manner.** THP-1 cells were preincubated with W-7 (calmodulin inhibitor) at indicated concentrations for 2 h in an atmosphere of 95% air and 5% CO_2 at 37 °C. After incubation, cells were subjected to adhesion assays on VCAM-1 or fibronectin for 5 min with (*open bar*) or without (*filled bar*) vortexing at 1,500 rpm for 5 s. Data represent the mean ± S.D. of triplicate measurements from three independent experiments.

DISCUSSION

In this study we have examined the effect of vortex-mediated mechanical stress on integrin-dependent cell adhesion in human monocytic THP-1 cells and have clearly shown that a brief period of vortex-mediated mechanical stress activated β1 integrin, resulting in cell adhesion to VCAM-1 and fibronectin in a transient and reversible manner. We have also shown that IP_3-dependent Ca^{2+} release from intracellular Ca^{2+} stores and calmodulin are involved in this integrin activation. This mechanism might explain why atherosclerosis is prone to progress in bifurcated or stenotic regions, and this may be a novel aspect of atherosclerosis and inflammation.

Most of the studies on mechanotransduction in the cardiovascular field have been done in endothelial cells and smooth muscle cells. The endothelial cells are normally subjected to mechanical stimuli from shear stress and from strain associated with stretch of the vessel wall. These stimuli can be detected by a mechanosensor that initiates a variety of signal transduction cascades (17, 27). For example, in response to the change in shear stress the endothelium can change the gene expression of various cytokines and adhesion molecules (15, 16, 28) that would be related to the promotion of atherosclerosis, thrombosis, and inflammation. Few studies, however, have been conducted to elucidate the changes in the adhesive property of leukocytes in the vortex flow, which might be also related to the induction of atherosclerosis. Fukuda *et al.* (11) have reported that human leukocytes respond to fluid shear stress by retracting pseudopods and down-regulate the integrin expression under the laminar flow condition, which would help leukocytes to run in the vessel wall. However, in the tortuous cardiovascular system, such as branching of the vessels and downstream of partially occluded vessels, leukocytes and plate-

lets can be subjected to differing shear forces under nonlaminar flow patterns (1, 12, 13). In this study, therefore, we exposed cells to vortex flow in order to mimic vortices that may occur in the cardiovascular system. In the study of platelet aggregation, a stirring bar has been used to expose platelets to vortex flow (19). Because it is important to expose whole cells to vortex flow instantaneously to mimic the *in vivo* situation, vortexing the cells in a vortex machine would be more reasonable to stimulate the cells *in vitro*. Establishing an *in vivo* model would be more important to show the relevance of this data to *in vivo* situations.

In previous studies, the endothelial intracellular Ca^{2+} concentration in response to mechanical stress is biphasic, consisting of an initial transient rise that depends on Ca^{2+} release from IP_3-sensitive stores, followed by a sustained elevation mediated by Ca^{2+} influx (22, 29, 30). However, in this report we have shown that Ca^{2+} influx from the extracellular space is not necessary for integrin activation induced by vortex-mediated mechanical stress on THP-1 cells. Our data also clearly indicate that IP_3-dependent Ca^{2+} release from intracellular Ca^{2+} stores plays a key role in this mechanism. Although the reason why only Ca^{2+} release from intracellular stores is required for vortex-mediated integrin activation remains unclear, it might be because of the shortness of vortex stimulation and integrin activation.

Calmodulin is a Ca^{2+} binding protein and is reported to be important for various cell responses, such as integrin activation leading to T cell adhesion (20) and aggregation (31). Our study clearly demonstrates that calmodulin also plays an essential role in regulating integrin activation induced by vortex-mediated mechanical stress as shown in various cell responses (32, 33). However, at present it is not clear how Ca^{2+} release from intracellular stores can be linked to the activation of calmodulin and integrin activation in THP-1 cells. Further studies, therefore, are required to clarify this mechanism.

In this study we have not been able to identify the sensing mechanism for vortex-induced mechanical stress in THP-1 cells. There is a possibility that a mechanosensor itself is not involved in this process. The forces applied at the cell surface might be transmitted to other locations via cytoskeleton. This kind of mechanotransduction is shown in the area of mechanical stretch (34). Therefore, an explanation of the sensing mechanism would be required to understand this process. Further understanding of how leukocyte adhesion functions in the tortuous cardiovascular system would enhance our knowledge of the nuances of the atherosclerotic and inflammatory process and should facilitate the development of drugs to regulate the process.

In summary, we have provided clear evidence that vortex-mediated mechanical stress on THP-1 cells quickly induces Ca^{2+}- and calmodulin-dependent integrin activation, and IP3-dependent Ca^{2+} release from intracellular Ca^{2+} stores is involved in its mechanism. These findings might enlighten another aspect of increased atherosclerosis at stenotic or bifurcated regions.

Acknowledgment—We thank Hitomi Sagawa for excellent technical assistance.

REFERENCES

1. Turitto, V. T., and Hall, C. L. (1998) *Thromb. Res.* **92**, (suppl.) 25–31
2. Malek, A. M., Gibbons, G. H., Dzau, V. J., and Izumo, S. (1993) *J. Clin. Invest.* **92**, 2013–2021
3. Resnick, N., Yahav, H., Khachigian, L. M., Collins, T., Anderson, K. R., Dewey, F. C., and Gimbrone, M. A., Jr. (1997) *Adv. Exp. Med. Biol.* **430**, 155–164
4. Mo, M., Eskin, S. G., and Schilling, W. P. (1991) *Am. J. Physiol.* **260**, H1698–1707
5. Sriramarao, P., Languino, L. R., and Altieri, D. C. (1996) *Blood* **88**, 3416–3423
6. Kroll, M. H., Hellums, J. D., McIntire, L. V., Schafer, A. I., and Moake, J. L. (1996) *Blood* **88**, 1525–1541
7. Miyazaki, Y., Nomura, S., Miyake, T., Kagawa, H., Kitada, C., Taniguchi, H., Komiyama, Y., Fujimura, Y., Ikeda, Y., and Fukuhara, S. (1996) *Blood* **88**, 3456–3464
8. Weiss, H. J., Hawiger, J., Ruggeri, Z. M., Turitto, V. T., Thiagarajan, P., and Hoffmann, T. (1989) *J. Clin. Invest.* **83**, 288–297
9. Butcher, E. C. (1991) *Cell* **67**, 1033–1036
10. Meazzam, F., DeLano, F. A., Zweifach, B. W., and Schmid-Schonbein, G. W. (1997) *Proc. Natl. Acad. Sci. U. S. A.* **94**, 5338–5343
11. Fukuda, S., Yasu, T., Predescu, D. N., and Schmid-Schonbein, G. W. (2000) *Circ. Res.* **86**, E13–18
12. Ku, D. N., Glagov, S., Moore, J. E., Jr., and Zarins, C. K. (1989) *J. Vasc. Surg.* **9**, 309–316
13. Cao, J., and Rittgers, S. E. (1998) *Ann. Biomed. Eng.* **26**, 190–199
14. Palmen, D. E., van de Vosse, F. N., Janssen, J. D., and van Dongen, M. E. (1994) *J. Biomech.* **27**, 681–690
15. Mohan, S., Mohan, N., Valente, A. J., and Sprague, E. A. (1999) *Am. J. Physiol.* **276**, C1100–1107
16. Nagel, T., Resnick, N., Atkinson, W. J., Dewey, C. F., Jr., and Gimbrone, M. A., Jr. (1994) *J. Clin. Invest.* **94**, 885–891
17. Brakemeier, S., Eichler, I., Hopp, H., Kohler, R., and Hoyer, J. (2002) *Cardiovasc. Res.* **53**, 209–218
18. Ashida, N., Arai, H., Yamasaki, M., and Kita, T. (2001) *J. Biol. Chem.* **276**, 16556–16560
19. Sonlau, G., Schechner, A. J., Alcaide, P. J., and Class, R. (2000) *Thromb. Res.* **97**, 15–27
20. van Kooyk, Y., Weder, P., Heije, K., de Waal Malefijt, R., and Figdor, C. G. (1993) *Cell Adhes. Commun.* **1**, 21–32
21. Yellowley, C. E., Jacobs, C. R., and Donahue, H. J. (1999) *J. Cell. Physiol.* **180**, 402–408
22. Oike, M., Droogmans, G., and Nilius, B. (1994) *Proc. Natl. Acad. Sci. U. S. A.* **91**, 2940–2944
23. Granfeldt, D., Samuelsson, M., and Karlsson, A. (2002) *J. Leukoc. Biol.* **71**, 611–617
24. Kuroiwa-Matsumoto, M., Hirano, K., Ahmed, A., Kawasaki, J., Nishimura, J., and Kanaide, H. (2000) *Br. J. Pharmacol.* **131**, 115–123
25. Sanderson, M. J., Charles, A. C., Boitano, S., and Dirksen, E. R. (1994) *Mol. Cell. Endocrinol.* **98**, 173–187
26. Meissner, G. (1986) *J. Biol. Chem.* **261**, 6300–6306
27. Lansman, J. B., Hallam, T. J., and Rink, T. J. (1987) *Nature* **325**, 811–813
28. Tsuboi, H., Ando, J., Korenaga, R., Takada, Y., and Kamiya, A. (1996) *Biochem. Biophys. Res. Commun.* **226**, 888–896
29. Geiger, R. V., Berk, B. C., Alexander, R. W., and Nerem, R. M. (1992) *Am. J. Physiol.* **262**, C1411–1417
30. Helmlinger, G., Berk, B. C., and Nerem, R. M. (1996) *J. Vasc. Res.* **33**, 360–369
31. Andrews, R. K., Suzuki-Inoue, K., Shen, Y., Tulasne, D., Watson, S. P., and Berndt, M. C. (2002) *Blood* **99**, 4219–4221
32. Exton, J. H. (1985) *Am. J. Physiol.* **248**, E633–647
33. Johns, A., Leijten, P., Yamamoto, H., Hwang, K., and van Breemen, C. (1987) *Am. J. Cardiol.* **59**, 18A–23A
34. Ingber, D. E. (1997) *Annu. Rev. Physiol.* **59**, 575–599

THE JOURNAL OF BIOLOGICAL CHEMISTRY
© 2003 by The American Society for Biochemistry and Molecular Biology, Inc.

Vol. 278, No. 20, Issue of May 16, pp. 18229–18234, 2003
Printed in U.S.A.

Growth Arrest-specific Gene 6 Is Involved in Glomerular Hypertrophy in the Early Stage of Diabetic Nephropathy*

Received for publication, December 30, 2002, and in revised form, March 17, 2003
Published, JBC Papers in Press, March 17, 2003, DOI 10.1074/jbc.M213266200

Kojiro Nagai‡, Hidenori Arai‡§, Motoko Yanagita‡, Takeshi Matsubara‡, Hiroshi Kanamori‡, Toru Nakano¶, Noriyuki Ieharaǁ, Atsushi Fukatsuǁ, Toru Kita, and Toshio Doi‡‡**

*From the Departments of ‡Geriatric Medicine, **Cardiovascular Medicine, and ǁArtificial Kidneys, Kyoto University Graduate School of Medicine, Kyoto 606-8507, Japan, the ¶Discovery Research Laboratory, Shionogi Co., Ltd., Osaka 553-0002, Japan, and the ‡‡Department of Clinical Biology and Medicine, Tokushima University, Tokushima 770-8503, Japan*

Nephropathy is one of the most common complications of diabetes mellitus. Glomerular hypertrophy is a hallmark in the early phase of the nephropathy. The mechanism of glomerular hypertrophy, however, remains incompletely understood. We have reported that Gas6 (growth arrest-specific gene 6) and its receptor, Axl, play a key role in the development of glomerulonephritis. Here we show the important role of Gas6/Axl in the pathogenesis of diabetic glomerular hypertrophy. In streptozotocin (STZ)-induced diabetic rats, mesangial and glomerular hypertrophy and an increase in the glomerular filtration rate (GFR) and albuminuria were observed after 12 weeks of STZ injection. The glomerular expression of Gas6 and Axl was increased in those rats. Administration of warfarin inhibited mesangial and glomerular hypertrophy and the increase in GFR and albuminuria in STZ rats. Moreover, we found less mesangial hypertrophy in STZ-treated Gas6 knockout mice than control mice. *In vitro* we found that stimulation of mesangial cells with Gas6 resulted in mesangial cell hypertrophy. Thus we have found a novel mechanism of glomerular hypertrophy through the Gas6/Axl-mediated pathway in the development of diabetic nephropathy. Inhibition of the Gas6/Axl pathway in diabetic patients might be beneficial to slow down the progression of diabetic nephropathy.

Diabetes is the most common cause of end stage renal disease in many countries. Approximately 30% of type 1 diabetic patients suffer from diabetic nephropathy (1, 2). Therefore, tremendous efforts have been made to elucidate the molecular mechanism of diabetic nephropathy to develop an effective treatment. The feature characteristic of diabetic nephropathy is persistent albuminuria and mesangial expansion followed by glomerulosclerosis and a decline in renal function. The development of glomerulosclerosis in diabetes mellitus is always preceded by the early hypertrophic processes in the glomerular compartment (3). Because it is important to regulate the early stage of the disease process, extensive efforts have been made to elucidate growth factors and cytokines involved in mesangial expansion or hypertrophy (4). Transforming growth factor-β1 (TGF-β1)[1] and angiotensin II are found to be implicated in the development of diabetic nephropathy among them (5). Although angiotensin-converting enzyme inhibitors and/or type I angiotensin receptor blockers are effective to some extent, angiotensin-converting enzyme inhibitors can decrease the risk of developing diabetic nephropathy by only 12.5% in type 2 diabetic patients (6). Therefore, additional pathogenetic mechanisms are being urgently investigated to help design novel therapies for patients with diabetic nephropathy.

Among other potential growth factors for glomerular cells, we have investigated the role of Gas6 (growth arrest-specific gene 6) in the pathogenesis of kidney disease. Gas6, cloned from serum-starved fibroblasts (7), is posttranslationally activated by γ-carboxylation of glutamate residues at its N terminus in the presence of vitamin K and inhibited by the anticoagulant warfarin (8, 9). Recently we showed that Gas6 is an autocrine growth factor for mesangial cells and that Gas6 and its receptor Axl play a critical role in the development of glomerulonephritis by showing that warfarin and the extracellular domain of Axl inhibit mesangial cell proliferation by specific blockade of the Gas6-mediated pathway in a mesangial proliferative model of glomerulonephritis (10, 11). However, the role of Gas6 and Axl in diabetic nephropathy is not determined.

The present study is designed to examine whether Gas6 and Axl can contribute to the pathogenesis of diabetic glomerular hypertrophy *in vivo* and *in vitro*. In this study, we specifically asked whether Gas6 and Axl can play an important role in mesangial cell hypertrophy, which is a feature seen in the early phase of diabetic nephropathy and whether inhibition of the Gas6/Axl pathway can affect the progression of diabetic nephropathy in streptozotocin (STZ) rats and mice.

EXPERIMENTAL PROCEDURES

Materials—STZ was obtained from Wako Pure Chemical Inc. Ltd. (Osaka, Japan). Recombinant human TGF-β1 was purchased from R&D Systems, Inc. (Minneapolis, MN).

Animals and Cell Culture—Male Sprague-Dawley rats weighing 170–200 g were purchased from Shimizu Laboratory Animal center (Hamamatsu, Japan). Gas6 knockout mice were generated with a targeted disruption of the *Gas6* gene as previously described (11). Control inbred C57BL/6 mice were obtained from Clea Japan, Inc. (Osaka, Japan). The animals were housed under specific pathogen-free conditions at the Animal Facilities of Kyoto University, Faculty of Medicine.

* This work was supported by Grants-in Aid 13307034 and 14570657 from the Ministry of Education, Science, Sports, and Culture of Japan, Center of Excellence Grant 12CE2006 from the Japanese Ministry of Education, Science, Sports, and Culture, and a research grant for health sciences from the Japanese Ministry of Health and Welfare. The costs of publication of this article were defrayed in part by the payment of page charges. This article must therefore be hereby marked "*advertisement*" in accordance with 18 U.S.C. Section 1734 solely to indicate this fact.

§ To whom correspondence should be addressed: Dept. of Geriatric Medicine, Kyoto University Graduate School of Medicine, 54 Kawahara-cho, Shogoin, Sakyo-ku, Kyoto 606-8507, Japan. Tel.: 81-75-751-3463; Fax: 81-75-751-3463; E-mail: harai@kuhp.kyoto-u.ac.jp.

[1] The abbreviation used are: TGF-β1, transforming growth factor-β1; STZ, streptozotocin; GFR, glomerular filtration rate; MAP, mitogen-activated protein.

All of the animal experiments were performed in accordance with institutional guidelines, and the Review Board of Kyoto University granted ethical permission to this study. The glomerular mesangial primary culture was established from glomeruli isolated from normal 4-week-old mice (C57BL/6JxSJL/J) and was identified according to the method previously described (12, 13). Phenotypically stable mesangial cells, 12th to 16th passages, were plated on 100-mm plastic dishes (Nalge Nunc International, Roskilde, Denmark) and maintained in growth medium (3:1 mixture of Dulbecco's modified Eagle's medium/Ham's F-12 medium modified trace elements) (Nissui Pharmaceutical Co., Ltd., Tokyo, Japan) supplemented with 1 mM glutamine, penicillin at 100 units/ml, streptomycin at 100 μg/ml (Invitrogen) and 20% fetal bovine serum (Cansera International Inc., Rexdale, Canada).

STZ-induced Diabetic Rats and Mice—Male rats weighing 170–200 g were made diabetic by a single intravenous injection of STZ (55 mg/kg body weight) in 0.05 mol/liter citrate buffer (pH 4.5). Weight-matched 8-week-old mice (17–20 g) were made diabetic by two consecutive daily intraperitoneal injections of STZ (150 mg/kg) dissolved in 0.01 mol/liter citrate buffer. Rats and mice receiving an injection of citrate buffer were used as controls. The levels of blood glucose were determined 2 days after injection of STZ or vehicle, and rats and mice with blood glucose levels more than >16.7 mmol/liter were used as diabetic (14, 15). Twelve weeks after STZ injection, the rats and mice were weighed and sacrificed.

Warfarin Treatment—The rats were divided into four groups: control rats without treatment, control rats with warfarin treatment, diabetic rats without treatment, and diabetic rats with warfarin treatment. The rats with warfarin treatment were administered with 0.25 mg/liter warfarin potassium (provided by Eisai Co. Ltd., Tokyo, Japan) in drinking water from the day of STZ injection. The dosage of warfarin was determined based on the previous report (10). Because diabetic rats drink much more water, the dosage of warfarin was reduced to 0.06 mg/liter from 2 days after injection of STZ. Twelve weeks after injection, the rats were weighed and sacrificed. Blood was collected at sacrifice. Prothrombin times, hematocrits, serum creatinine, and plasma concentrations of warfarin were measured as described (10). HbA1c was measured using DCA2000 analyzer (Bayer Medical, Tokyo, Japan). Before sacrifice, creatinine and albumin were measured from 24-h urine collection.

Immunohistochemistry—Kidney tissues from each animal were snap frozen in cold acetone in optimal cutting temperature compound (Sakura Finetechnical Co. Ltd., Tokyo, Japan), and cryostat sections (4 μm) were stained by indirect immunofluorescence procedure with the following primary antibodies: rabbit polyclonal antibodies against rat Gas6 (16) and human Axl (generous gift from Dr. Brian Varnum, Amgen, Thousand Oaks, CA).

Isolation of Glomeruli—Glomeruli were isolated from renal cortices of rats using the differential sieving method (17, 18). The purity of the glomeruli was >90%.

Western Blotting—Isolated glomeruli were suspended in RIPA buffer (50 mM Tris, pH 7.5, 150 mM NaCl, 1% Nonidet P-40, 0.25% SDS, 1 mM Na_3VO_4, 2 mM EDTA, 1 mM phenylmethylsulfonyl fluoride, 10 μg/ml of aprotinine), and incubated for 1 h at 4 °C. After centrifugation, the supernatants were used as total cell lysates. 60 μg of each sample was applied to SDS-PAGE. After electrophoresis, the proteins were transferred to nitrocellulose filters (Schleicher & Schuell). The blots were subsequently incubated with rabbit anti-rat Gas6, anti-human Axl, rabbit anti-phospho-p44/p42 mitogen-activated protein (MAP) kinase polyclonal antibody (Cell Signaling Technology, Beverly, MA), or rabbit anti-MAP kinase polyclonal antibody (Oncogene, San Diego, CA), followed by incubation with horseradish peroxidase-conjugated goat anti-rabbit IgG (Amersham Biosciences). The immunoreactive bands were visualized using horseradish peroxidase-conjugated secondary antibody and the enhanced chemiluminescent system (Amersham Biosciences).

Histological Examination—The mesangial cell area was measured in a hematoxylin eosin staining section by Image-Pro Plus (Media Cybernetics, Silver Spring, MD). For each animal, 50 mesangial cell areas were analyzed. The glomerular surface area and the periodic acid-methenamine-silver-positive area were determined using an image analyzer (Image Processor for Analytical Pathology; Sumitomo Chemical Co., Tokyo, Japan) (19, 20). For each animal, 50 glomeruli were analyzed.

Glomerular Filtration Rate (GFR) and the Measurement of Urinary Albumin Excretion—Urine volume (V_u) was measured at 12 weeks by 24-h urine collection from rats housed in individual metabolic cages. During the urine collection, the rats were allowed free access to food and water. Serum and urine creatinine concentrations (C_s and C_u) were measured, and GFR was calculated by the following equation: GFR = (C_u/C_s) × V_u/body weight (21). The albumin concentration in the urine was measured by Nephrat (Exocell Inc., Philadelphia, PA).

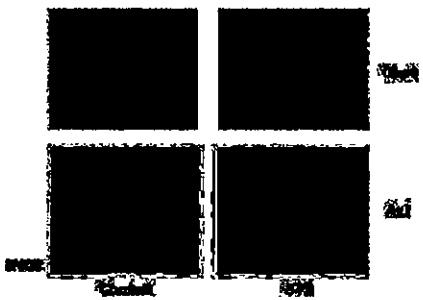

FIG. 1. **Expression of Gas6 and Axl in STZ-induced diabetic rat kidney.** Kidney tissues from each animal were snap frozen in cold acetone in OCT compound. The cryostat sections (4 μm) were stained using indirect immunofluorescence procedure with anti-Gas6 or anti-Axl antibody. The original magnification was ×400.

[^{3}H]Leucine Incorporation and Determination of Cell Number—Mesangial cells were plated at 1.5×10^4 cells/well in 24-well dishes. After 48 h, the cells were serum-starved in Dulbecco's modified Eagle's medium containing 0.5% bovine serum albumin (Sigma-Aldrich) for 48 h. The medium was then replaced with the fresh starving medium including various concentrations of agonist or left untreated. After 18 h, the cells were labeled with [^{3}H]leucine (2 μCi/ml; Amersham Biosciences) for 6 h, and the incorporation of [^{3}H]leucine into acid-precipitable materials was then determined. For determination of cell number, the cells were trypsinized, resuspended in phosphate-buffered saline, and counted with a Coulter counter Z1 (Coulter Electronics Ltd., Hialeah, FL). The data were normalized by dividing incorporation counts by the cell number and showed as fold increases over control.

Flow Cytometry—Mesangial cells were plated at 4.5×10^6 cells/well in 100-mm plates. The cells were treated as the [^{3}H]leucine incorporation procedure. After treatment, mesangial cells were harvested by tripsinization, washed with phosphate-buffered saline, centrifuged at 1,500 rpm for 10 min, and then resuspended in ice-cold 70% ethanol added dropwise while vortexing. Ethanol-fixed mesangial cells were then analyzed by forward light scattering on a Becton Dickinson flow cytometer (BD Biosciences, San Jose, CA).

Statistical Analyses—The data are expressed as the means ± S.D. Comparison among each group was performed by one-way analysis of variance followed by Neuman-Keuls test to evaluate the statistical significance between two groups. A p value of <0.05 was considered to be significant.

RESULTS

Expression of Gas6 and Axl in STZ-induced Diabetic Rats—Our preliminary data showed that glomerular hypertrophy and an increase in GFR and albuminuria were observed after 12 weeks of STZ injection in rats. Therefore, to examine the role of Gas6/Axl in the early phase of diabetic nephropathy *in vivo*, we used STZ-induced diabetic rat kidney. We analyzed the glomerulus after 12 weeks of STZ injection and found that expression of both Gas6 and Axl was significantly increased in the STZ-treated group and that they were mostly localized at endothelial and mesangial cells (Fig. 1).

Warfarin Treatment Inhibits Induced Expression of Axl and Phosphorylation of p44/42 MAP Kinase—Because expression of Gas6 and Axl was induced in diabetic rats, the Gas6/Axl pathway seems to play a role in the development of diabetic nephropathy in the early phase of the disease process. Therefore, we next examined whether inhibiting this pathway can be effective in treating this experimental diabetic nephropathy. We treated rats with warfarin in drinking water as shown in Fig. 2. Plasma concentrations of warfarin in these rats were 0.71 ± 0.05 and 0.67 ± 0.05 μM, which were significantly lower

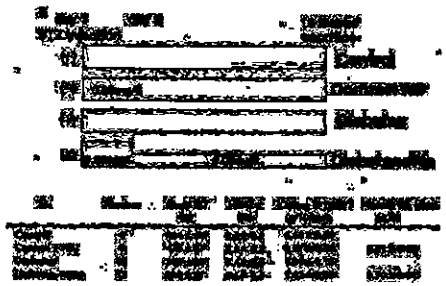

FIG. 2. **Protocol of warfarin treatment (A) and physiological characteristics of control and diabetic rats with or without warfarin treatment after 12 weeks (B).** A single intravenous injection of 55 mg/kg of STZ was performed on day 1 to make diabetic rats. The rats were separated into control and diabetic groups with or without warfarin treatment. Rats with warfarin treatment (*Wa*) were administered with 0.25 mg/liter warfarin in drinking water. Because diabetic rats drink much more water, the dosage of warfarin was reduced to 0.06 mg/liter from 2 days after injection of STZ. *B*, after 12 weeks of STZ injection, the rats were weighed and sacrificed. Blood was taken to evaluate HbA1c and plasma concentrations of warfarin. Kidney weight was also measured.

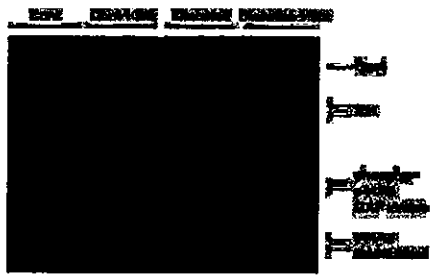

FIG. 3. **Effect of warfarin on the expression of Gas6 and Axl and expression and phosphorylation of p44/42 MAP kinase in STZ rat glomeruli.** After 12 weeks of STZ injection, the rats were sacrificed, and glomeruli were isolated by a sieving method. The isolated glomeruli were suspended in RIPA buffer. After centrifugation, the supernatants were used as total cell lysates. 60 μg of each sample was analyzed by Western blotting with the antibodies indicated. Each lane represents a representative Western blot for the cell lysate from each rat. *Wa*, warfarin treatment; *Cont*, control.

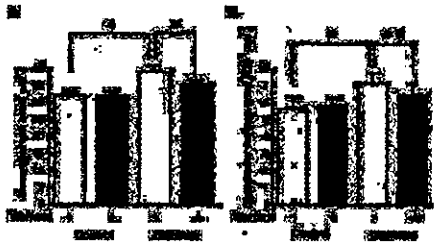

FIG. 4. **Effect of warfarin on mesangial (A) and glomerular hypertrophy (B).** The mesangial cell area was measured in a hematoxylin eosin staining section by Image-Pro Plus. For each animal, 50 mesangial cell areas were calculated. The glomerular surface area was determined using an image analyzer. The data are expressed as the means ± S.D. (n = 6 in the control group and n = 10 in the diabetic group). *, $p < 0.01$; **, $p < 0.05$.

than the ordinary therapeutic concentrations as an anticoagulant. The body weight and kidney weight/body weight values were not changed by warfarin treatment. Significant prolongation of prothrombin times, anemia, or bleeding tendency was not observed in all the rats during the whole period of warfarin treatment as we already found in our previous study (data not shown).

After 12 weeks of STZ injection, we isolated glomeruli from the rats and found increased glomerular expression of Gas6 and Axl by Western blotting (Fig. 3) as shown in Fig. 1. When we treated STZ rats with warfarin, we found that the expression of Axl was markedly inhibited in warfarin-treated STZ rats than untreated STZ rats. Although warfarin treatment did not affect Gas6 expression, it might be due to the fact that the antibody used for Western blotting cannot discriminate active or inactive Gas6.

Because we have shown that Gas6 can activate p44/42 MAP kinase *in vitro* (16), we examined whether p44/42 MAP kinase can be phosphorylated in diabetic glomerular lysates and whether warfarin treatment can affect the phosphorylation. As shown in Fig. 3, p44/42 MAP kinase was phosphorylated in the glomerular lysates in STZ rats, and warfarin treatment abolished their phosphorylation.

Warfarin Shows a Beneficial Effect on Mesangial and Glomerular Hypertrophy—Because glomerular hypertrophy is one of the earliest structural alterations in diabetic nephropathy, we measured mesangial cell and glomerular surface areas in diabetic rat kidney and examined the effect of warfarin on glomerular hypertrophy. After 12 weeks of STZ injection, both areas were significantly enlarged compared with control rats, and administration of warfarin prevented the increase of mesangial and glomerular areas (Fig. 4). Because accumulation of mesangial extracellular matrix components is also an early structural change in diabetic nephropathy, we also measured the periodic acid-methenamine-silver-positive area in both groups. However, there was no change in the periodic acid-methenamine-silver-positive area between control and diabetic groups, indicating that there is no glomerular sclerotic change after 12 weeks of STZ injection (data not shown).

Warfarin Treatment Improves Hyperfiltration and Excretion of Urinary Albumin—In the early phase of diabetic nephropathy, GFR is increased in most of diabetic patients. Therefore, we examined whether GFR is increased in STZ rats and whether warfarin treatment can affect GFR. After 12 weeks of STZ injection, GFR and urinary albumin excretion were significantly increased, and the increased GFR and albuminuria were suppressed by warfarin treatment (Fig. 5).

STZ-treated Gas6 Knockout Mice Showed Less Glomerular Hypertrophy—To confirm the specificity of warfarin on the Gas6/Axl pathway, we used STZ-treated Gas6 knockout mice. Our preliminary data showed that glomerular hypertrophy was observed after 12 weeks of STZ injection in mice. Therefore, we analyzed mesangial and glomerular hypertrophy in Gas6 knockout and wild type mice after 12 weeks of STZ injection. As shown in Fig. 6*A*, Gas6 knockout mice were smaller than wild type mice, and HbA1c was higher in Gas6 knockout mice than in wild type mice. However, the blood glucose levels were almost the same throughout the study period (data not shown). Although the kidney weight/body weight was smaller in diabetic Gas6 knockout mice compared with diabetic wild type mice, there was no statistically significant difference. As shown in Fig. 6 (*B* and *C*), mesangial cell and glomerular surface areas in diabetic wild type mice were significantly larger than those in wild type untreated mice. However, in diabetic Gas6 knockout mice, the increase of both areas was significantly

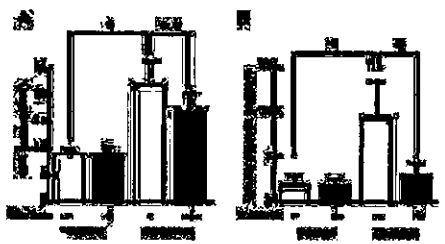

FIG. 5. **Effect of warfarin on hyperfiltration (A) and urinary albumin excretion (B).** Urine volume was measured at 12 weeks from 24-h urine collection. Serum and urine creatinine concentrations were measured, and GFR was calculated by an equation described under "Experimental Procedures." Albumin concentrations in the urine were measured by Nephrat. The data are expressed as the means ± S.D. (n = 6 in the control group and n = 10 in the diabetic group). *, $p < 0.01$; **, $p < 0.05$.

A	Number	Body WT (g)	HbA1c (%)	Kidney WT/BWT (g/100gs)
WT Control	6	22.9±0.9	3.6±0.1	1.26±0.06
KO Control	6	21.1±1.0	4.2±0.6	1.23±0.10
WT Diabetes	5	19.6±2.3	9.6±0.3	2.11±0.45
KO Diabetes	6	19.2±1.1	10.4±1.3	1.73±0.15

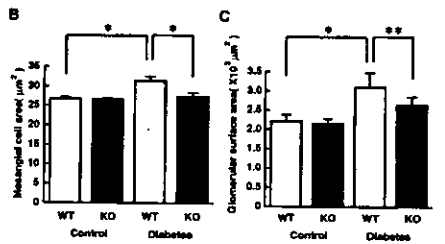

FIG. 6. **Effect of Gas6 deficiency on mesangial and glomerular hypertrophy in STZ-treated mice.** Diabetes was induced by two consecutive daily intraperitoneal injections of STZ (150 mg/kg). Wild type (*WT*) and Gas6 knockout mice (*KO*) (12 each) were divided into two groups: untreated (*Control*) or STZ-treated (*Diabetes*). Twelve weeks after STZ injection, HbA1c, body weight, and kidney weight were measured (*A*). Mesangial cell (*B*) and glomerular surface areas (*C*) were also measured as described under "Experimental Procedures." For each mouse, 50 mesangial cell and glomerular surface areas were calculated. The data are expressed as the means ± S.D. (n = 6 in each group). *, $p < 0.01$; **, $p < 0.05$.

suppressed. These data also indicate that Gas6 is involved in the development of the initial phase of diabetic nephropathy and suggest that warfarin inhibits diabetic nephropathy specifically through the Gas6-mediated pathway.

Gas6 Induces Mesangial Cell Hypertrophy in Vitro—To investigate the mechanism by which Gas6 is involved in glomerular hypertrophy in diabetic rats, we examined whether Gas6 can cause mesangial cell hypertrophy *in vitro*. We measured [^{3}H]leucine incorporation in mouse mesangial cells as a marker of cellular hypertrophy after incubation with various concentrations of Gas6. Recombinant Gas6 increased incorporation of [^{3}H]leucine incorporation dose-dependently, with a 1.5-fold increase at maximum (Fig. 7). The same dose of Gla-defective Gas6, which is an inactive form of Gas6 without γ-carboxylation, did not affect [^{3}H]leucine incorporation in mouse mesangial cells. The Gas6-mediated increase in [^{3}H]leucine incorporation was almost the same as that of TGF-β1 (1 ng/ml). To clarify whether mesangial cell hypertrophy is mediated specifically through the Gas6-Axl pathway, we used the recombinant extracellular domain of Axl (Axl-Fc), which is a recombinant fusion protein of the extracellular domain of Axl and human Fc portion, as an inhibitor of the Gas6-Axl pathway. After preincubation with 10 nM Axl-Fc in starving medium for 1 h, Gas6 (100 ng/ml) was added to the serum-starved mesangial cells, and [^{3}H]leucine incorporation was then measured. The addition of Axl-Fc inhibited the increased [^{3}H]leucine incorporation by Gas6, suggesting that the effect of Gas6 on hypertrophy is specific for the Gas6-Axl interaction. Further, we checked the cellular size of mesangial cells by flow cytometry under the same protocol as [^{3}H]leucine incorporation (Fig. 8). We found that treatment of the cells with Gas6 100 ng/ml or TGF-β1 increased the cellular size by 1.1-fold but not Gla-defective Gas6.

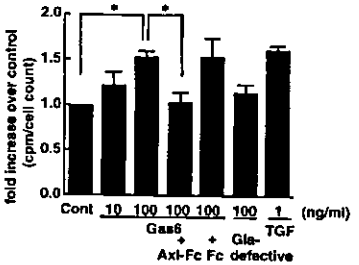

FIG. 7. **[^{3}H]Leucine incorporation in mouse mesangial cells by Gas6.** Mesangial cells were plated at 1.5×10^4 cells/well in 24-well dishes. After 48 h, the cells were serum-starved in Dulbecco's modified Eagle's medium containing 0.5% bovine serum albumin for 48 h. Then the medium was replaced with the fresh starving medium including various concentrations of agonist or left untreated. After 18 h, the cells were labeled with [^{3}H]leucine (2 μCi/ml) for 6 h, and the incorporation of [^{3}H]leucine into acid-precipitable materials was determined. The data were normalized by dividing incorporated counts with cell number and showed as fold increases over control. The values expressed are the means ± S.D. of six independent experiments. *, $p < 0.01$.

DISCUSSION

In this study, we have shown a novel mechanism of mesangial hypertrophy in diabetic nephropathy mediated by Gas6. This is the first demonstration that Gas6 can induce mesangial cell hypertrophy characteristic of the early stage of diabetic nephropathy and that warfarin is effective to prevent the progression of diabetic nephropathy. Our study implies that Gas6 can be a novel growth factor that plays a crucial role in the development of the initial phase of diabetic nephropathy.

Here we have found a novel aspect of warfarin as an antihypertrophic agent. Our data also show that warfarin treatment ameliorated hyperfiltration and urinary albumin excretion in STZ rats. Thus hypertrophy and hyperfiltration might be an interactive mechanism and presumed to be causally linked (22). It is conceivable, therefore, that blocking the Gas6/Axl pathway can improve the vicious cycle in diabetic nephropathy. Therefore, treating diabetic patients with warfarin to prevent the nephropathy would be one of the options for treatment. However, the side effect of warfarin should be noted if we treat diabetic patients with warfarin. Warfarin has long been used as an anticoagulant to prevent thrombosis and embolism (23, 24), and patients prescribed with this agent are monitored by measuring prolongation of prothrombin times to achieve its anticoagulant effect. These patients have to be treated for the

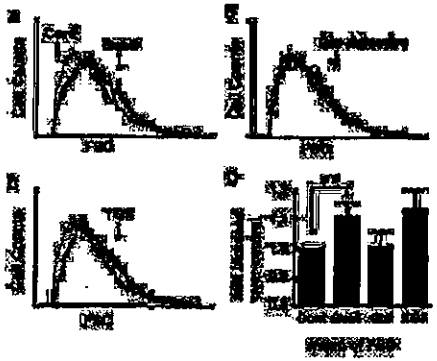

FIG. 8. **Flow cytometric analysis of mesangial cell size.** The cells were treated as described in Fig. 7. After treatment, the mesangial cells were harvested by tripsinization, washed with phosphate-buffered saline, centrifuged at 1,500 rpm for 10 min, and then resuspend in ice-cold 70% ethanol. Ethanol-fixed mesangial cells were then analyzed by forward light scattering on a Becton Dickinson flow cytometer. The data are representative of six independent experiments with qualitatively similar changes. *Thin line*, control (*Cont*); *bold line*, agonist. *A*, 100 ng/ml of Gas6; *B*, 100 ng/ml of Gla-defective Gas6; *C*, 1 ng/ml of TGF-β1. *D*, means of forward scatter of mesangial cells after treatment. The data are shown as fold increases over control. The values are the means ± S.D. of six independent experiments. **, $p < 0.05$. *FSC*, forward scatter.

risk of bleeding (25). However, the anti-hypertrophic effect of warfarin was achieved at serum concentrations of 0.7 μM, which is significantly lower than the ordinary therapeutic concentrations as an anticoagulant (4–5 μM) (26). The prothrombin times of rats treated with warfarin in our experiments were not significantly prolonged, and no bleeding tendency or anemia was observed (data not shown), whereas mesangial cell hypertrophy was significantly inhibited. Although we have shown the clear effect of warfarin on the development of diabetic nephropathy, the question remains about the specificity of the effect of warfarin. We have already shown that in mesangial cells warfarin specifically inhibits the Gas6/Axl pathway *in vitro* (16). To further confirm the specificity, we have treated Gas6-deficient mice (11) with STZ (15) and found that both mesangial and glomerular areas were significantly decreased in Gas6-deficient mice compared with wild type mice. Therefore, we can conclude that this effect of warfarin would be mediated specifically through the inhibition of Gas6.

Hypercoagulability in glomeruli has also been reported in diabetic nephropathy (27), which might worsen the renal function. Recently, Angelillo-Scherrer *et al.* (28) reported that a deficiency of Gas6 protects mice from thrombosis. In this study, we used a low dose of warfarin, and at these concentrations we found no prolongation of prothrombin time (data not shown). However, we already reported that even under these concentrations, warfarin can inhibit the activation of Gas6 *in vitro* and *in vivo* (10, 16, 29). It is still possible that warfarin could affect the coagulation cascades and prevent thrombotic events even at low concentrations. Therefore, Gas6 might affect the development of diabetic renal disease by improving the coagulation state.

The increase of extracellular matrix followed by mesangial cell hypertrophy is one of the major characteristics in diabetic nephropathy (30). Mauer *et al.* (31) investigated the structural-functional relationship in a cross-section of patients with type 1 diabetes. They found a close correlation between mesangial expansion and clinical manifestations of diabetic nephropathy. Ziyadeh (3) also showed that the development of irreversible renal changes in diabetes mellitus, such as glomerulosclerosis, is always preceded by the early hypertrophic processes in the glomerular compartment. In our experiment, however, we could not find an excessive accumulation of extracellular matrix in STZ rats at 12 weeks, although other investigators have reported increased deposition of extracellular matrix in a later phase of nephropathy in STZ rats (32). Because our purpose in this study is to determine the role of Gas6 in the initial phase of diabetic nephropathy, we analyzed up to 12 weeks after STZ injection. The correlation between Gas6 and diabetic glomerulosclerosis should be evaluated by treating the rats with warfarin for a longer time or using another animal model. Treating STZ rats with a high protein diet would be another way to accelerate the glomerulosclerosis (33) and should be tested in the future experiments.

We have already shown that Gas6 is a growth factor for mesangial cells *in vitro* and that Gas6 plays a key role in acute and chronic forms of glomerulonephritis *in vivo* (10, 16, 29). In those studies, we have shown that Gas6 can induce mesangial proliferation through a tyrosine kinase, Axl (11, 16) and a transcription factor signal transducer and activator of transcription 3 (29). However, in this study we have clearly shown that Gas6 can induce mesangial hypertrophy *in vivo* and *in vitro*. Therefore, the obvious question is why Gas6 only induces mesangial hypertrophy without affecting the mesangial proliferation in this diabetic rat model. Although we determined the mesangial cell area in the kidney of diabetic rats, we did not notice that the glomerular cell number was increased in diabetic rats (data not shown). Although Young *et al.* (34) reported that diabetic nephropathy may be associated with some glomerular cell proliferation, hypertrophy is the major finding of diabetic nephropathy. It remains uncertain why Gas6 can be induced in both glomerulonephritis and diabetic nephropathy and why Gas6 does not induce cell proliferation in diabetic nephropathy. It is conceivable that some other growth factor or cytokine is playing an additional role in determining the fate of mesangial cell in the disease process.

We have clearly shown that p42/44 MAP kinase was phosphorylated in the glomeruli after 12 weeks of STZ injection and that warfarin treatment abolished the phosphorylation. In the case of insulin-like growth factor 1, Akt seems to be responsible for its hypertrophic effect in skeletal myotube (35), and endothelin-induced hypertrophy requires activation of p42/44 MAP kinase, c-Jun N-terminal kinase/stress-activated protein kinase, and phosphatidylinositol 3-kinase pathways (36). Although we have no definite evidence to indicate the role of p42/44 MAP kinase in mesangial cell hypertrophy so far, phosphorylation of p42/44 MAP kinase might be used as a marker for the hypertrophy in diabetic nephropathy. The molecular mechanism of mesangial cell hypertrophy in diabetic nephropathy should be further clarified in future studies.

In summary, this is the first demonstration that Gas6 and Axl are involved in the development of the initial phase of diabetic nephropathy by inducing mesangial cell hypertrophy. This is a completely novel mechanism explaining the development of diabetic nephropathy. Blocking this pathway would be beneficial to prevent the progression of nephropathy in diabetic patients.

Acknowledgments—We thank Drs. Hideharu Abe (Tokushima University) and Daisuke Koya (Shiga University of Medical Science) for helpful comments. We also thank Toshiko Hori (Kyoto University) and Hideo Uchiyama (Taigenkai Hospital) for excellent technical assistance.

REFERENCES

1. Bojestig, M., Arnqvist, H. J., Hermansson, G., Karlberg, B. E., and Ludvigsson, J. (1994) *N. Engl. J. Med.* **330**, 15–18
2. Krolewski, M., Eggers, P. W., and Warram, J. H. (1996) *Kidney Int.* **50**, 2041–2046
3. Ziyadeh, F. N. (1993) *Am. J. Kidney Dis.* **22**, 736–744
4. Wolf, G. (2000) *Kidney Int. Suppl.* **77**, S59–S66
5. Lehmann, R., and Schleicher, E. D. (2000) *Clin. Chim. Acta* **297**, 135–144
6. Ravid, M., Brosh, D., Levi, Z., Bar-Dayan, Y., Ravid, D., and Rachmani, R. (1998) *Ann. Intern. Med.* **128**, 982–988
7. Manfioletti, G., Brancolini, C., Avanzi, G., and Schneider, C. (1993) *Mol. Cell. Biol.* **13**, 4976–4985
8. Nakano, T., Higashino, K., Kikuchi, N., Kishino, J., Nomura, K., Fujita, H., Ohara, O., and Arita, H. (1995) *J. Biol. Chem.* **270**, 5702–5705
9. Nakano, T., Kawamoto, K., Kishino, J., Nomura, K., Higashino, K., and Arita, H. (1997) *Biochem. J.* **323**, 387–392
10. Yanagita, M., Arai, H., Ishii, K., Nakano, T., Ohashi, K., Mizuno, K., Varnum, B., Fukatsu, A., Doi, T., and Kita, T. (2001) *Am. J. Pathol.* **158**, 1423–1432
11. Yanagita, M., Ishimoto, Y., Arai, H., Nagai, K., Ito, T., Nakano, T., Salant, D. J., Fukatsu, A., Doi, T., and Kita, T. (2002) *J. Clin. Invest.* **110**, 239–246
12. Doi, T., Vlassara, H., Kirstein, M., Yamada, Y., Striker, G. E., and Striker, L. J. (1992) *Proc. Natl. Acad. Sci. U. S. A.* **89**, 2873–2877
13. MacKay, K., Striker, L. J., Elliot, S., Pinkert, C. A., Brinster, R. L., and Striker, G. E. (1988) *Kidney Int.* **33**, 677–684
14. Koya, D., Jirousek, M. R., Lin, Y. W., Ishii, H., Kuboki, K., and King, G. L. (1997) *J. Clin. Invest.* **100**, 115–126
15. Flyvbjerg, A., Bennett, W. F., Rasch, R., Kopchick, J. J., and Scarlett, J. A. (1999) *Diabetes* **48**, 377–382
16. Yanagita, M., Ishii, K., Ozaki, H., Arai, H., Nakano, T., Ohashi, K., Mizuno, K., Kita, T., and Doi, T. (1999) *J. Am. Soc. Nephrol.* **10**, 2503–2509
17. Ziswiler, R., Steinmann-Niggli, K., Kappeler, A., Daniel, C., and Marti, H. P. (1998) *J. Am. Soc. Nephrol.* **9**, 2056–2066
18. Pippin, J. W., Qu, Q., Meijer, L., and Shankland, S. J. (1997) *J. Clin. Invest.* **100**, 2512–2520
19. Yamamoto, Y., Kato, I., Doi, T., Yonekura, H., Ohashi, S., Takeuchi, M., Watanabe, T., Yamagishi, S., Sakurai, S., Takasawa, S., Okamoto, H., and Yamamoto, H. (2001) *J. Clin. Invest.* **108**, 261–268
20. Hirata, M., Makibayashi, K., Katsumata, K., Kusano, K., Watanabe, T., Fukushima, N., and Doi, T. (2002) *Nephrol. Dial. Transplant* **17**, 2132–2137
21. Stockelman, M. G., Lorens, J. N., Smith, F. N., Boivin, G. P., Sahota, A., Tischfield, J. A., and Stambrook, P. J. (1996) *Am. J. Physiol.* **275**, F154–F163
22. Hostetter, T. H. (2001) *J. Clin. Invest.* **107**, 161–162
23. Gallus, A. S., Baker, R. I., Chong, B. H., Ockelford, P. A., and Street, A. M. (2000) *Med. J. Aust.* **172**, 600–605
24. Booth, S. L., and Mayer, J. (2000) *Nutr. Rev.* **58**, 20–22
25. Schulman, S., and Lindmarker, P. (2000) *N. Engl. J. Med.* **342**, 1953–1958
26. Holford, N. H. (1986) *Clin. Pharmacokinet.* **11**, 483–504
27. Kanzu, K., Uriu, K., Hashimoto, O., and Eto, S. (1991) *J. Diabet. Complications* **5**, 92–94
28. Angelillo-Scherrer, A., de Frutos, P., Aparicio, C., Melis, E., Savi, P., Lupu, F., Arnout, J., Dewerchin, M., Hoylaerts, M., Herbert, J., Collen, D., Dahlback, B., and Carmeliet, P. (2001) *Nat. Med.* **7**, 215–221
29. Yanagita, M., Arai, H., Nakano, T., Ohashi, K., Mizuno, K., Fukatsu, A., Doi, T., and Kita, T. (2001) *J. Biol. Chem.* **276**, 42364–42369
30. Wolf, G., and Ziyadeh, F. N. (1999) *Kidney Int.* **56**, 393–405
31. Mauer, S. M., Steffes, M. W., Ellis, E. N., Sutherland, D. E., Brown, D. M., and Goetz, F. C. (1984) *J. Clin. Invest.* **74**, 1143–1155
32. Makino, H., Yamasaki, Y., Hiramata, K., and Ota, Z. (1992) *Virchows Arch. B Cell Pathol. Incl. Mol. Pathol.* **62**, 19–24
33. Zatz, R., Meyer, T. W., Rennke, H. G., and Brenner, B. M. (1985) *Proc. Natl. Acad. Sci. U. S. A.* **82**, 5963–5967
34. Young, B. A., Johnson, R. J., Alpers, C. E., Eng, E., Gordon, K., Floege, J., Couser, W. G., and Seidel, K. (1995) *Kidney Int.* **47**, 935–944
35. Rommel, C., Bodine, S. C., Clarke, B. A., Rossman, R., Nunez, L., Stitt, T. N., Yancopoulos, G. D., and Glass, D. J. (2001) *Nat. Cell Biol.* **3**, 1009–1013
36. Goruppi, S., Bonvecchio, J. V., and Kyriakis, J. M. (2002) *EMBO J.* **21**, 5427–5436

THE JOURNAL OF BIOLOGICAL CHEMISTRY
© 2003 by The American Society for Biochemistry and Molecular Biology, Inc.

Vol. 278, No. 29, Issue of July 18, pp. 26374–26379, 2003
Printed in U.S.A.

Direct Demonstration of Involvement of Protein Kinase Cα in the Ca^{2+}-induced Platelet Aggregation*

Received for publication, December 5, 2002, and in revised form, March 31, 2003
Published, JBC Papers in Press, April 30, 2003, DOI 10.1074/jbc.M212407200

Arata Tabuchi, Akira Yoshioka‡, Tomohito Higashi, Ryutaro Shirakawa, Hiroaki Nishioka§, Toru Kita¶, and Hisanori Horiuchi‖

From the Department of Geriatric Medicine and ¶Cardiovascular Medicine, Graduate School of Medicine, Kyoto University, 606-8507 Kyoto, Japan

Platelets play critical roles in hemostasis and thrombosis through their aggregation following activation of integrin $\alpha_{IIb}\beta_3$. However, the molecular mechanism of the integrin activation inside platelets remains largely unknown. Pharmacological experiments have demonstrated that protein kinase C (PKC) plays an important role in platelet aggregation. Because PKC inhibitors can have multiple substrates and given that non-PKC-phorbol ester-binding signaling molecules have been demonstrated to play important roles, the precise involvement of PKC in cellular functions requires re-evaluation. Here, we have established an assay for analyzing the Ca^{2+}-induced aggregation of permeabilized platelets. The aggregation of platelets was inhibited by the addition of the arginine-glycine-aspartate-serine peptide, an integrin-binding peptide inhibitor of $\alpha_{IIb}\beta_3$, suggesting that the aggregation was mediated by the integrin. The aggregation was also dependent on exogenous ATP and platelet cytosol, indicating the existence of essential cytosolic factors required for the aggregation. To examine the role of PKC in the aggregation assay, we immunodepleted PKCα and β from the cytosol. The PKC-depleted cytosol lost the aggregation-supporting activity, which was recovered by the addition of purified PKCα. Furthermore, the addition of purified PKCα in the absence of cytosol did not support the aggregation, whereas the cytosol containing less PKC supported it efficiently, suggesting that additional factors besides PKC would also be required. Thus, we directly demonstrated that PKCα is involved in the regulation of Ca^{2+}-induced platelet aggregation.

Platelets play critical roles in hemostasis and thrombosis through aggregation following activation of integrin $\alpha_{IIb}\beta_3$ (1–3). Although $\alpha_{IIb}\beta_3$ of platelets in the resting stage does not bind fibrinogen or von Willebrand factors (vWF),[1] the activation of platelets results in conformation changes, which allow $\alpha_{IIb}\beta_3$ to bind these ligands (1–3). When fibrinogen or vWF binds to $\alpha_{IIb}\beta_3$, the ligand-occupied integrin signals downstream to stabilize platelet aggregation through reorganization of the actin cytoskeletal network and the release of bioactive substances stored in the granules (1–3). Thus, the process of platelet activation and aggregation consists of a series of orchestrated responses (1–3). However, the molecular mechanisms that underlie this process remain unclear because it is difficult to use molecular biology and biochemistry in platelets that do not synthesize new proteins. To overcome this difficulty, semi-intact assays using permeabilized platelets have been established for the study of granule secretion (4–8). Although some semi-intact aggregation assays have now been developed, it has been difficult to demonstrate a cytosol dependence in these experiments (8).

Protein kinase C (PKC) family members are important signaling molecules regulating many cellular functions (9, 10). Among the family members, conventional PKCs (cPKC), which include PKCα, βI, βII, and γ, have regulatory Ca^{2+}- and phorbol ester-binding domains (9, 10). The involvement of cPKCs in the cellular functions has been analyzed mainly pharmacologically using cell-permeable small compounds of inhibitors and stimulators such as phorbol esters. However, these experiments are somewhat indirect because 1) no inhibitors have absolute specificity and 2) important signaling molecules other than PKCs have also been demonstrated to contain phorbol ester-binding C1-domains, which were first identified in cPKC (9, 10). For example, Ras-guanyl nucleotide-releasing protein (11, 12) contains the C1 domain at its C terminus and acts as a stimulator for small GTPase Ras involved in the regulation of cell growth. Chimerin (13, 14) also contains a C1 domain and acts as a GTPase-activating protein of small GTPase Rac involved in the regulation of cytoskeletal reorganization. Thus, the effects of phorbol esters could be through multiple pathways. Therefore, it is important to re-evaluate and demonstrate the involvement of PKCs in certain cellular functions in a direct fashion (15).

In platelets, PKC has been considered to play important roles in aggregation (16, 17) and granule secretion (18). For the granule secretion, we have recently demonstrated the direct involvement of PKC (19). We have established a semi-intact secretion assay (19, 20) where the secretion does not occur upon stimulation without adding exogenous cytosol, indicating the existence of cytosolic essential factors. We purified an essential factor for the secretion and identified it to be PKCα (19). On the other hand, it has been so far difficult to demonstrate the involvement of PKC in platelet aggregation without using small compounds of PKC inhibitors or phorbol esters. Here, we directly demonstrate the involvement of PKCα in the regulation of platelet aggregation by using a stable semi-intact aggregation assay with cytosol dependence.

* This work was supported by Research Grants from Ministry of Education, Science, Sports, and Culture of Japan (Grants 15590740 (to H. H.) and 12CE2006 and 13307034 (to T. K.)), Research Grants from Ministry of Health, Labor, and Welfare of Japan (Comprehensive Research on Aging and Health Grant H14-choju-012 (to T. K. and H. H.)), and partially by grants from Takeda Science Foundation, Suzuken Memorial Foundation, Study Group of Molecular Cardiology and Novartis Foundation for Gerontrogical Research (to H. H.). The costs of publication of this article were defrayed in part by the payment of page charges. This article must therefore be hereby marked "*advertisement*" in accordance with 18 U.S.C. Section 1734 solely to indicate this fact.

‡ Present address: Dept. of Internal Medicine, Mitsubishi Kyoto Hospital, 615-8087 Kyoto, Japan.

§ Present address: Sir William Dunn School of Pathology, University of Oxford, South Parks Rd., Oxford OX1 3RE, United Kingdom.

‖ To whom correspondence should be addressed. E-mail: horiuchi@kuhp.kyoto-u.ac.jp.

[1] The abbreviations used are: vWF, von Willebrand factors; PKC, protein kinase C; cPKC, conventional protein kinase C; SLO, streptolysin-O; RGDS, arginine-glycine-aspartate-serine; RGES, arginine-glycineglutamate-serine.

EXPERIMENTAL PROCEDURES

Materials—Anti-PKCα and anti-*pan*-PKCβ mouse monoclonal antibodies were purchased from Transduction Laboratories. This anti-PKCα antibody, which was described in the manufacturer's instruction to interact with PKCβ but not with other PKCs, was used for immunodepletion experiments. Another anti-PKCα mouse monoclonal antibody purchased from Santa Cruz Biotechnology had no cross-reactivity with PKCβ and was used for the immunoblotting. Anti-PKCγ, anti-PKCδ, and anti-PKCθ mouse monoclonal antibodies were from Transduction Laboratories, and anti-PKCβI and anti-PKCβII rabbit polyclonal antibodies were from Santa Cruz Biotechnology. A control mouse IgG used for the immunodepletion experiment was from Zymed Laboratories Inc. Horseradish peroxidase-labeled anti-mouse and anti-rabbit IgG polyclonal antibodies were from Amersham Biosciences, which were used as secondary antibodies for immunoblotting visualized by enhanced chemiluminescence method (Amersham Biosciences). Unless otherwise specified, all of the chemicals including peptides of arginine-glycine-aspartate-serine (RGDS) and arginine-glycine-glutamate-serine (RGES) were purchased from Sigma with the exception of SLO, which was from Dr. Bhakdi (Mainz University, Mainz, Germany). Protein concentrations were determined by the Bradford method (Bio Rad) (21) or densitometric scanning of the Coomassie Blue-stained band in sodium dodecyl sulfate-polyacrylamide gel electrophoresis (22) using bovine serum albumin as a standard.

The Aggregation Assay with Permeabilized Platelets—The aggregation assay was established by modification of our previous assay (23). Unless otherwise specified, the standard assay method was used as follows. Washed human platelets from healthy donors were prepared (24), resuspended in ice-cold Buffer A (50 mM Hepes/KOH, pH 7.2, 78 mM KCl, 4 mM $MgCl_2$, 0.2 mM $CaCl_2$, 2 mM EGTA, 1 mM dithiothreitol, and the calculated free $[Ca^{2+}]$ was ~20 nM (25)) containing 4 mg/ml bovine serum albumin and 20 ng/ml prostaglandin E_1 and kept at 4 °C. The platelets were incubated with 0.6 μg/ml SLO at 4 °C for 10 min and washed once to remove unbound SLO (19, 20, 26, 27). The treated platelets were resuspended in ice-cold Buffer A containing 4 mg/ml bovine serum albumin at a density of 5×10^9/ml, quantified with a Coulter Counter, and incubated at 30 °C for 5 min to make holes in their plasma membrane (19, 20, 26, 27). The permeabilized platelets were kept on ice for 15–30 min with 2 mg of proteins/ml human platelet cytosol (or rat brain cytosol), an ATP-regenerating system (19, 20, 26, 27), and tested substances. Because fibrinogen has been added in previously established aggregation assays using washed platelets at 0.4 mg/ml by Kinlough-Rathbone *et al.* (28) and 0.38 mg/ml by Santos *et al.* (29), we also added fibrinogen (Sigma) in our assay at the concentration of 0.4 mg/ml. The platelets then were incubated at 37 °C for 3 min and stimulated by the addition of calcium chloride to make final $[Ca^{2+}]$ at 200 μM (25). The aggregation was measured by a light transmission aggregometer, MCM HEMA TRACER 212 (MC Medical). For the morphological analysis, permeabilized platelets were incubated with 200 μM or 20 nM Ca^{2+} for 20 min in the standard assay condition. The samples then were immediately examined with a phase-contrast microscopy.

Cytosol Preparation—For generation of platelet cytosol, platelets from healthy donors were washed and resuspended in ice-cold Buffer A containing a protease inhibitor mixture (Sigma). The platelets then were sonicated, and the supernatant after the low speed centrifugation at 1000 × *g* for 10 min was further centrifuged at 100,000 × *g* for 30 min. The final supernatant was dialyzed extensively with Buffer A and kept as platelet cytosol at −80 °C until use. The cytosol of rat brain was prepared in a similar way except using a Potter-type blender instead of sonication. For generating the PKC-depleted cytosol, the human platelet cytosol (0.4 mg of proteins) was incubated with protein A-agarose beads (Roche Diagnostics) coated with 25 μg of the anti-PKCα antibody (Transduction Laboratories) or the control mouse IgG for 6 h at 4 °C. After the beads were removed by centrifugation, the supernatants were used as the PKC-depleted cytosol and the control cytosol, respectively. PKCα was purified from rat brain cytosol as described previously (19).

RESULTS

Establishment of an Assay Analyzing the Ca^{2+}-induced Aggregation of Permeabilized Platelets—We have established an aggregation assay with platelets permeabilized by SLO, which has been shown to form pores of ~30 nm in diameter in the membrane (27). In this method, we permeabilized only the plasma membrane judging from observations that the intracellular membrane structures of the platelets appeared to be intact morphologically (30) and that vWF stored in α-granules did not leak out (19, 20). Because the condition used here with 0.6 μg/ml SLO induced leakage of 80% cytosolic lactate dehydrogenase from platelets (19, 20), it was presumed that most of ATP and cytosol were also lost by diffusion through the pores in the plasma membrane. Therefore, we exogenously added ATP and cytosol in the assay to reconstitute the aggregation. We also added 0.4 mg/ml fibrinogen in our assay, which would bridge the activated integrin $\alpha_{IIb}\beta_3$ on both sides of platelets to be aggregated (2, 3). Because calcium ionophore has been demonstrated to induce platelet aggregation (31, 32), we used calcium ions at a calculated concentration at 200 μM (25) as a stimulus.

We first examined morphologically whether aggregates of permeabilized platelets were indeed generated in the assay. After confirming the Ca^{2+}-induced aggregation by the light-transmission aggregometer (data not shown), the samples were subjected to observation with a phase-contrast microscopy. A typical set of photographs showed that many platelet aggregates were formed upon stimulation with 200 μM Ca^{2+}, whereas the permeabilized platelets incubated with 20 nM Ca^{2+} remained unaggregated (Fig. 1*A*). The quantification of the platelets in the images revealed that unaggregated platelets were reduced upon Ca^{2+} stimulation (Fig. 1*B*) and that the aggregates consisting of >10 platelets were drastically increased (Fig. 1*C*). Thus, the formation of the aggregates in the assay was confirmed morphologically.

We next examined the effects of Ca^{2+} concentrations on the platelet aggregation. Although Ca^{2+} at 20 and 200 nM did not induce the platelet aggregation, Ca^{2+} at 2–200 μM efficiently induced the aggregation (Fig. 2). Because it has been shown that $[Ca^{2+}]$ in resting platelet cytosol is around 10 nM and that it increases to 1–10 μM upon platelet activation (33), the Ca^{2+} sensitivity of the aggregation in the assay using permeabilized platelets was similar to physiological conditions.

Aggregation of Permeabilized Platelets Was Mediated by the Integrin—It has been well known that platelet aggregation is mediated by activated integrin $\alpha_{IIb}\beta_3$ (2, 3). We examined whether it was the case for the aggregation of permeabilized platelets. RGD is the integrin-binding sequence (34), which is present in both fibrinogen and vWF, and the aggregation of intact platelets has been shown to be inhibited by the addition of the RGD-containing peptide (35, 36). As shown in Fig. 3, the RGDS peptide inhibited the Ca^{2+}-induced aggregation of permeabilized platelets, whereas the control RGES peptide did not. Furthermore, when fibrinogen was omitted from the assay, the aggregation was also inhibited (data not shown). Taken together, the aggregation in the assay was mediated by the integrin.

Platelet Aggregation Was Cytosol-dependent—ATP and cytosol in the permeabilized platelets would be lost by diffusion through the pores. Without the addition of ATP, the permeabilized platelets did not aggregate upon the Ca^{2+} stimulation (data not shown), indicating that ATP is essential for the aggregation. When the cytosol was not added exogenously into the assay, the permeabilized platelets did not aggregate upon the Ca^{2+} stimulation in the condition where ATP and fibrino-

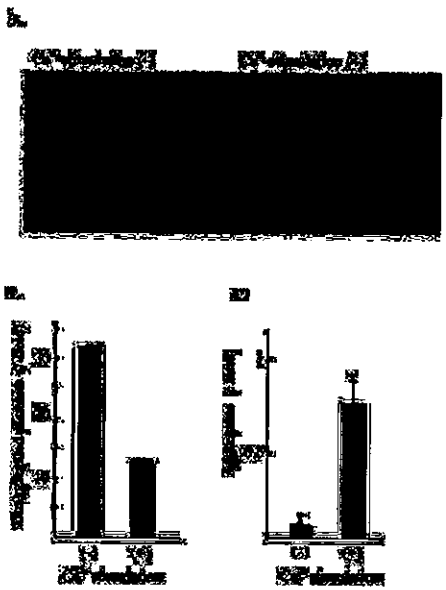

FIG. 1. **Morphological examination of the Ca^{2+}-induced aggregation of permeabilized platelets.** *A*, the permeabilized platelets were incubated with 20 nM Ca^{2+} (Ca^{2+} stimulation (−)) or 200 μM Ca^{2+} (Ca^{2+} stimulation (+)) at 37 °C for 20 min and examined by phase-contrast microscopy (×1000) as described under "Experimental Procedures." An *arrowhead* and an *arrow* indicate an unaggregated platelet and an aggregate consisting of >10 platelets, respectively. *B* and *C*, 20 individual fields of the sample after the incubation were randomly selected, and numbers of unaggregated platelets (*B*) and aggregates consisting of >10 platelets (*C*) were counted. The data shown are expressed as means + S.E. of four independent experiments.

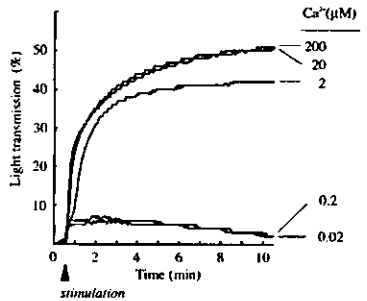

FIG. 2. **The Ca^{2+} concentration-dependent aggregation of the permeabilized platelets.** Permeabilized platelets were first incubated for 30 min at 4 °C with 2 mg of proteins/ml rat brain cytosol followed by stimulation with indicated concentrations of Ca^{2+} (25) as described under "Experimental Procedures." The data shown are the representative of four independent experiments with similar results.

gen were sufficiently supplemented (Fig. 4*A*). On the other hand, the aggregation was reconstituted by the addition of platelet cytosol in a concentration-dependent manner (Fig. 4*A*).

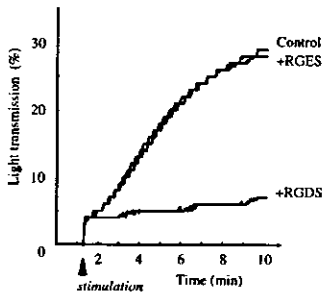

FIG. 3. **The Ca^{2+}-induced aggregation was inhibited by the RGDS peptide, an integrin $\alpha_{IIb}\beta_{III}$ inhibitor.** Permeabilized platelets were first incubated for 30 min at 4 °C with 2 mg of proteins/ml rat brain cytosol in the absence or presence of 1 μM RGDS-peptide or RGES-peptide, and the Ca^{2+}-induced aggregation was analyzed as described under "Experimental Procedures." The data shown are the representative of four independent experiments with similar results.

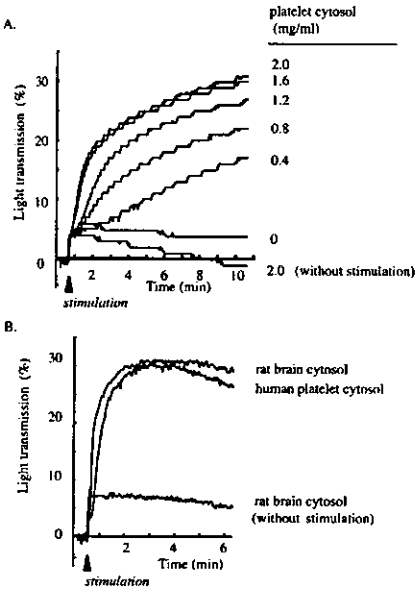

FIG. 4. **The Ca^{2+}-induced aggregation was cytosol-dependent.** *A*, the permeabilized platelets were first incubated for 15 min at 4 °C with indicated concentrations of platelet cytosol, and the Ca^{2+}-induced aggregation was analyzed as described under "Experimental Procedures." *B*, the permeabilized platelets were first incubated for 15 min at 4 °C with rat brain cytosol or human platelet cytosol at 1.5 mg of proteins/ml, and the Ca^{2+}-induced aggregation was analyzed as described under "Experimental Procedures." The data shown are the representative of four independent experiments with similar results.

These results indicated the existence of cytosolic essential factor(s). We next tested rat brain cytosol for the reconstitution of the aggregation. The rat brain cytosol also supported the aggregation as efficiently as the human platelet cytosol (Fig. 4*B*).

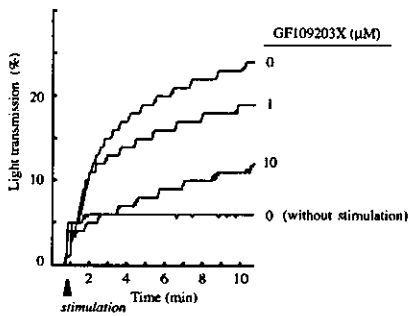

FIG. 5. **The Ca^{2+}-induced aggregation was inhibited by GF109203X, a cPKC inhibitor.** The permeabilized platelets were first incubated for 30 min at 4 °C with indicated concentration of GF109203X, and the Ca^{2+}-induced aggregation was then analyzed as described under "Experimental Procedures." The data shown are the representative of four independent experiments with similar results.

These results indicated that cytosolic essential factor(s) were expressed ubiquitously.

Involvement of PKC in the Regulation of Platelet Aggregation—The cytosol dependence of the aggregation indicates that some cytosolic factors are required for the platelet aggregation. Although the identity of these factors is unknown, one important factor could be cPKC. As shown previously with intact platelets (37), GF109203X, an inhibitor of cPKCs, also affected the Ca^{2+}-induced aggregation in our semi-intact assay in a concentration-dependent manner (Fig. 5).

To examine the involvement of PKC directly, we first prepared PKC-depleted platelet cytosol. As shown in Fig. 6*A*, PKCα was completely depleted from the platelet cytosol with the anti-PKCα antibody-coated beads while PKCα stayed in the cytosol after the same procedure with control IgG-coated beads. Among other cPKCs, PKCβI and PKCβII were detected in platelets, whereas PKCγ, a neuronal specific cPKC, was not (data not shown). By the immunodepletion, PKCβ was also completely depleted because of the cross-reactivity of the antibody (Fig. 6*A*). When we used lower amounts of the anti-PKCα antibody for the immunodepletion, PKCβ was completely depleted while PKCα still remained in the cytosol (data not shown), suggesting that platelet cytosol contained more PKCα than PKCβ. As expected, although PKCδ and PKCθ, both of which are classified as novel PKCs, were detected in platelets, they were not affected by the immunodepletion procedure either with anti-PKCα antibody or control IgG (Fig. 6*A*).

The PKC-depleted cytosol lost the aggregation activity, whereas the Ca^{2+}-induced platelet aggregation was efficiently reconstituted with the cytosol treated with the control IgG (Fig. 6*C*). When PKCα purified from rat brain (Fig. 6*B*) (19) was supplemented to the PKC-depleted cytosol, the aggregation activity was recovered (Fig. 6*C*), indicating that cPKC, possibly PKCα, is an essential cytosolic factor for the platelet aggregation. We next examined whether PKCα is a sufficient cytosolic factor for the aggregation. As shown in Fig. 7, purified PKCα (50 nM) alone was not sufficient to support the Ca^{2+}-induced platelet aggregation. On the other hand, platelet cytosol at 0.6 mg of proteins/ml, which contained 16 nM PKCα determined by Western blot with the anti-PKCα antibody using purified PKCα as a control (data not shown), efficiently induced platelet aggregation (Fig. 7). Thus, PKCα is not a sufficient cytosolic factor for platelet aggregation. Furthermore, the addition of purified PKCα to the low concentration of cytosol (0.6 mg of

FIG. 6. **The PKC-depleted cytosol lost the aggregation-supporting activity, which was recovered by the addition of purified PKCα.** *A*, platelet cytosol (*lane 1*) was incubated with the anti-PKCα antibody-coated beads (Transduction Laboratories) (*lane 3*) or the control mouse IgG (*lane 2*) at 4 °C for 6 h, and the supernatant after removing the beads was examined by immunoblotting using another PKCα-specific antibody (Sigma) and anti *pan* PKCβ, anti PKCδ, and anti-PKCθ antibodies as described under "Experimental Procedures." *B*, PKCα was purified from rat brain cytosol and analyzed by sodium dodecyl sulfate-polyacrylamide gel electrophoresis stained by Coomassie Blue as described under "Experimental Procedures." *C*, the permeabilized platelets were first incubated for 30 min at 4 °C with 2 mg of proteins/ml of the treated platelet cytosol and/or purified PKCα at 50 nM as indicated in the figure, and the Ca^{2+}-induced aggregation was then analyzed as described under "Experimental Procedures." The data shown are the representative of four independent experiments with similar results.

proteins/ml) strongly enhanced the platelet aggregation, suggesting that PKCα is a limiting factor for the Ca^{2+}-induced platelet aggregation. Thus, PKCα is an essential but not sufficient cytosolic factor for the Ca^{2+}-induced platelet aggregation.

DISCUSSION

Here we established an aggregation assay system using permeabilized platelets, and using this assay, we first directly demonstrated that PKC is an essential but not sufficient factor in the cytosol for platelet aggregation.

Because platelets lack the protein-producing activity, it is difficult to apply molecular biology for investigating the molecular mechanism of aggregation and granule secretion inside activated platelets. Therefore, the research in these fields has been performed mainly pharmacologically. To overcome this difficulty, much effort has been made to establish semi-intact assay systems using permeabilized platelets. In the research of platelet granule secretion, several semi-intact assays have been established (4–8, 19, 20). However, for platelet aggregation, only a few semi-intact aggregation assays have been established (8), and as far as we know, no stable assays with cytosol dependence have been established.

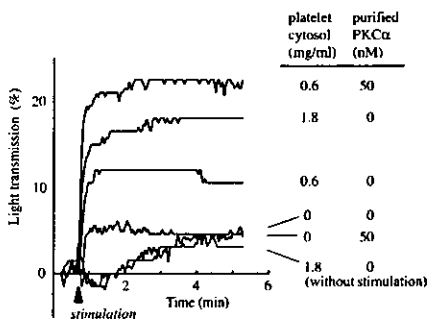

FIG. 7. **Purified PKCα alone without addition of cytosol did not support the Ca^{2+}-induced aggregation.** Permeabilized platelets were first incubated for 15 min at 4 °C with indicated concentrations of platelet cytosol and/or purified PKCα, and the Ca^{2+}-induced aggregation was analyzed as described under "Experimental Procedures." It is noted that 1 mg of proteins/ml platelet cytosol contains 25 nM PKC. The data shown are the representative of four independent experiments with similar results.

We have previously established an aggregation assay system with SLO-permeabilized platelets and demonstrated that small GTPase Rho plays an important role in thrombin-induced aggregation (23). However, the assay did not demonstrate cytosol dependence since a low concentration of SLO (0.1 μg/ml) was used for the permeabilization and the aggregation was induced without adding exogenous cytosol (23). Here, we have established another semi-intact aggregation assay by modifying the previous one (23). The aggregation of the permeabilized platelets in our *in vitro* assay appears physiological since the time course, the Ca^{2+} sensitivity and the involvement of the integrin are similar to those of intact platelets. Since the cytosol was extensively depleted from the permeabilized platelets in our semi-intact aggregation assay using a higher concentration of SLO than that used previously (23), permeabilized platelets did not aggregate in response to calcium stimulation without adding exogenous cytosol. This cytosol dependence would widen the application of the assay to investigate the molecular mechanism of platelet aggregation.

The cytosol dependence also indicated the existence of essential cytosolic factor(s) for aggregation. A cytosolic protein PKC has been shown to play an important role in platelet aggregation by pharmacological experiments using cell-permeable small compounds of inhibitors and stimulators such as phorbol esters (16, 17). However, the results obtained from such experiments appear somewhat indirect because the specificity of inhibitors is not absolutely strict and important signaling molecules containing the phorbol ester-binding C1 domain other than PKC have been recently identified such as Ras-guanyl nucleotide-releasing protein (11, 12) and chimerin (13, 14). Munc13-1 present in the presynapse also contains the C1 domain (38), and it has very recently been demonstrated that the effect of phorbol ester in the neurotransmitter release is through Munc13-1 (39). Thus, at the moment, it is ambiguous whether phorbol esters exert their functions through PKC or other non-PKC-signaling molecules. Therefore, re-evaluation and direct demonstration are required in various cell functions where PKCs have been suggested to be involved (15, 43).

Using the semi-intact aggregation assay, we have directly demonstrated the involvement of PKCα in the Ca^{2+}-induced platelet aggregation. First, an inhibitor of conventional PKC affected the aggregation. Second, immunodepletion of PKCα and PKCβ from the cytosol abolished the Ca^{2+}-induced aggregation. Third, the aggregation-supporting activity of PKCα/β-depleted cytosol was rescued by supplementation of purified PKCα. Supplementation of PKCα alone to the PKCα/β-depleted cytosol was enough to reconstitute the aggregation, suggesting that PKCα but not PKCβ is the essential factor or otherwise that the activity of cPKC, namely PKCα or PKCβ, is essential. Because PKCα and PKCβ show similar substrate specificity *in vitro* (40), we cannot exclude a possibility that added PKCα covered the lack of PKCβ activity in the assay. Although cPKC is an essential factor for the aggregation, it is not a sufficient cytosolic factor since the addition of purified PKCα alone without exogenous cytosol did not support the aggregation. Furthermore, platelet cytosol containing less PKC supported the aggregation efficiently, and purified PKCα strongly enhanced the aggregation in the presence of low concentration of cytosol, suggesting that PKCα is a limiting factor in the cytosol for the aggregation and that additional factors besides PKC would also be required for the aggregation.

PKCα and PKCβ are known to be activated by Ca^{2+}, diacylglycerol, and phosphatidylserine (9, 10). Although we did not add these stimulators besides Ca^{2+}, the purified PKCα added to the assay was indeed active since the purified PKCα phosphorylated a PKC substrate efficiently in the similar assay condition used here (19). We speculate that the components inside the platelets, possibly including phosphatidylserine, help support the activity of PKCα (19). Furthermore, because PKC increases the intracellular Ca^{2+} concentration by modulating Ca^{2+} channels in the plasma membrane in neurons (41, 42), it remains unclear whether PKC acts upstream and/or downstream of increased Ca^{2+}. Because we used Ca^{2+} as a stimulus, we could safely say that PKCα plays an important role at least at the downstream of increased Ca^{2+}. Further investigation is required for elucidation of how PKCα activates the integrin $\alpha_{IIb}\beta_3$ and induces platelet aggregation. The assay established here will be a powerful tool for future experiments aimed at elucidating these mechanisms.

Acknowledgments—We are grateful to Dr. H. McBride and Dr. H. Arai for the critical reading of the paper and to T. Matsubara for excellent technical assistance.

REFERENCES

1. Shattil, S. J., Kashiwagi, H., and Pampori, N. (1998) *Blood* **91**, 2645–2657
2. Plow, E. F., and Ginsberg, M. H. (2000) in *Hematology: Basic Principles and Practice* (Hoffman, R., Benz, E. J., Jr., Shattil, S. J., Furie, B., Cohen, H. J., Silberstein, L. E., and McGlave, P., eds) 3rd Ed., pp. 1741–1752, Churchill Livingston, New York
3. Brass, L. F. (2000) in *Hematology: Basic Principles and Practice* (Hoffman, R., Benz, E. J., Jr., Shattil, S. J., Furie, B., Cohen, H. J., Silberstein, L. E., and McGlave, P., eds) 3rd Ed., pp. 1763–1770, Churchill Livingston, New York
4. Authi, K. S., Rao, G. H., Evenden, B. J., and Crawford, N. (1988) *Biochem. J.* **255**, 885–893
5. Flaumenhaft, R., Furie, B., and Furie, B. C. (1999) *J. Cell. Physiol.* **179**, 1–10
6. Sloan, D. C., and Haslam, R. J. (1997) *Biochem. J.* **328**, 13–21
7. Lemons, P. P., Chen, D., Bernstein, A. M., Bennett, M. K., and Whiteheart, S. W. (1997) *Blood* **90**, 1490–1500
8. Hers, I., Donath, J., Litjens, P. E., van Willigen, G., and Akkerman, J. W. (2000) *Arterioscler. Thromb. Vasc. Biol.* **20**, 1651–1660
9. Nishizuka, Y. (1992) *Science* **258**, 607–614
10. Newton, A. C., and Johnson, J. E. (1998) *Biochim. Biophys. Acta* **1376**, 155–172
11. Ebinu, J. O., Bottorff, D. A., Chan, E. Y., Stang, S. L., Dunn, R. J., and Stone, J. C. (1998) *Science* **280**, 1082–1086
12. Tognon, C. E., Kirk, H. E., Passmore, L. A., Whitehead, I. P., Der, C. J., and Kay, R. J. (1998) *Mol. Cell. Biol.* **18**, 6995–7008
13. Ball, C., Monfries, C., Smith, P., Lim, H. H., Kozma, R., Ahmed, S., Vasudevaraghavan, V., Leung, T., and Lim, L. (1990) *J. Mol. Biol.* **211**, 11–16
14. Wang, H., and Kazanietz, M. G. (2002) *J. Biol. Chem.* **277**, 4541–4550
15. Kazanietz, M. G., Caloca, M. J., Eroles, P., Fujii, T., Garcia-Bermejo, M. L., Reilly, M., and Wang, H. (2000) *Biochem. Pharmacol.* **60**, 1417–1424
16. Kaibuchi, K., Takai, Y., Sawamura, M., Hoshijima, M., Fujikura, T., and Nishizuka, Y. (1983) *J. Biol. Chem.* **258**, 6701–6704
17. Siess, W., and Lapetina, E. G. (1988) *Biochem. J.* **255**, 309–318

18. Gerrard, J. M., Beattie, L. L., Park, J., Israels, S. J., McNicol, A., Lint, D., and Cragoe, E. J., Jr. (1989) *Blood* **74**, 2405–2413
19. Yoshioka, A., Shirakawa, R., Nishioka, H., Tabuchi, A., Higashi, T., Ozaki, H., Yamamoto, A., Kita, T., and Horiuchi, H. (2001) *J. Biol. Chem.* **276**, 39379–39385
20. Shirakawa, R., Yoshioka, A., Horiuchi, H., Nishioka, H., Tabuchi, A., and Kita, T. (2000) *J. Biol. Chem.* **275**, 33844–33849
21. Bradford, M. M. (1976) *Anal. Biochem.* **72**, 248–254
22. Laemmli, U. K. (1970) *Nature* **227**, 680–685
23. Nishioka, H., Horiuchi, H., Tabuchi, A., Yoshioka, A., Shirakawa, R., and Kita, T. (2001) *Biochem. Biophys. Res. Commun.* **280**, 970–975
24. Phillips, D. R., and Agin, P. P. (1977) *J. Clin. Invest.* **60**, 535–545
25. Fabiato, A., and Fabiato, F. (1979) *J. Physiol. (Paris)* **75**, 463–505
26. Ullrich, O., Horiuchi, H., Bucci, C., and Zerial, M. (1994) *Nature* **368**, 157–160
27. Palmer, M., Harris, R., Freytag, C., Kehoe, M., Tranum-Jensen, J., and Bhakdi, S. (1988) *EMBO J.* **17**, 1598–1606
28. Kinlough-Rathbone, R. L., Perry, D. W., Rand, M. L., and Packham, M. A. (1999) *Thromb. Res.* **95**, 315–323
29. Santos, M. T., Moscardo, A., Valles, J., Martinez, M., Pinon, M., Aznar, J., Broekman, M. J., and Marcus, A. J. (2000) *Circulation* **102**, 1924–1930
30. Yoshioka, A., Horiuchi, H., Shirakawa, R., Nishioka, H., Tabuchi, A., Higashi, T., Yamamoto, A., and Kita, T. (2001) *Ann. N. Y. Acad. Sci.* **947**, 403–406
31. Girolami, A., Fabris, F., Marco, L., and Peruffo, R. (1976) *Acta Haematol.* **56**, 151–159
32. Botteschia, D., Fentin, G., Gruppo, F., and Nasruato, G. (1976) *Haemostasis* **5**, 176–188
33. Knight, D. E., Hallam, T. J., and Scrutton, M. C. (1982) *Nature* **296**, 256–257
34. Pierschbacher, M. D., and Ruoslahti, E. (1984) *Nature* **309**, 30–33
35. Lefkovits, J., Plow, E. F., and Topol, E. J. (1995) *N. Engl. J. Med.* **332**, 1553–1559
36. Basani, R. B., D'Andrea, G., Mitra, N., Vilaire, G., Richberg, M., Kowalska, M. A., Bennett, J. S., and Poncz, M. (2001) *J. Biol. Chem.* **276**, 13978–13981
37. Toullec, D., Pianetti, P., Coste, H., Bellevergue, P., Grand-Perret, T., Ajakane, M., Baudet, V., Boissin, P., Boursier, E., Loriolle, F., Duhamel, L., Charon, D., and Kirilovsky, J. (1991) *J. Biol. Chem.* **266**, 15771–15781
38. Brose, N., Hofmann, K., Hata, Y., and Sudhof, T. C. (1995) *J. Biol. Chem.* **270**, 25273–25280
39. Rhee, J. S., Betz, A., Pyott, S., Reim, K., Varoqueaux, F., Augustin, I., Hesse, D., Sudhof, T. C., Takahashi, M., Rosenmund, C., and Brose, N. (2002) *Cell* **108**, 121–133
40. Hofmann, J. (1997) *FASEB J.* **11**, 649–669
41. Swartz, K. J. (1993) *Neuron* **11**, 305–320
42. Stea, A., Soong, T. W., and Snutch, T. P. (1995) *Neuron* **15**, 929–940
43. Brose, N., and Rosenmund, C. (2000) *J. Cell. Sci.* **115**, 4399–4411

MOLECULAR AND CELLULAR BIOLOGY, May 2003, p. 3593–3606 Vol. 23, No. 10
0270-7306/03/$08.00+0 DOI: 10.1128/MCB.23.10.3593–3606.2003

Cardiac p300 Is Involved in Myocyte Growth with Decompensated Heart Failure

Tetsuhiko Yanazume,[1] Koji Hasegawa,[1]* Tatsuya Morimoto,[1] Teruhisa Kawamura,[1] Hiromichi Wada,[1] Akira Matsumori,[1] Yosuke Kawase,[2] Maretoshi Hirai,[1] and Toru Kita[1]

Department of Cardiovascular Medicine, Graduate School of Medicine, Kyoto University, Shogoin, Sakyo-ku, Kyoto 606-8507,[1] and Pharmacological Technology Laboratory, Chugai Pharmaceutical Co., Ltd., Shizuoka,[2] Japan

Received 13 January 2003/Accepted 20 February 2003

A variety of stresses on the heart initiate a number of subcellular signaling pathways, which finally reach the nuclei of cardiac myocytes and cause myocyte hypertrophy with heart failure. However, common nuclear pathways that lead to this state are unknown. A zinc finger protein, GATA-4, is one of the transcription factors that mediate changes in gene expression during myocardial-cell hypertrophy. p300 not only acts as a transcriptional coactivator of GATA-4, but also possesses an intrinsic histone acetyltransferase activity. In primary cardiac myocytes derived from neonatal rats, we show that stimulation with phenylephrine increased an acetylated form of GATA-4 and its DNA-binding activity, as well as expression of p300. A dominant-negative mutant of p300 suppressed phenylephrine-induced nuclear acetylation, activation of GATA-4-dependent endothelin-1 promoters, and hypertrophic responses, such as increase in cell size and sarcomere organization. In sharp contrast to the activation of cardiac MEK-1, which phosphorylates GATA-4 and causes compensated hypertrophy in vivo, p300-mediated acetylation of mouse cardiac nuclear proteins, including GATA-4, results in marked eccentric dilatation and systolic dysfunction. These findings suggest that p300-mediated nuclear acetylation plays a critical role in the development of myocyte hypertrophy and represents a pathway that leads to decompensated heart failure.

Heart failure arises from a number of diverse primary cardiovascular disorders and is associated with significant morbidity and mortality. Therefore, elucidating the mechanisms of this disease is of clinical importance. Previous studies have demonstrated that a variety of stresses on the heart activate neuronal and hormonal factors, such as the renin-angiotensin system and factors regulating the sympathetic nervous systems. These factors initiate a number of subcellular signaling pathways, which finally reach the nuclei of cardiac myocytes and change the pattern of gene expression associated with hypertrophy (reviewed in references 14 and 53). In order to establish appropriate therapy for heart failure, it is critical to identify a common nuclear pathway which can be targeted by pharmacological agents in the future.

We have been interested in transcription factors that mediate changes in gene expression during myocardial-cell hypertrophy. A zinc finger protein, GATA-4, is one such factor and is required for transcriptional activation of cardiac genes whose expression is upregulated during myocardial-cell hypertrophy (22, 25; reviewed in reference 46). While overexpression of GATA-4 in cardiac myocytes causes hypertrophy, expression of a dominant-negative form of GATA-4 inhibits Gq protein-coupled receptor agonist-induced hypertrophy (37). During myocardial-cell hypertrophy, GATA-4 is phosphorylated at a serine residue and shows increased DNA-binding ability (38, 47). Phosphorylation of cardiac GATA-4 requires activation of MEK1/extracellular signal-regulated kinase (ERK) 1/2. On the other hand, activation of MEK1 in cardiac myocytes results in phosphorylation of GATA-4 and in concentric left-ventricular hypertrophy in vivo (9). Other transcription factors that control myocardial-cell hypertrophy include myocyte-enhancing factor 2 (MEF2) (34), serum response factor (49), TEF-1 (32), and AP-1 (25). MEF2 is a downstream target for calmodulin-dependent protein kinase IV, the activation of which is sufficient to induce cardiac hypertrophy in vivo (50). The involvement of multiple transcription factors in hypertrophic responses suggests that these factors are activated through some common pathway during myocardial-cell hypertrophy. Regarding this hypothesis, Molkentin et al. have reported that the calcineurin–NF-AT pathway is one of the common pathways that transduces signals for cardiac hypertrophy (45). However, several studies have demonstrated that blockade of calcineurin fails to inhibit the development of heart failure in pathophysiological settings, suggesting the existence of redundant networks in cardiac nuclear signaling (63; reviewed in reference 44).

p300 is an adenovirus E1A-associated protein that acts as a transcriptional coactivator that mediates the interaction of DNA-binding transactivators with the basal transcriptional complex (17). Consistent with this function, p300 protein interacts directly with components of the basal transcriptional apparatus (62) and diverse enhancer-binding proteins, modulating many examples of enhancer-mediated transcription. Several lines of evidence suggest that p300 plays a critical role in the physiological growth and differentiation of cardiac myocytes during development. Mice lacking a functional p300 gene die between days 9 and 11.5 of gestation, exhibiting defects of cardiac muscle differentiation and trabeculation (61). The expression of myocardial contractile proteins is clearly reduced in the mutants compared with the wild type (WT). Furthermore, p300 is required for maintenance of the G_1 phase of the cell cycle in differentiated cardiac myocytes (5, 39). p300 protein also serves as an adaptor for hypertrophy-responsive transcription factors, such as GATA-4, MEF2, serum response factor, and AP-1, and these interactions are required for the full transcriptional activities of these factors (16, 31, 56). However, the direct roles of p300 in cardiac myocyte hypertrophy have not been clarified.

In addition to its "bridging function," p300 protein possesses an intrinsic histone acetyltransferase (HAT) activity (48) which promotes a transcriptionally active chromatin configuration. The HAT activity of p300 is required for the functions of diverse proteins in transcriptional activation (42, 52, 54). The PHD finger of p300 has been reported to be dispensable for its HAT activity and its transactivating function (7). p300 protein can also acetylate certain nonhistone transcription-related proteins, including transcriptional activators (20), coactivators (12), and basal transcription factors (28). Acetylation is emerging as a posttranslational modification of nuclear proteins that is essential for the regulation of transcription and that modifies transcription factor affinity for binding sites on DNA, stability, and/or nuclear localization. However, it is unknown whether p300 is able to acetylate hypertrophy-responsive transcription factors such as GATA-4 and, if so, whether p300-mediated acetylation plays a role in myocardial-cell hypertrophy.

For all of these reasons, we were interested in clarifying the role of the intrinsic HAT activity of p300 in myocardial-cell hypertrophy. We show here that p300 acetylates GATA-4 and increases its DNA-binding ability, as well as causing nuclear hyperacetylation of cardiac myocytes. In addition, this process is closely associated with the development of myocardial-cell hypertrophy. In sharp contrast to MEK1 transgenic (TG) mice (which exhibit concentric hypertrophy with normal systolic function), acetylation of cardiac nuclear proteins, including GATA-4, by overexpression of p300 in mice results in marked left-ventricular dilatation and systolic dysfunction. Thus, p300-mediated acetylation may be involved in the development of decompensated heart failure and represents a pharmacological target of heart failure therapy in humans.

MATERIALS AND METHODS

Plasmid constructs. The expression vectors pcDNAG4, pCMVβ-gal, pCMVwtp300, and pCMV1514-1922p300 contain the cytomegalovirus promoter-enhancer fused to murine GATA-4 cDNA (4, 29), β-galactosidase cDNA, a full-length human p300 cDNA (17), and a portion of p300 cDNA encoding amino acid residues 1514 to 1922 (62), respectively. Plasmid pwtE1A is an expression vector for WT 12S E1A. pwtE1A and pCMVwtp300 were gifts from Richard Eckner and David M. Livingston (Harvard Medical School, Boston, Mass.), and pCMV1514-1922p300 was provided by Antonio Giordano (Thomas Jefferson University, Philadelphia, Pa.). pRSVCAT and pRSVluc contain chloramphenicol acetyltransferase (CAT) and Luc genes, respectively, driven by Rous sarcoma virus long terminal repeat sequences (22, 23). The plasmid construct pETCAT contains the transcription start site-proximal 204 bp of the WT rat endothelin-1 (ET-1) promoter fused to a bacterial CAT gene (33) and was a gift of Thomas Quertermous (Stanford University, Palo Alto, Calif.).

Transfection and luciferase-CAT assays. COS7 cells were maintained in Dulbecco's modified Eagle's medium with 10% fetal bovine serum. The cells were washed twice with serum-free medium and then transfected with a total of <12 μg of DNA in 100-mm-diameter plates using Lipofectamine (Life Technologies, Inc.) according to the manufacturer's recommendation. After a 5-h incubation with DNA-Lipofectamine complex, the cells were washed twice with serum-free medium and further incubated in the medium with 10% fetal bovine serum for 48 h. The cells were then washed twice with ice-cold phosphate-buffered saline and lysed as described previously (31, 47). Luc and CAT activities were determined in the same cell lysate as described previously (31). The relative CAT activity was calculated from the ratio of CAT background to Luc background and was expressed as the mean ± standard error.

Primary neonatal rat ventricular cardiac myocytes were prepared as previously described (23, 31, 47). Cardiac myocytes were cotransfected with the appropriate amounts of DNA using Lipofectamine Plus (Life Technologies, Inc.) according to the manufacturer's recommendation. After a 2-h incubation with DNA-Lipofectamine complex, the cells were washed twice with serum-free medium and further incubated for 48 h in serum-free medium in the presence of 10^{-5} M phenylephrine (PE) or saline as a control. The cells were then washed twice with ice-cold phosphate-buffered saline, lysed with lysis buffer, and subjected to assays for luciferase and CAT activities as described previously (47).

Analysis of the acetylation state of GATA-4 and Western blotting. In analysis of the acetylation state of GATA-4, 50 mM NaF and 1 mM Na_3VO_4 were added to all buffers. For pulse-labeling, COS7 cells (10^6) transfected with GATA-4 were resuspended in 2.5 ml of medium containing 0.05 mCi of [1-^{14}C]acetic acid sodium salt/ml (200 μCi/ml; Amersham Pharmacia Biotech) and incubated for 3 h. Ethanol, the solvent of [1-^{14}C]acetic acid sodium salt, was evaporated to minimize the cytotoxic effect of the ethanol in the culture medium. Nuclear extracts from these cells were immunoprecipitated using anti-GATA-4 antibody (Santa Cruz Biotechnology, Inc.) or normal goat immunoglobulin G (IgG) in low-stringency buffer (50 mM Tris, pH 7.4, 0.15 M NaCl, 0.5% Nonidet P-40, 1 mM EDTA, 10 mg each of aprotinin and leupeptin/ml, and 0.5 mM phenylmethylsulfonyl fluoride; all from Sigma) for 16 h at 4°C and incubated with protein G beads for 1 h at 4°C. The precipitate was washed four times in the same buffer, resuspended in 50 ml of sodium dodecyl sulfate (SDS) lysis buffer (20 mM Tris, pH 7.5, 50 mM NaCl, 0.5% SDS, 1 mM dithiothreitol), heated to 95°C for 2 min, electrophoresed on an SDS-polyacrylamide gel (10% acrylamide), fixed, and autoradiographed using a bioimaging analyzer (BAS 2000; FUJIX, Tokyo, Japan).

For immunoprecipitation and Western blotting, nuclear extracts were immunoprecipitated with anti-GATA-4 antibody (Santa Cruz Biotechnology, Inc.), which was captured by adding protein G beads. The precipitate was washed four times in the low-stringency buffer, resolved by SDS-polyacrylamide gel electrophoresis, transferred to immobilon membranes, and reacted with anti-acetylated lysine antibody (New England Biolabs, Inc.), which was subsequently detected using horseradish peroxidase-conjugated anti-rabbit IgG. Signals were detected using the ECL Western blotting detection system (Amersham Pharmacia Biotech) according to the manufacturer's instructions. To normalize for protein loading after immunoprecipitation, the blots were stripped by incubation in 62.5 mM Tris-HCl, pH 6.8, 100 mM β-mercaptoethanol, and 2% SDS for 30 min at 50°C, washed twice with phosphate-buffered saline and 0.05% Tween, and then probed with anti-GATA-4 antibody. The primary antibody for p300/CBP associated factor (PCAF) was obtained from Santa Cruz Biotechnology, Inc. Western blotting for GATA-4, p300, E1A, and β-actin was performed as described previously (23, 31, 47).

Electrophoretic mobility shift assays (EMSAs). Double-stranded oligonucleotides were designed to contain GATA motifs from the rat ET-1 promoter. The sequences of the sense strands of these oligonucleotides were as follows: WT, 5′-CCTCTAGAGCCGGGTCTTATCTCCGGCTGCACGTTGC-3′, and mut-GATA, 5′-CCTCTAGAGCCGGGTCTGCACTCCGGCTGCACGTTGC-3′ (mutated sequences are in italics).

We also used a double-stranded oligonucleotide (purchased from Santa Cruz Biotechnology, Inc.) that contained the Sp-1 binding site as a control probe. EMSAs were carried out at 4°C for 20 min in 15-μl reaction mixtures containing 10 μg of nuclear extract, 0.25 ng (>20,000 cpm) of radiolabeled double-stranded oligonucleotide, 500 ng of poly(dI-dC), 5 mM Tris-HCl (pH 7.5), 1 mM EDTA, 0.5 mM dithiothreitol, 37.5 mM KCl, and 4% Ficoll 400. For cold competition experiments, a 100 M excess of unlabeled competitor oligonucleotide was included in the binding reaction mixture. Protein-DNA complexes were separated by electrophoresis on 4% nondenaturing polyacrylamide gels in 0.25× TBE (1× TBE is 100 mM Tris, 100 mM boric acid, and 2 mM EDTA) at 4°C.

Immunocytochemistry and measurement of cell diameter. The cardiac myocytes were grown in flask style chambers with glass slides (Nalgen Nunc) and stained for β-myosin heavy chain (MHC) using the indirect immunofluorescence method, as previously described (60). Immunocytochemical staining for acety-

* Corresponding author. Mailing address: Department of Cardiovascular Medicine, Graduate School of Medicine, Kyoto University, 54 Kawara-cho, Shogoin, Sakyo-ku, Kyoto, 606-8507, Japan. Phone: 81-75-751-3190. Fax: 81-75-751-3203. E-mail: koj@kuhp.kyoto-u.ac.jp.

lated lysine was performed using the indirect immuno-alkaline phosphatase method. Cells were incubated with anti-acetylated lysine polyclonal antibody (New England Biolabs, Inc.) at a dilution of 1:30. Signals of acetylated lysine were detected using anti-rabbit alkaline phosphatase-conjugated secondary antibody (Sigma) at a dilution of 1:250 for 45 min.

Measurement of cell diameter was performed in cardiac myocytes stained by anti-β-MHC antibody as previously described (60).

Creation of TG mice and Southern analysis. The α-MHC–p300 DNA plasmid was constructed by subcloning a *NotI-HindIII* fragment of pCMVwtp300 (kindly donated by Richard Eckner, Zurich, Switzerland) into the *SalI-HindIII* site of clone 26, a 5.5-kb mouse α-MHC promoter-containing construct (kindly donated by Jeffery Robbins, Cincinnati, Ohio). The α-MHC–p300 DNA fragment was gel purified and injected into newly fertilized C57BL/6 oocytes, which were transferred to the oviducts of pseudopregnant C57BL/6 recipients. TG founders were identified by Southern blotting using the ^{32}P-labeled 450-bp α-MHC–p300 sequence region as a probe.

RNA analysis. Detection of mRNA for β-MHC, atrial natriuretic factor (ANF), and glyceraldehyde-3-phosphate dehydrogenase (GAPDH) was performed by Northern blot analysis as previously described (22, 23, 31).

To detect prepro-ET-1 mRNA, reverse transcriptase (RT) PCR was carried out as described previously (30). The PCR primers were designed on the basis of the published cDNA sequence for mouse ET-1 and GAPDH as follows: sense for ET-1, 5′-CATCATCTGGGTCAACACTC-3′; antisense for ET-1, 5′-CATGGGCTCGCACTATATA-3′; sense for GAPDH, 5′-TTGCCATCAACGACCCCTTC-3′; and antisense for GAPDH, 5′-TTGTCATGGATGACCTTGGC-3′. To define the optimal amplification conditions, a series of pilot studies were performed by the use of various amounts of RT products and 20 to 45 cycles of PCR amplification as described previously (30). On the basis of these initial experiments, the linear portion of the amplification was determined for the ET-1 and GAPDH genes.

Transthoracic echocardiography. The cardiac functions of WT and TG mice were evaluated noninvasively by echocardiography. The animals were anesthetized with ketamine (50 μg/g of body weight) and xylazine (2.5 μg/g). Transthoracic echocardiography was performed with a cardiac ultrasound recorder (Toshiba Power Vision, Tokyo, Japan), using a 7.5-MHz transducer. After the acquisition of high-quality two-dimensional images, M mode images of the left ventricle were recorded. Measurements of left-ventricular end diastolic (LVDD) and end systolic (LVESD) internal dimensions were performed according to the leading edge-to-leading edge convention adopted by the American Society of Echocardiography. Percent fractional shortening (%FS) was calculated as follows: %FS = [(LVDD − LVESD)/LVDD] × 100. At least three independent M mode measurements per animal were obtained by an examiner blinded to the genotype of the animal.

Statistical analysis. Data are presented as means ± standard errors. Statistical comparisons were performed using unpaired two-tailed Student's *t* tests or analysis of variance with Scheffe's test where appropriate, with a probability value of <0.05 taken to indicate significance.

RESULTS

p300 protein acetylates lysine residues of GATA-4, enhances its DNA-binding activity, and participates in GATA-4-dependent ET-1 transcription. To give positive proof of GATA-4 acetylation, expression plasmids encoding GATA-4 (pcDNAG4) and p300 (pCMVwtp300) were transfected into COS7 cells, which lack all GATA factors (31, 47). These cells were pulse-labeled with the [^{14}C]acetic acid, sodium salt and subjected to immunoprecipitation with antiserum against GATA-4 or with normal goat IgG as a negative control. As shown in Fig. 1, GATA-4 protein incorporated sodium [^{14}C]acetate, indicating acetylation of GATA-4.

To determine whether GATA-4 is acetylated by p300, expression plasmids encoding GATA-4 (pcDNAG4), p300 (pCMVwtp300), and E1A (pwtE1A) were transfected (Fig. 2) into COS7 cells. Nuclear extracts from these cells were subjected to immunoprecipitation with an anti-GATA-4 antibody, followed by Western blotting using anti-acetylated lysine antibody. As shown in Fig. 2A, the forced expression of p300

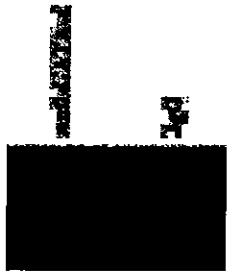

FIG. 1. In vitro acetylation of GATA-4 in COS7 cells. COS7 cells were transfected with 2 μg of pcDNAG4 and 9 μg of pCMVwtp300 and were pulse-labeled with [^{14}C]acetic acid sodium salt for 3 h. The nuclear extracts were immunoprecipitated with anti-GATA-4 antibody or with normal goat IgG, resolved by SDS-polyacrylamide gel electrophoresis, fixed, and autoradiographed using a bioimaging analyzer.

induced acetylation of GATA-4. However, when E1A, which disrupts p300 function, was expressed in addition to p300, it almost completely inhibited this acetylation. Expression of p300 or E1A did not influence the amounts of GATA-4 and β-actin produced by transfecting pcDNAG4 (Fig. 2B). To determine whether acetylation of GATA-4 by p300 modulates the DNA-binding activity of GATA-4, EMSAs were performed. The same nuclear extracts used to detect acetylation were probed with a radiolabeled double-stranded oligonucleotide containing the GATA-4 site of the rat ET-1 promoter. As shown in Fig. 2C, competition EMSAs demonstrated that the retarded band represented specific binding, as evidenced by the fact that it was competed out by an excess of unlabeled ET-1 GATA oligonucleotide (fourth lane from left) but not by the same amount of an oligonucleotide containing the ET-1 GATA site with a mutation (fifth lane). To further confirm that the retarded band represents an interaction of the probe with GATA-4, we performed supershift experiments. The retarded band was supershifted by anti-GATA-4 antibody (seventh lane) but not by control goat IgG (sixth lane). The amount of specific complex formed with GATA-4 markedly increased in nuclear extracts from p300-expressing cells (second lane) compared with those from β-galactosidase (β-Gal)-expressing cells (first lane). Coexpression of E1A, which inhibited GATA-4 acetylation, blocked the p300-mediated increase in GATA-4–DNA binding (third lane).

To examine whether p300-mediated acetylation is involved in GATA-4-dependent ET-1 transcription, we performed transient-transfection experiments. As seen in Fig. 2D, the expression of GATA-4 resulted in a 22-fold activation of the 204-bp rat ET-1 promoter (pETCAT), and coexpression of E1A almost completely blocked this increase. Consistent with the acetylation of GATA-4 by p300, expression of p300 dramatically potentiated GATA-4-mediated transactivation of the ET-1 promoter (252-fold). This potentiation was also repressed by coexpression of E1A, which inhibits p300-mediated acetylation.

PE induces acetylation and DNA-binding of GATA-4, as well

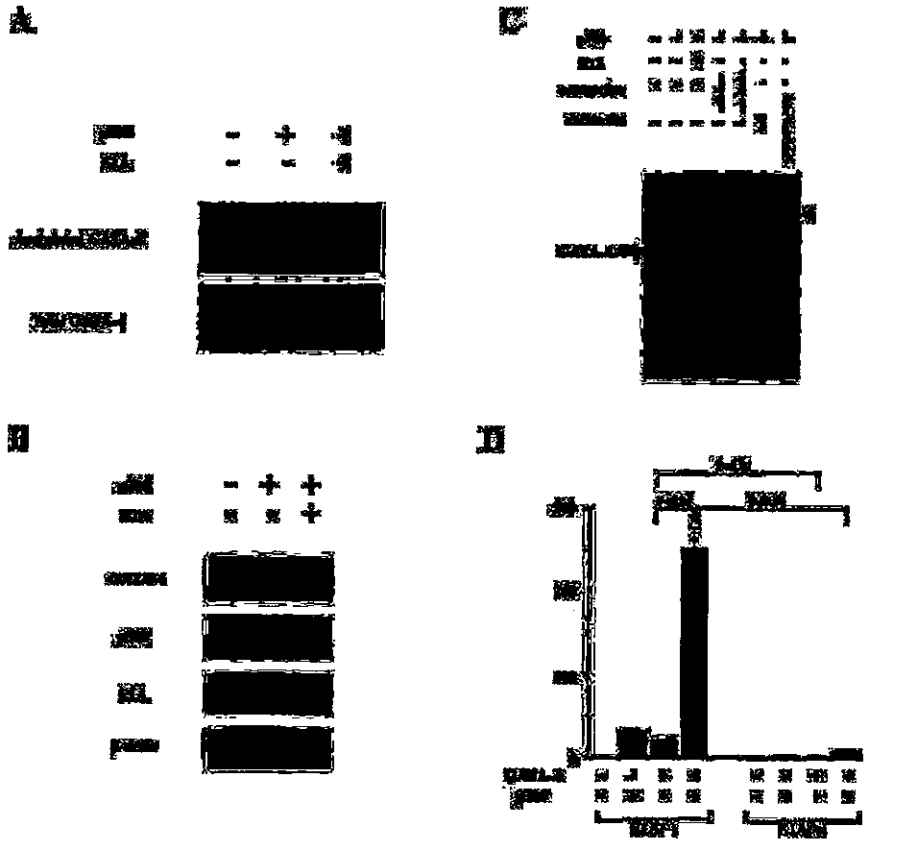

FIG. 2. p300 acetylates lysine residues of GATA-4, enhances its DNA-binding activity, and is involved in GATA-4-dependent ET-1 transcription. (A) COS7 cells were transfected with 2 μg of pcDNAG4 or with (+) 9 μg of pCMVwtp300 (p300) and/or 1 μg of pwtE1A (E1A) as indicated. The total amount of DNA was kept constant by cotransfecting pCMVβ-gal. Nuclear extracts (300 μg of protein) from these cells were immunoprecipitated with anti-GATA-4 antibody, followed by sequential Western blotting with anti-acetylated lysine antibody and with anti-GATA-4 antibody. (B) The nuclear extracts used for panel A before immunoprecipitation were subjected to Western blotting using the anti-GATA-4 antibody, anti-p300 antibody, anti-E1A antibody, or anti-β-actin antibody. (C) The same nuclear extracts were probed with a radiolabeled double-stranded oligonucleotide containing the GATA-4 site in the ET-1 promoter. Ab, antibody; small arrow, supershifted band of GATA-4. (D) COS7 cells were transfected with 2.0 μg of pETCAT, 0.1 μg of pRSVluc, 0.5 μg of pcDNAG4 or pCMVβ-gal, 2.5 μg of pCMVwtp300 or pCMVβ-gal, and 0.3 μg of pwtE1A or pCMVβ-gal. The results are expressed as *n*-fold activation of the normalized CAT activity (CAT/luc) relative to that resulting from transfection with 3.3 μg of pCMVβ-gal without pcDNAG4, pCMVwtp300, or pwtE1A. The data shown are the means and standard errors of the mean from three independent experiments.

as p300 expression in cardiac myocytes. To examine whether acetylation of GATA-4 actually occurs during myocardial-cell hypertrophy, cultured ventricular myocytes prepared from neonatal rats were incubated with an α_1-adrenergic agonist, PE, at 10^{-5} M or with saline as a control for 48 h. As shown in Fig. 3A, the expression levels of GATA-4, PCAF, and β-actin were similar in saline- and PE-stimulated cells. In contrast, p300 levels were markedly increased by PE. Nuclear extracts from cardiac myocytes were immunoprecipitated with anti-GATA-4 antibody, followed by Western blotting with anti-acetylated lysine antibody. As shown in Fig. 3B, PE treatment resulted in a marked increase in the level of the acetylated form of GATA-4. To correct for differences in protein loading after immunoprecipitation, the same membrane was reblotted

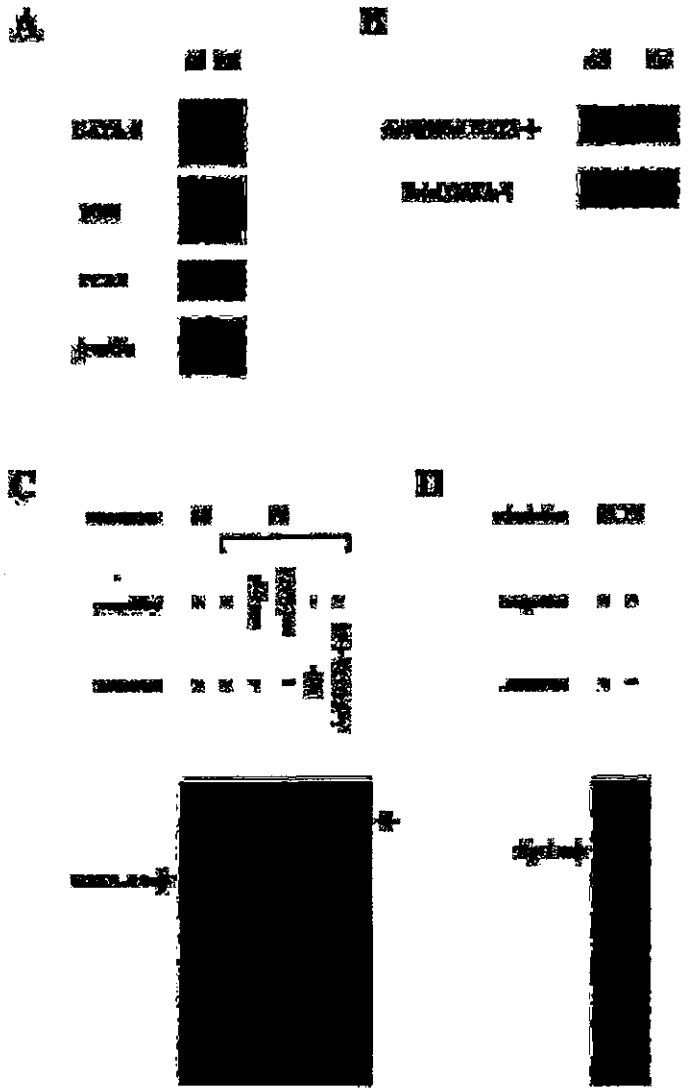

FIG. 3. PE induces p300 expression, acetylation, and DNA binding of GATA-4 in cardiac myocytes. (A) Primary cardiac myocytes from neonatal rats were stimulated with saline (SS) or PE (10^{-5} M) for 48 h. Nuclear extracts from these cells were subjected to Western blotting with anti-GATA-4 antibody, anti-p300 antibody, anti-PCAF antibody, or anti-β-actin antibody. (B) The same nuclear extracts (100 μg of protein) were immunoprecipitated with anti-GATA-4 antibody and sequentially subjected to Western blotting with anti-acetylated lysine antibody and with anti-GATA-4 antibody. (C and D) The same nuclear extracts were probed with a radiolabeled double-stranded oligonucleotide containing the ET-1 GATA site (C) and with one containing the Sp-1 site (D). −, absent.

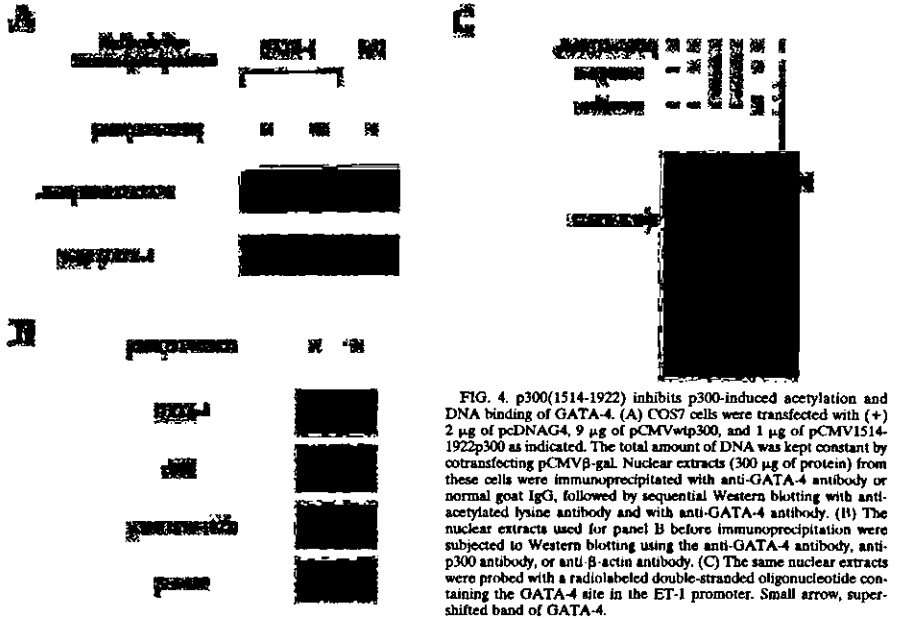

FIG. 4. p300(1514-1922) inhibits p300-induced acetylation and DNA binding of GATA-4. (A) COS7 cells were transfected with (+) 2 μg of pcDNAG4, 9 μg of pCMVwtp300, and 1 μg of pCMV1514-1922p300 as indicated. The total amount of DNA was kept constant by cotransfecting pCMVβ-gal. Nuclear extracts (300 μg of protein) from these cells were immunoprecipitated with anti-GATA-4 antibody or normal goat IgG, followed by sequential Western blotting with anti-acetylated lysine antibody and with anti-GATA-4 antibody. (B) The nuclear extracts used for panel B before immunoprecipitation were subjected to Western blotting using the anti-GATA-4 antibody, anti-p300 antibody, or anti-β-actin antibody. (C) The same nuclear extracts were probed with a radiolabeled double-stranded oligonucleotide containing the GATA-4 site in the ET-1 promoter. Small arrow, supershifted band of GATA-4.

with anti-GATA-4 antibody. The amounts of total GATA-4 in lysates after immunoprecipitation were similar in saline- and PE-stimulated cells. Therefore, PE markedly increased the ratio of the acetylated form of GATA-4 relative to the total GATA-4 in cardiac myocytes.

To determine whether PE stimulation influences the DNA-binding activity of GATA-4 in cardiac myocytes, EMSAs were performed with a radiolabeled double-stranded oligonucleotide containing the ET-1 GATA site. As shown in Fig. 3C, a retarded band indicated sequence-specific binding (third and fourth lanes from left), and it was supershifted by anti-GATA-4 antibody (sixth lane) but not by control goat IgG (fifth lane). These findings demonstrate that this band represents a specific GATA-4 complex. The intensity of this band was increased in nuclear extracts from PE-stimulated cardiac myocytes (second lane) compared with those from saline-stimulated cells (first lane). However, the DNA-binding activities of Sp-1 in cells stimulated with saline (Fig. 3D, left lane) and those stimulated with PE (Fig. 3D, right lane) did not differ.

p300(1514-1922) inhibits p300-induced acetylation and DNA binding of GATA-4. Yuan et al. reported that the portion of p300 containing the affinity to MyoD was detected in fragment 1514 to 1922, covering the third cysteine-histidine-rich conserved domain (62). Dai and Markham showed that this cysteine-histidine-rich region of p300 interacts with N and C zinc finger domains of GATA-4 (16). However, this small fragment of p300(1514-1922) lacks the HAT activity, suggesting that this fragment may act as a dominant-negative mutant and impair the function of endogenous p300. To determine whether p300(1514-1922) inhibits p300-induced acetylation of GATA-4, expression plasmids encoding GATA-4 (pcDNAG4), p300 (pCMVwtp300), and p300(1514-1922) (pCMV1514-1922p300) were transfected into COS7 cells. Nuclear extracts from these cells were subjected to immunoprecipitation with an anti-GATA-4 antibody (first two lanes on the left) or with normal goat IgG as a negative control (third lane), followed by Western blotting using anti-acetylated lysine antibody. As shown in Fig. 4A, the extent of GATA-4 acetylation decreased when p300(1514-1922) was expressed in addition to p300. Expression of p300 or p300(1514-1922) did not influence the amount of GATA-4 produced by transfecting pcDNAG4 (Fig. 4B). To determine whether p300(1514-1922) modulates the DNA-binding activity of GATA-4, EMSAs were performed (Fig. 4C). The same nuclear extracts used to detect acetylation were probed with a radiolabeled double-stranded oligonucleotide containing the GATA-4 site of the rat ET-1 promoter. The specific band indicating GATA-4 binding was determined by competition EMSAs and by supershift experiments (third to sixth lanes from the left). Coexpression of p300(1514-1922), which inhibited GATA-4 acetylation, also decreased GATA-4–DNA binding (compare the first and second lanes).

p300 protein is involved in PE-induced nuclear acetylation of cardiac myocytes. We next evaluated whether nuclear hyperacetylation of cardiac myocytes occurs during hypertrophy and, if so, whether p300 is involved in the process. Cardiac myocytes were transfected with a plasmid encoding p300(1514-

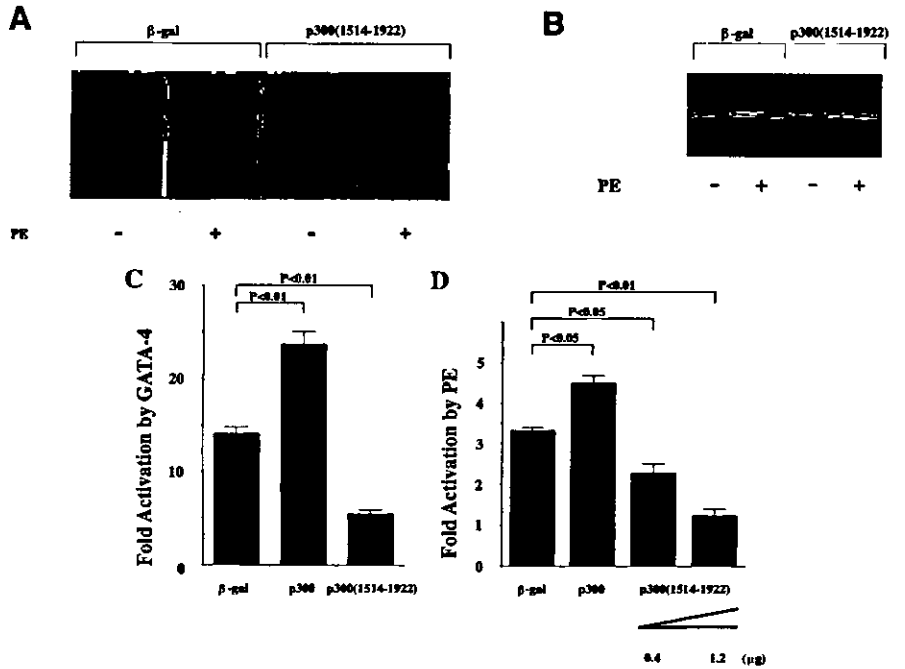

FIG. 5. p300(1514-1922) inhibits PE-induced nuclear hyperacetylation and GATA-4-dependent and PE-induced ET-1 transcription in cardiac myocytes. (A) Cardiac myocytes were transfected with 0.7 μg of pCMV1514-1922p300 or pCMVβ-gal (β-gal). Then, these cells were stimulated with saline or PE (10^{-5} M) for 48 h and subjected to immunocytochemical staining with antibody against acetylated lysine. +, present. (B) Nuclear extracts from these cells were subjected to Western blotting using the anti-p300 and anti-β-actin antibodies. (C) Cardiac myocytes were cotransfected with 1 μg of pETCAT, 0.05 μg of pRSVluc, 0.25 μg of pcDNAG4 or pCMVβ-gal, and 1.25 μg of pCMVwtp300, pCMV1514-1922p300, or pCMVβ-gal. The results are expressed as *n*-fold activation by GATA-4 of the normalized CAT activity (CAT/luc). The data shown are the means and standard errors of the mean of two independent experiments, each carried out in duplicate. (D) Cardiac myocytes were cotransfected with 2 μg of pETCAT, 0.1 μg of pRSVluc, and 0.4 μg of pCMVwtp300 or 0.4 or 1.2 μg of pCMV1514-1922p300. The total DNA content was equalized in each sample with pCMVβ-gal. The results are expressed as *n*-fold activation by PE of the normalized CAT activity (CAT/luc). The data shown are the means and standard errors of the mean of two independent experiments, each carried out in duplicate.

1922), or β-Gal as a control, and stimulated with saline or 10^{-5} M PE for 48 h. By Western blotting, the specific band indicating p300(1514-1922) was intensely detected in cardiac myocytes transfected with pCMV1514-1922p300 but not in myocytes transfected with pCMVβ-gal (Fig. 5B). Then, these cells were immunostained with an anti-acetylated lysine antibody. As shown in Fig. 5A, in β-Gal-transfected cardiac myocytes, PE stimulation markedly induced nuclear staining, indicating hyperacetylation. This change in β-Gal-expressing cells was compared with that in p300(1514-1922)-expressing cells. PE-induced nuclear hyperacetylation was almost completely blocked by transfection of an expression plasmid encoding p300(1514-1922).

p300 protein is involved in PE-induced ET-1 transcription and hypertrophy in cardiac myocytes. To test whether p300 is involved in GATA-4- and PE-induced ET-1 transcription in cardiac myocytes, we transfected an ET-1 reporter plasmid into cardiac myocytes. As shown in Fig. 5C and D, coexpression of WT p300 further activated GATA-4- and PE-induced ET-1 promoter activities. However, coexpression of p300 (1514-1922), which blocks PE-induced nuclear acetylation, inhibited GATA-4- and PE-induced ET-1 transcription.

To investigate whether p300 is involved in hypertrophic responses, such as increase in cell size and sarcomere organization, cardiac myocytes were subjected to immunofluorescence with an antibody against β-MHC. As shown in Fig. 6A, in β-Gal-expressing cardiac myocytes, PE stimulation caused increases in cell size and in the thickness and density of striated sarcomeric actin fibers compared with saline stimulation. Expression of p300(1514-1922) markedly inhibited PE-induced changes of cell size and myofibrillar organization. As shown in Fig. 6B, p300(1514-1922) dose-dependently inhibited the increase of cell diameter induced by PE or ET-1. However, p300 (1514-1922) alone did not affect the cell diameter in saline-stimulated cardiac myocytes. These data demonstrate that p300 (1514-1922) selectively suppresses hypertrophic responses.

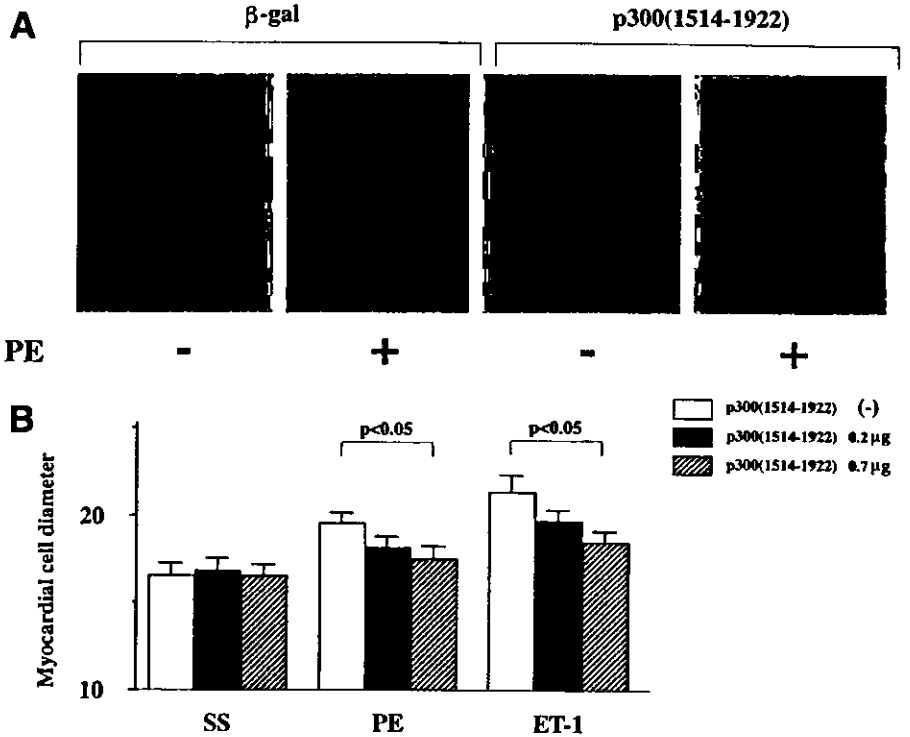

FIG. 6. p300(1514-1922) blocks hypertrophic responses in cardiac myocytes. (A) Cardiac myocytes were transfected with a total of 0.7 μg of pCMV1514-1922p300 or pCMVβ-gal, stimulated with saline (SS) or PE (10^{-5} M) for 48 h, and subjected to immunofluorescent staining with antibody to β-MHC. −, absent; +, present. (B) Measurement of cell diameter (in micrometers). The values are means and standard errors of the mean. The data are from 50 cells in each group.

Cardiac overexpression of p300 in vivo results in increased level of acetylation and DNA binding of GATA-4. To further investigate the role of p300 in cardiac hypertrophy and heart failure in vivo, we generated TG mice expressing p300 in the heart. The injected construct consisted of the full-length human p300 cDNA driven by a cardiomyocyte-specific 5.5-kb mouse α-MHC promoter. Three p300 TG founders were identified by Southern blotting analysis and bred with C57BL/6 mice to generate F_1 heterozygotes. To examine the expression of the p300 transgene in different tissues of TG mice, we performed RT-PCR using primers that specifically recognize the p300 transgene but not the endogenous p300 gene. The expression of the p300 transgene in all lines of TG mice was detected in the heart but not in the lung, liver, or kidney. These findings are consistent with prior observations that the α-MHC promoter specifies cardiac-restricted transgene expression (51).

Myocardial expression levels of p300 protein were determined by Western blot analysis. Cardiac nuclear extracts isolated from 8-week-old TG and WT mice were subjected to Western blotting with anti-p300 antibody, which recognizes both the transgene and endogenous p300. TG mouse hearts showed an eightfold increase in total p300 content compared with WT mouse hearts, whereas the total amounts of cardiac GATA-4 and β-actin in WT and TG mice did not differ (Fig. 7A). Next, we investigated whether cardiac p300 overexpression results in acetylation of GATA-4 in mice. Nuclear extracts isolated from TG and WT mouse hearts were subjected to immunoprecipitation with anti-GATA-4 antibody or with normal goat IgG as a negative control, followed by sequential Western blotting with anti-acetylated lysine antibody and anti-GATA-4 antibody. As shown in Fig. 7B, the ratio of the acetylated form of GATA-4 to total GATA-4 was markedly increased in TG

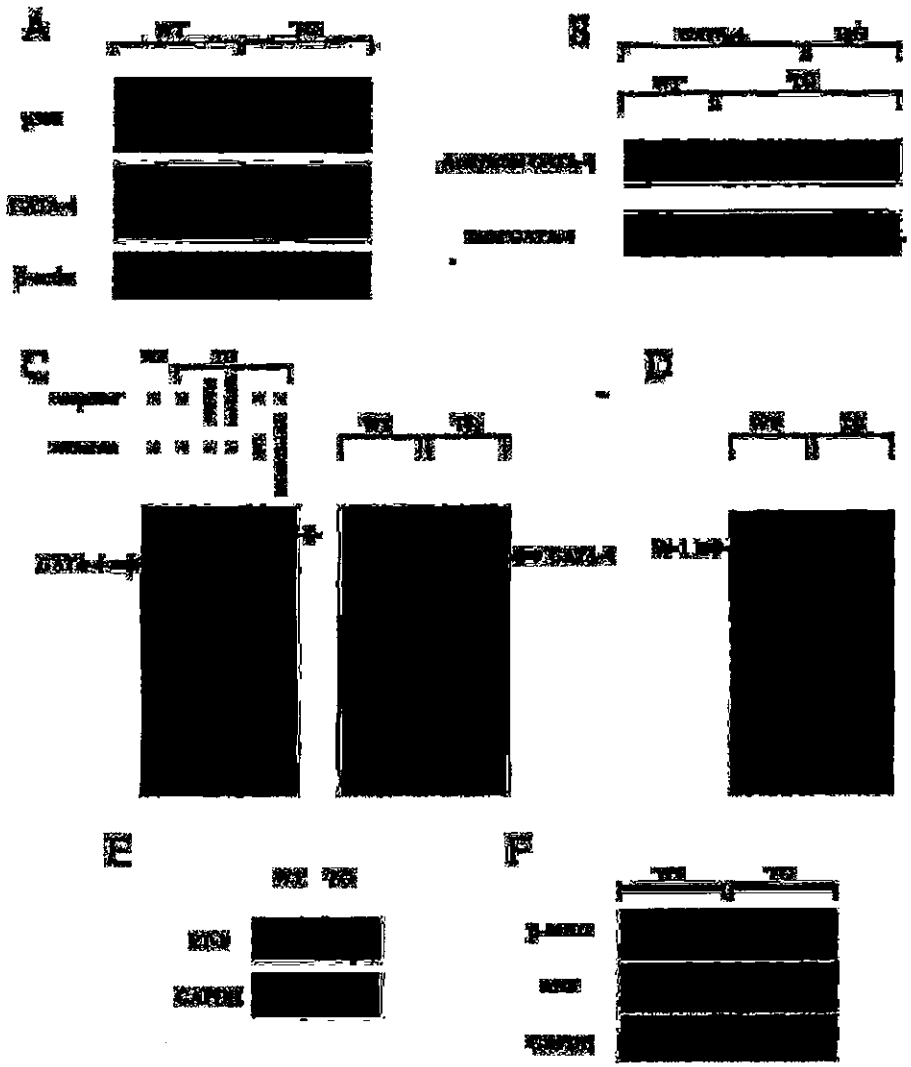

FIG. 7. Cardiac overexpression of p300 results in acetylation and increased DNA-binding activity of GATA-4. (A) Nuclear extracts (10 μg of protein) from WT or p300 TG mouse hearts were subjected to Western blotting with anti-p300 antibody, anti-GATA-4 antibody, or anti-β-actin antibody. (B) Nuclear extracts (400 μg of protein) from WT or TG mouse hearts were immunoprecipitated with anti-GATA-4 antibody and control goat IgG and sequentially subjected to Western blotting with anti-acetylated lysine antibody and anti-GATA-4 antibody. (C and D) Nuclear extracts from WT and TG mouse hearts were probed with a radiolabeled double-stranded oligonucleotide containing the GATA-4 site in the ET-1 promoter (C) and with one containing the Sp-1 site (D). Small arrow, supershifted band of GATA-4. (E) Analysis of ET-1 mRNA levels in WT and TG mouse hearts was performed by RT-PCR. (F) Northern blotting of total RNA from WT and TG mouse hearts for β-MHC, ANF, and GAPDH.

mouse hearts compared with that in WT mouse hearts, indicating hyperacetylation of GATA-4 by p300 expression.

To determine whether GATA-4 acetylation results in increased DNA-binding activity of cardiac GATA-4 in p300 TG mouse hearts, EMSAs were performed with cardiac nuclear extracts from 8-week-old WT and TG mice. Nuclear extracts were probed with a radiolabeled double-stranded oligonucleotide containing the GATA-4 site of the ET-1 promoter. Competition and supershift experiments demonstrated that the band represents an interaction of the probe with cardiac GATA-4 (Fig. 7C, left gel, third to sixth lanes from left). As shown in Fig. 7C, the intensity of the specific band indicating GATA-4 binding was increased in cardiac nuclear extracts from TG mice (second lane in the left gel and fourth to sixth lanes in the right gel) compared with those from WT mice (first lane in the left gel and first to third lanes in the right gel). In contrast, Sp-1 binding activities did not differ in WT and TG mouse hearts (Fig. 7D).

Cardiac overexpression of p300 results in increased expression of GATA-4-dependent hypertrophy-responsive genes. To determine if cardiac p300 overexpression alters the expression of GATA-4-dependent hypertrophy-responsive genes, RNA isolated from mouse ventricles was subjected to RT-PCR for the detection of prepro-ET-1 mRNA and to Northern blotting for detection of ANF and β-MHC mRNAs. TG ventricles showed markedly increased levels of ET-1 (Fig. 7E), ANF, and β-MHC (Fig. 7F) mRNAs compared with WT ventricles. However, the levels of ventricular control GAPDH mRNA in WT and TG mice did not differ.

Cardiac overexpression of p300 results in increased mortality and left-ventricular myocyte hypertrophy, dilatation, and dysfunction. Finally, we evaluated whether TG mice exhibit representative symptoms of heart failure, such as increased mortality, reduced systolic function, and dilatation of the left ventricles. TG mice were prone to premature death after 20 weeks of age and displayed significantly lower survival rates than WT mice at 42 weeks of age (WT [$n = 45$], 100%; TG [$n = 45$], 76%; $P < 0.0001$). TG mice sacrificed at the age of 24 weeks demonstrated dilatation of the left ventricles without a significant increase in wall thickness (Fig. 8A). Hearts from TG mice showed a significant ($P < 0.01$) increase in the heart weight-to-body weight ratio (Fig. 8B). Histological analysis demonstrated that TG mouse hearts showed obvious hypertrophy of individual myocytes but no evidence of an increase in fibrosis, myofibrillar disarray, or inflammatory changes compared with WT mouse hearts (Fig. 8C). The cross-sectional myocardial-cell diameter was significantly ($P < 0.01$) increased in the TG mice compared with the WT mice (Fig. 8D). To determine the effects of cardiac p300 overexpression on ventricular function, we performed echocardiography. As shown in Fig. 9, TG mice at the age of 24 weeks revealed markedly depressed fractional shortening and increased cavity diameter of the left ventricles. However, the left-ventricular wall thicknesses and heart rates in WT and TG mice did not differ. These changes were observed in all three lines of p300 TG mice.

DISCUSSION

GATA-4 acetylation as a new mode of posttranslational modification during myocardial-cell hypertrophy. GATA-4 is a member of the GATA family of zinc finger transcription factors and plays a critical role in heart development (57). GATA-4 also mediates hypertrophic responses of cardiac myocytes (22, 25; reviewed in reference 46). p300 protein serves as a transcriptional coactivator of GATA-4 and provides a bridge between GATA-4 and the basal transcriptional machinery (16, 31). In addition to its bridging function, p300 exhibits HAT activity and is able to acetylate DNA-binding transcription factors, as well as histones (20). p300 protein also frequently forms complexes with other HATs, including PCAF (48), SRC-1 (58), and P/CIP/ACTR/AIBI (13). Protein acetylation often facilitates protein-protein and protein-DNA interactions. The present study has demonstrated that p300 is sufficient to induce GATA-4 acetylation, which results in an increase in the DNA-binding activity of GATA-4. Adenovirus E1A oncoprotein, which inhibited p300-mediated acetylation, also perturbed p300/GATA-4 dependent transcription. These results suggest that p300-mediated acetylation of GATA-4 is required for its full activity as a transcriptional regulator. The lysine residues acetylated by p300/CBP in GATA-1/3 have been mapped (8, 59). Although these residues are not conserved in GATA-4, several lysine residues are possible acetylation sites around the DNA-binding domain of GATA-4. Dissecting these sites remains a major theme for future study.

The present study demonstrates that E1A inhibits p300-mediated acetylation of GATA-4. Our data are compatible with the finding that E1A interferes in the association of p300/CBP with DNA-binding transcription factors, such as p53 and GATA-1, and inhibits acetylation of these factors (10, 26). However, there are reports indicating that E1A does not interfere with the activity of p300 to acetylate histones (3, 6, 19). The reasons for this discrepancy are unclear at present. It is possible that E1A weakens the acetylation of transcription factors by disrupting the association of p300 with these factors rather than affecting HAT activity itself. Alternatively, E1A might have some other direct or indirect effects on histones to reinforce the HAT activity of p300/CBP. Further studies of how E1A regulates the HAT activity of p300/CBP are needed.

During myocardial-cell hypertrophy, the DNA binding of GATA-4 markedly increases while the level of expression of GATA-4 remains unchanged. These findings suggest that posttranslational mechanisms are involved in the activation of cardiac GATA-4 during the process of hypertrophy. One such mechanism is phosphorylation of GATA-4, which requires activation of MEK1/ERKs by Gq protein-coupled receptor agonists (38, 47). The present study demonstrated that during myocardial-cell hypertrophy, an acetylated form of GATA-4 markedly increases, which results in an increase in the DNA-binding activity of cardiac GATA-4. These findings provide evidence that the acetylation of GATA-4 is a novel mode of posttranslational modification during hypertrophic responses. However, the time courses of phosphorylation and acetylation are clearly distinct. The acetylation of cardiac GATA-4 occurs 48 h after agonist stimulation. In contrast, the phosphorylation occurs at much earlier stages (3 and 12 h after stimulation) and decreases at later stages (47). These findings suggest that these two modes of posttranslational modification are regulated through independent mechanisms.

Role of p300 in nuclear hyperacetylation of cardiac myo-

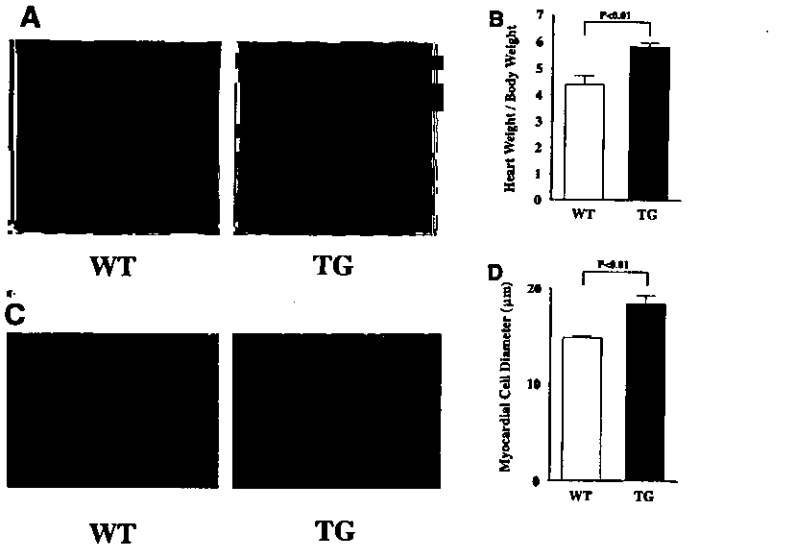

FIG. 8. Histological sections of hearts from WT and p300 TG mice. (A) Gross view of histological sections of WT and TG mice at 24 weeks of age. Both sections were cut at the midsagittal level and parallel to the base. (B) Heart weight/body weight ratio (1,000) of WT and TG mice at 24 weeks of age (n = 5 for each group). (C) Histological sections at a magnification of ×200. (D) Cell diameter was measured as described in Materials and Methods. The values are means and standard errors of the mean. The data are from 50 cells in each group.

cytes during hypertrophy. Histone acetylation is now recognized as one of the hallmark properties of transcriptionally active chromatin (24), and it appears to influence cell cycle progression (35), chromosome dynamics (18), and DNA recombination (55), as well as DNA repair and apoptosis (27). The present study provides the first evidence that nuclear hyperacetylation of cardiac myocytes occurs during hypertrophic responses. Acetylation is regulated not only by intrinsic HATs, such as p300, but also by histone deacetylases. Activation of calcium-calmodulin-dependent protein kinase signaling, which generally occurs during myocardial-cell hypertrophy (50), releases MEF2 from histone deacetylases 4 and 5 (40, 41, 43). This results in unmasking of MEF2 transcriptional activity and in nuclear export of histone deacetylases. It is also possible that the exit of histone deacetylases from the nucleus contributes to nuclear hyperacetylation of hypertrophied cardiac myocytes. The present study demonstrated that expression of p300 in cardiac myocytes is markedly increased during hypertrophy and that a dominant-negative form of p300 blocks the acetylation caused by a hypertrophic agonist. These findings suggest that p300 is required for nuclear hyperacetylation of hypertrophied myocytes. However, they do not exclude the possibility that other HATs, such as CBP and PCAF, play a role in acetylation of GATA-4 in cardiac myocytes.

The question arises as to how the HAT activity of p300 is regulated during myocardial-cell hypertrophy. Increased levels of p300 protein may contribute to the nuclear hyperacetylation of hypertrophied myocytes. In addition, phosphorylation of p300 has been reported to influence the HAT activity of p300/CBP. For example, the HAT activity of p300/CBP increases in association with cyclin E/CDK-mediated phosphorylation of p300/CBP at the G_1/S boundary of the mammalian cell cycle (1). It has been proposed that activation of p44 MAP kinase leads to enhanced phosphorylation of p300/CBP in the C-terminal region and thereby enhances its HAT activity (2). Protein kinase A (15), calcium-calmodulin-dependent kinase N (11), and MAP kinase (2) are known to phosphorylate p300/CBP, thereby enhancing p300/CBP-mediated transcriptional activation. In contrast, the transcriptional regulator Twist appears to reduce p300/CBP HAT activity (21). Further studies are needed to clarify how the HAT activity of p300 is regulated during myocardial-cell hypertrophy.

Nuclear acetylation by p300 causes decompensated heart failure in mice. Phosphorylation of GATA-4 is one mechanism by which its DNA-binding activity is increased during myocardial-cell hypertrophy (38, 47). Activation of MEK1/ERK1/ERK2 either by agonist stimulation or by expression of a constitutively active form of MEK1 results in phosphorylation of GATA-4 at serine residue 105 (38). TG mice overexpressing a constitutively active form of MEK1 in the heart exhibit concentric hypertrophy associated with hyperdynamic systolic function (9). To test whether acetylation of cardiac GATA-4 by p300 in vivo results in a cardiac phenotype similar to or distinct from that induced by phosphorylation of GATA-4, we have

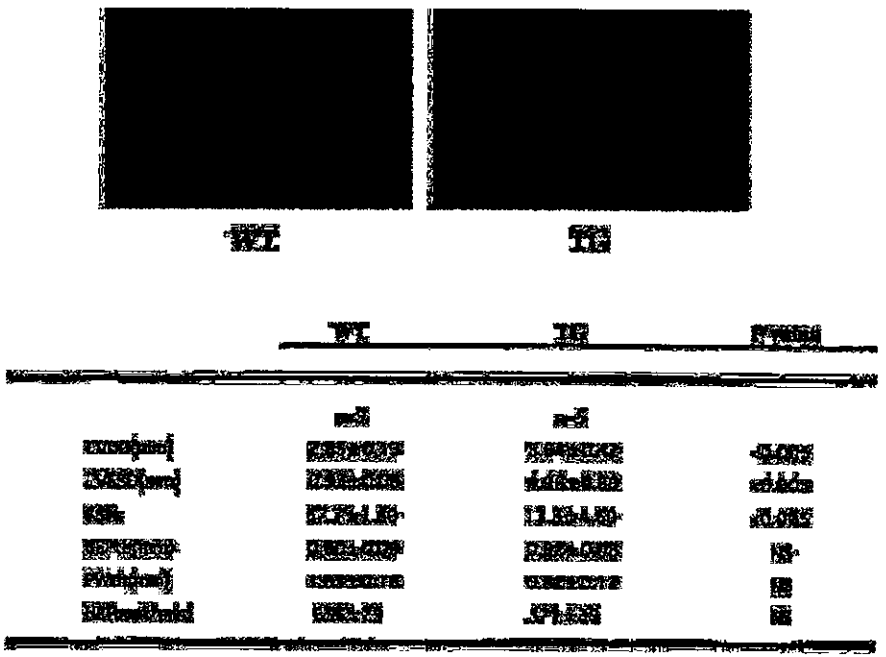

FIG. 9. Echocardiographic parameters of WT and p300 TG mice. TG mice or WT littermates at the age of 24 weeks were subjected to transthoracic echocardiography. SEPth, septal wall thickness; PWth, left-ventricular posterior-wall thickness; HR, heart rate; FS, fractional shortening, which was calculated as [(LVDD − LVESD)/LVDD] × 100.

generated TG mice overexpressing p300 under the control of the cardiac-specific α-MHC promoter. In contrast to mice with cardiac MEK-1 activation, mice overexpressing p300 in the heart exhibit increased mortality and marked eccentric dilatation and systolic dysfunction of the left ventricles. In these mice, acetylation and the increased DNA-binding activity of cardiac GATA-4 occurred as early as 8 weeks of age and preceded the development of left-ventricular dilatation and dysfunction. These findings raise the hypothesis that two modes of posttranslational modification, phosphorylation and acetylation, are involved in distinct cardiac phenotypes: concentric hypertrophy with normal systolic function and eccentric dilatation with systolic dysfunction, respectively. However, the present study provides insufficient evidence that p300-mediated acetylation and the resultant increase in the DNA-binding activity of cardiac GATA-4 are the primary causes of heart failure in these mice. To confirm this hypothesis, it is necessary to perform further studies using TG mice expressing equivalent amounts of p300 mutant lacking the HAT activity.

The cardiac phenotype of p300 TG mice also significantly differs from that of GATA-4 TG mice (37). These two kinds of TG mice exhibit similar increases (30 to 40%) in the heart weight/body weight ratio at 6 to 8 months of age. At that stage, the left ventricles of p300 TG mice show a 98% increase in the end diastolic dimension and an 80% decrease in fractional shortening compared with those of WT mice. In contrast, GATA-4 TG mice exhibit an increase in the end diastolic dimension of only 11% and a 42% decrease in fractional shortening. Thus, overexpression of p300 induces similar levels of cardiac growth but much more severe left-ventricular dilatation and dysfunction than overexpression of GATA-4. While the mechanisms that account for this difference are unclear at present, p300 may activate (acetylate) not only GATA-4 but also other transcription factors, including MEF2, serum response factor, and AP-1. Activation of multiple transcription factors may be involved in the more severe dilatation and systolic dysfunction of the left ventricles than those caused by increased levels of GATA-4 protein alone.

The present study demonstrated that a dominant-negative form of p300 inhibits not only nuclear hyperacetylation but also all of the characteristics of hypertrophic responses examined. These findings suggest that acetylation, which results in transcriptionally active chromatin, plays a key role in the development of hypertrophy, as well as changes in cardiac gene expression during this process. In addition, p300-mediated acetylation of cardiac nuclear proteins, including GATA-4, in

mice results in pathophysiological changes that mimic those associated with heart failure in humans. These findings suggest that acetylation by p300 provides a pharmacological target for the treatment of heart failure. Recently, Lau et al. reported that Lys-coenzyme A is a selective inhibitor of p300 HAT activity (36). The selectivity of this compound for p300 is at least 400 times higher than that for PCAF. The search for cardiac-specific HAT inhibitors will be of considerable importance in establishing a novel therapy modality for heart failure in humans.

ACKNOWLEDGMENTS

This work was supported in part by the Advanced and Innovational Research program in Life Science and by grants to T.K. and K.H. from the Ministry of Education, Science and Culture of Japan.

We thank N. Sowa for his excellent technical assistance.

Three authors, T. Yanazume, T. Morimoto, and T. Kawamura, equally contributed to this work.

REFERENCES

1. **Ait-Si-Ali, S., A. Polesskaya, S. Filleur, R. Ferreira, A. Duquet, P. Robin, A. Vervish, D. Trouche, F. Cabon, and A. Harel-Bellan.** 2000. CBP/p300 histone acetyl-transferase activity is important for the G1/S transition. Oncogene 19:2430–2437.
2. **Ait-Si-Ali, S., D. Carlisi, S. Ramirez, L. C. Upegui-Gonzalez, A. Duquet, P. Robin, B. Rudkin, A. Harel-Bellan, and D. Trouche.** 1999. Phosphorylation by p44 MAP kinase/ERK1 stimulates CBP histone acetyl transferase activity in vitro. Biochem. Biophys. Res. Commun. 262:157–162.
3. **Ait-Si-Ali, S., S. Ramirez, F. X. Barre, F. Dkhissi, L. Magnaghi-Jaulin, J. A. Girault, P. Robin, M. Knibiehler, L. L. Pritchard, B. Ducommun, D. Trouche, and A. Harel-Bellan.** 1998. Histone acetyltransferase activity of CBP is controlled by cycle-dependent kinases and oncoprotein E1A. Nature 396:184–186.
4. **Arceci, R. J., A. A. King, M. C. Simon, S. H. Orkin, and D. B. Wilson.** 1993. Mouse GATA-4: a retinoic acid-inducible GATA-binding transcription factor expressed in endodermally derived tissues and heart. Mol. Cell. Biol. 13:2235–2246.
5. **Avantaggiati, M. L., V. Ogryzko, K. Gardner, A. Giordano, A. S. Levine, and K. Kelly.** 1997. Recruitment of p300/CBP in p53-dependent signal pathways. Cell 89:1175–1184.
6. **Bannister, A. J., and T. Kouzarides.** 1996. The CBP co-activator is a histone acetyltransferase. Nature 384:641–643.
7. **Bordoli, L., S. Hunger, U. Lathi, M. Netsch, H. Osmani, and R. Eckner.** 2001. Functional analysis of the p300 acetyltransferase domain: the PHD finger of p300 but not of CBP is dispensable for enzymatic activity. Nucleic Acids Res. 29:4462–4471.
8. **Boyes, J., P. Byfield, Y. Nakatani, and V. Ogryzko.** 1998. Regulation of activity of the transcription factor GATA-1 by acetylation. Nature 396:594–598.
9. **Bueno, O. F., L. J. De Windt, K. M. Tymitz, S. A. Witt, T. R. Kimball, R. Klevitsky, T. R. Hewett, S. P. Jones, D. J. Lefer, C. F. Peng, R. N. Kitsis, and J. D. Molkentin.** 2000. The MEK1-ERK1/2 signaling pathway promotes compensated cardiac hypertrophy in transgenic mice. EMBO J. 19:6341–6350.
10. **Chakravarti, D., V. Ogryzko, H. Y. Kao, A. Nash, H. Chen, Y. Nakatani, and R. M. Evans.** 1999. A viral mechanism for inhibition of p300 and PCAF acetyltransferase activity. Cell 96:393–403.
11. **Chawla, S., G. R. Hardingham, D. R. Quinn, and H. Bading.** 1998. CBP: a signal-regulated transcriptional coactivator controlled by nuclear calcium and CaM kinase IV. Science 281:1505–1509.
12. **Chen, H., R. J. Lin, W. Xie, D. Wilpitz, and R. M. Evans.** 1999. Regulation of hormone-induced histone hyperacetylation and gene activation via acetylation of an acetylase. Cell 98:675–686.
13. **Chen, H., R. J. Lin, R. L. Schiltz, D. Chakravarti, A. Nash, L. Nagy, M. L. Privalsky, Y. Nakatani, and R. M. Evans.** 1997. Nuclear receptor coactivator ACTR is a novel histone acetyltransferase and forms a multimeric activation complex with P/CAF and CBP/p300. Cell 90:569–580.
14. **Chien, K. R., H. Zhu, K. U. Knowlton, W. Miller-Hance, M. van Bilsen, T. X. O'Brien, and S. M. Evans.** 1993. Transcriptional regulation during cardiac growth and development. Annu. Rev. Physiol. 55:77–95.
15. **Chrivia, J. C., R. P. Kwok, N. Lamb, M. Hagiwara, M. R. Montminy, and R. H.Goodman.** 1993. Phosphorylated CREB binds specifically to the nuclear protein CBP. Nature 365:855–859.
16. **Dai, Y. S., and B. E. Markham.** 2001. p300 functions as a coactivator of transcription factor GATA-4. J. Biol. Chem. 276:37178–37185.
17. **Eckner, R., M. E. Ewen, D. Newsome, M. Gerdes, J. A. DeCaprio, J. B. Lawrence, and D. M. Livingston.** 1994. Molecular cloning and functional analysis of the adenovirus E1A-associated 300-kD protein (p300) reveals a protein with properties of a transcriptional adaptor. Genes Dev. 8:869–884.
18. **Ekwall, K., T. Olsson, B. M. Turner, G. Cranston, and R. C. Allshire.** 1997. Transient inhibition of histone deacetylation alters the structural and functional imprint at fission yeast centromeres. Cell 91:1021–1032.
19. **Fax, P., O. Lehmkuhler, C. Kahn, H. Esche, and D. Brockmann.** 2000. E1A12S-mediated activation of the adenovirus type 12 E2 promoter depends on the histone acetyltransferase activity of p300/CBP. J. Biol. Chem. 275:40554–40560.
20. **Gu, W., and R. G. Roeder.** 1997. Activation of p53 sequence-specific DNA binding by acetylation of the p53 C-terminal domain. Cell 90:595–606.
21. **Hamamori, Y., V. Sartorelli, V. Ogryzko, P. L. Puri, H. Y. Wu, J. Y. Wang, Y. Nakatani, and L. Kedes.** 1999. Regulation of histone acetyltransferases p300 and PCAF by the bHLH protein twist and adenoviral oncoprotein E1A. Cell 96:405–413.
22. **Hasegawa, K., S. J. Lee, S. M. Jobe, B. E. Markham, and R. N. Kitsis.** 1997. *cis*-Acting sequences that mediate induction of beta-myosin heavy chain gene expression during left ventricular hypertrophy due to aortic constriction. Circulation 96:3943–3953.
23. **Hasegawa, K., M. B. Meyers, and R. N. Kitsis.** 1997. Transcriptional coactivator p300 stimulates cell type-specific gene expression in cardiac myocytes. J. Biol. Chem. 272:20049–20054.
24. **Hebbes, T. R., A. W. Thorne, and C. Crane-Robinson.** 1988. A direct link between core histone acetylation and transcriptionally active chromatin. EMBO J. 7:1395–1402.
25. **Herzig, T. C., S. M. Jobe, H. Aoki, J. D. Molkentin, A. W. Cowley, Jr., S. Izumo, and B. E. Markham.** 1997. Angiotensin II type 1a receptor gene expression in the heart: AP-1 and GATA-4 participate in the response to pressure overload. Proc. Natl. Acad. Sci. USA 94:7543–7548.
26. **Hung, H. L., J. Lee, A. Y. Kim, M. J. Weiss, and G. A. Biebel.** 1999. CREB-binding protein acetylates hematopoietic transcription factor GATA-1 at functionally important sites. Mol. Cell. Biol. 19:3496–3505.
27. **Ikura, T., V. V. Ogryzko, M. Grigoriev, R. Groisman, J. Wang, M. Horikoshi, R. Scully, J. Qin, and Y. Nakatani.** 2000. Involvement of the TIP60 histone acetylase complex in DNA repair and apoptosis. Cell 102:463–473.
28. **Imhof, A., X. J. Yang, V. V. Ogryzko, Y. Nakatani, A. P. Wolffe, and H. Ge.** 1997. Acetylation of general transcription factors by histone acetyltransferases. Curr. Biol. 7:689–692.
29. **Ip, H. S., D. B. Wilson, M. Heikinheimo, Z. Tang, C. N. Ting, M. C. Simon, J. M. Leiden, and M. S. Parmacek.** 1994. The GATA-4 transcription factor transactivates the cardiac muscle-specific troponin C promoter-enhancer in nonmuscle cells. Mol. Cell. Biol. 14:7517–7526.
30. **Kaburagi, S., K. Hasegawa, T. Morimoto, M. Araki, T. Sawamura, T. Masaki, and S. Sasayama.** 1999. The role of endothelin-converting enzyme-1 in the development of α1-adrenergic-stimulated hypertrophy in cultured neonatal rat cardiac myocytes. Circulation 99:292–298.
31. **Kakita, T., K. Hasegawa, T. Morimoto, S. Kaburagi, H. Wada, and S. Sasayama.** 1999. p300 protein as a coactivator of GATA-5 in the transcription of cardiac-restricted atrial natriuretic factor gene. J. Biol. Chem. 274:34096–34102.
32. **Karlyn, K., J. K. Farrusco, and P. C. Simpson.** 1993. Transcriptional enhancer factor-1 in cardiac myocytes interacts with an alpha 1-adrenergic- and beta-protein kinase C-inducible element in the rat beta-myosin heavy chain promoter. J. Biol. Chem. 268:26658–26662.
33. **Kawana, M., M. E. Lee, E. E. Quertermous, and T. Quertermous.** 1995. Cooperative interaction of GATA-2 and AP1 regulates transcription of the endothelin-1 gene. Mol. Cell. Biol. 15:4225–4231.
34. **Kolodziejczyk, S. M., L. Wang, K. Balazsi, Y. DeRepentigny, R. Kothary, and L. A. Megeney.** 1999. MEF2 is upregulated during cardiac hypertrophy and is required for normal post-natal growth of the myocardium. Curr. Biol. 9:1203–1206.
35. **Kreba, J. E., C. J. Fry, M. L. Samuels, and C. L. Peterson.** 2000. Global role for chromatin remodeling enzymes in mitotic gene expression. Cell 102:587–598.
36. **Lau, O. D., T. K. Kundu, R. E. Soccio, S. Ait-Si-Ali, E. M. Khalil, A. Vassilev, A. P. Wolffe, Y. Nakatani, R. G. Roeder, and P. A. Cole.** 2000. HATs off: selective synthetic inhibitors of the histone acetyltransferases p300 and PCAF. Mol. Cell 5:589–595.
37. **Liang, Q., L. J. De Windt, S. A. Witt, T. R. Kimball, B. E. Markham, and J. D. Molkentin.** 2001. The transcription factors GATA-4 and GATA-6 regulate cardiomyocyte hypertrophy in vitro and in vivo. J. Biol. Chem. 276:30245–30253.
38. **Liang, Q., R. J. Wiese, O. F. Bueno, Y. S. Dai, B. E. Markham, and J. D. Molkentin.** 2001. The transcription factor GATA-4 is activated by extracellular signal-regulated kinase 1- and 2-mediated phosphorylation of serine 105 in cardiomyocytes. Mol. Cell. Biol. 21:7460–7469.
39. **Lill, N. L., S. R. Grossman, D. Ginsberg, J. DeCaprio, and D. M. Livingston.** 1997. Binding and modulation of p53 by p300/CBP coactivators. Nature 387:823–827.
40. **Lu, J., T. A. McKinsey, C. L. Zhang, and E. N. Olson.** 2000. Regulation of skeletal myogenesis by association of the MEF2 transcription factor with class II histone deacetylases. Mol. Cell 6:233–244.
41. **Lu, J., T. A. McKinsey, R. L. Nicol, and E. N. Olson.** 2000. Signal-dependent activation of the MEF2 transcription factor by dissociation from histone deacetylases. Proc. Natl. Acad. Sci. USA 97:4070–4075.
42. **Martinez-Balbas, M. A., U. M. Bauer, S. J. Nielsen, A. Brehm, and T. Kouzarides.** 2000. Regulation of E2F1 activity by acetylation. EMBO J. 19:662–671.
43. **McKinsey, T. A., C. L. Zhang, J. Lu, and E. N. Olson.** 2000. Signal-dependent nuclear export of a histone deacetylase regulates muscle differentiation. Nature 408:106–111.
44. **Molkentin, J. D.** 2000. Calcineurin and beyond: cardiac hypertrophic signaling. Circ. Res. 87:731–738.
45. **Molkentin, J. D., J. R. Lu, C. L. Antos, B. Markham, J. Richardson, J. Robbins, S. R. Grant, and E. N. Olson.** 1998. A calcineurin-dependent transcriptional pathway for cardiac hypertrophy. Cell 93:215–228.
46. **Molkentin, J. D., and E. N. Olson.** 1997. GATA4: a novel transcriptional regulator of cardiac hypertrophy? Circulation 96:3833–3835.
47. **Morimoto, T., K. Hasegawa, S. Kaburagi, T. Kakita, H. Wada, T. Yanazume, and S. Sasayama.** 2000. Phosphorylation of GATA-4 is involved in α1-adrenergic agonist-responsive transcription of the endothelin-1 gene in cardiac myocytes. J. Biol. Chem. 275:13721–13726.
48. **Ogryzko, V. V., R. L. Schiltz, V. Russanova, B. H. Howard, and Y. Nakatani.** 1996. The transcriptional coactivators p300 and CBP are histone acetyltransferases. Cell 87:953–959.
49. **Paradis, P., W. R. MacLellan, N. S. Belaguli, R. J. Schwartz, and M. D. Schneider.** 1996. Serum response factor mediates AP-1-dependent induction of the skeletal alpha-actin promoter in ventricular myocytes. J. Biol. Chem. 271:10827–10833.
50. **Passier, R., H. Zeng, N. Frey, F. J. Naya, R. L. Nicol, T. A. McKinsey, P. Overbeek, J. A. Richardson, S. R. Grant, and E. N. Olson.** 2000. CaM kinase signaling induces cardiac hypertrophy and activates the MEF2 transcription factor in vivo. J. Clin. Investig. 105:1395–1406.
51. **Robbins, J., J. Palecmo, and H. Rindt.** 1995. In vivo definition of a cardiac specific promoter and its potential utility in remodeling the heart. Ann. N. Y. Acad. Sci. 752:492–505.
52. **Roth, S. Y., J. M. Denu, and C. D. Allis.** 2001. Histone acetyltransferases. Annu. Rev. Biochem. 70:81–120.

53. **Sadoshima, J., and S. Izumo.** 1997. The cellular and molecular response of cardiac myocytes to mechanical stress. Annu. Rev. Physiol. 59:551–571.
54. **Sartorelli, V., J. Huang, Y. Hamamori, and L. Kedes.** 1997. Molecular mechanisms of myogenic coactivation by p300: direct interaction with the activation domain of MyoD and with the MADS box of MEF2C. Mol. Cell. Biol. 17:1010–1026.
55. **Schlissel, M. S.** 2000. Perspectives: transcription. A tail of histone acetylation and DNA recombination. Science 287:438–440.
56. **Slepak, T. I., K. A. Webster, J. Zang, H. Prentice, A. O'Dowd, M. N. Hicks, and N. H. Bishopric.** 2001. Control of cardiac-specific transcription by p300 through myocyte enhancer factor-2D. J. Biol. Chem. 276:7575–7585.
57. **Soudais, C., M. Bielinska, M. Heikinheimo, C. A. MacArthur, N. Narita, J. E. Saffitz, M. C. Simon, J. M. Leiden, and D. B. Wilson.** 1995. Targeted mutagenesis of the transcription factor GATA-4 gene in mouse embryonic stem cells disrupts visceral endoderm differentiation in vitro. Development 121:3877–3888.
58. **Spencer, T. E., G. Jeanter, M. M. Burcin, C. D. Allis, J. Zhou, C. A. Mizzen, N. J. McKenna, S. A. Onate, S. Y. Tsai, M. J. Tsai, and B. W. O'Malley.** 1997. Steroid receptor coactivator-1 is a histone acetyltransferase. Nature 389:194–198.
59. **Yamagata, T., K. Mitani, H. Oda, T. Suzuki, H. Honda, T. Asai, K. Maki, T. Nakamoto, and H. Hirai.** 2000. Acetylation of GATA-3 affects T-cell survival and homing to secondary lymphoid organs. EMBO J. 19:4676–4687.
60. **Yanazume, T., K. Hasegawa, H. Wada, T. Morimoto, M. Abe, T. Kawamura, and S. Sasayama.** 2002. Rho/ROCK pathway contributes to the activation of extracellular signal-regulated kinase/GATA-4 during myocardial cell hypertrophy. J. Biol. Chem. 277:8618–8625.
61. **Yao, T. P., S. P. Oh, M. Fuchs, N. D. Zhou, L. E. Ch'ng, D. Newsome, R. T. Bronson, E. Li, D. M. Livingston, and R. Eckner.** 1998. Gene dosage-dependent embryonic development and proliferation defects in mice lacking the transcriptional integrator p300. Cell 93:361–372.
62. **Yuan, W., G. Condorelli, M. Caruso, A. Felsani, and A. Giordano.** 1996. Human p300 protein is a coactivator for the transcription factor MyoD. J. Biol. Chem. 271:9009–9013.
63. **Zhang, W., R. C. Kewal, F. Rauscat, R. A. Sikkink, E. N. Olson, and R. G. Victor.** 1999. Failure of calcineurin inhibitors to prevent pressure-overload left-ventricular hypertrophy in rats. Circ. Res. 84:722–728.

CUTTING EDGE

Cutting Edge: SR-PSOX/CXC Chemokine Ligand 16 Mediates Bacterial Phagocytosis by APCs Through its Chemokine Domain[1]

Takeshi Shimaoka, Takashi Nakayama,‡ Noriaki Kume,† Shu Takahashi,§ Junko Yamaguchi,§ Manabu Minami,† Kazutaka Hayashida,† Toru Kita,† Jun Ohsumi,§ Osamu Yoshie,‡ and Shin Yonehara[2]**

SR-PSOX and CXC chemokine ligand (CXCL)16, which were originally identified as a scavenger receptor and a transmembrane-type chemokine, respectively, are indicated to be identical. In this study, we demonstrate that membrane-bound SR-PSOX/CXCL16 mediates adhesion and phagocytosis of both Gram-negative and Gram-positive bacteria. Importantly, our prepared anti-SR-PSOX mAb, which suppressed chemotactic activity of SR-PSOX, significantly inhibited bacterial phagocytosis by human APCs including dendritic cells. Various scavenger receptor ligands inhibited the bacterial phagocytosis of SR-PSOX. In addition, the recognition specificity for bacteria was determined by only the chemokine domain of SR-PSOX/CXCL16. Thus, SR-PSOX/CXCL16 may play an important role in facilitating uptake of various pathogens and chemotaxis of T and NKT cells by APCs through its chemokine domain. The Journal of Immunology, 2003, 171: 1647–1651.

The scavenger receptor family is a highly heterogenous group of cell surface molecules that commonly bind and uptake oxidized low density lipoprotein (OxLDL)[3] (1). Currently, scavenger receptors are categorized into almost 10 classes on the basis of structure, even though there are few structural and primary amino acid similarities among the classes. Scavenger receptors have been primarily studied for their roles in foam cell formation and the pathogenesis of atherosclerosis. Some scavenger receptors have also been shown to bind a broad range of ligands including bacteria (2–5). Studies with scavenger receptor class-A (SR-A) knockout mice revealed that a deficiency of SR-A enhances sensitivities for infection of *Staphylococcus aureus* and *Listeria* (6, 7), suggesting that its function as a pattern recognition receptor plays potential roles in innate immunity and in the initiation of acquired immune responses (8).

Previously, we identified a novel scavenger receptor capable of binding and uptaking phosphatidylserine and OxLDL, and termed it SR-PSOX (scavenger receptor that binds phosphatidylserine and oxidized lipoprotein) (9). Surprisingly, SR-PSOX was indicated to be identical to CXC chemokine ligand (CXCL)16 (10, 11), which was identified as the ligand for an orphan G-protein coupled chemokine receptor Bonzo/CXCR6. CXCL16 is the second transmembrane-type chemokine with a chemokine-domain fused to a mucin-like stalk, a structure very similar to that of fractalkine/CX_3CL1 (12, 13). CXCL16 selectively expresses on APCs such as dendritic cells (DCs) and macrophages, while its receptor Bonzo/CXCR6 expresses on naive CD8 T cells, NKT cells, and type 1-polarized CD4 and CD8 T cells (10, 11, 14). Thus, SR-PSOX/CXCL16 is a multifunctional molecule that may link the family of scavenger receptors and that of chemokines.

In the present study, we have demonstrated that SR-PSOX/CXCL16 expressed by macrophages and DCs supports binding and phagocytosis of both Gram-negative and Gram-positive bacteria through the chemokine domain. SR-PSOX/CXCL16 should play a role in facilitating uptake of various pathogens and chemotaxis of T and NKT cells by professional APCs.

Materials and Methods

Cells

DCs were generated from peripheral blood monocytes isolated from human blood (a gift from Kyoto Red Cross Blood Center, Kyoto, Japan) by cultivation with 20 ng/ml IL-4 and 50 ng/ml GM-CSF (PeproTech, Rocky Hill, NJ) for 7 days. DCs were confirmed to express CD1a, CD40, CD80, HLA-DR, and HLA-ABC at high levels, and CD14 at a low level by flow cytometry. L1.2 murine pre-B cells stably expressing CXCR6 (L-CXCR6 cells) and CX_3CR1 (L-CX_3CR1 cells) were generated as described previously (15).

Monoclonal anti-human SR-PSOX Abs

BALB/c female mice were immunized with SR-PSOX-Fc fusion protein produced by COS-7 cells transfected with a fusion construct consisting of the extracellular domain of human SR-PSOX (amino acids 1–206) fused at its C terminus with Fc fragment of human IgG_1. According to the method described previously (16), we generated three anti-human SR-PSOX mAbs 22-19-12, 49-36, and 28-12.

*Graduate School of Biostudies and Institute for Virus Research, and †Department of Cardiovascular Medicine, Graduate School of Medicine, Kyoto University, Sakyo-ku, Kyoto, Japan; ‡Department of Microbiology, Kinki University School of Medicine, Osaka-Sayama, Japan; and §Biomedical Research Laboratories and Molecular Biology Research Laboratories, Sankyo, Shinagawa-ku, Tokyo, Japan

Received for publication April 25, 2003. Accepted for publication June 20, 2003.

The costs of publication of this article were defrayed in part by the payment of page charges. This article must therefore be hereby marked *advertisement* in accordance with 18 U.S.C. Section 1734 solely to indicate this fact.

0022-1767/03/$02.00

[1] This work was supported in part by Grants-in-Aid from the Ministry of Education, Culture, Sports, Science and Technology of the Japanese Government.

[2] Address correspondence and reprint requests to Dr. Shin Yonehara, Graduate School of Biostudies and Institute for Virus Research, Kyoto University, Shogoin Kawahara-cho 53, Sakyo-ku, Kyoto 606-8507, Japan. E-mail: syonehar@virus.kyoto-u.ac.jp

[3] Abbreviations used in this paper: OxLDL, oxidized low-density lipoprotein; SR-A, scavenger receptor class A; CXCL, CXC chemokine ligand; DC, dendritic cell; LTA, lipoteichoic acid; LOX-1, lectin-like OxLDL receptor-1; dSR-CI, *Drosophila* scavenger receptor CI; SEAP, secreted form of placental alkaline phosphatase.

Binding and phagocytosis of bacteria

Bacterial adhesion and phagocytosis assays were conducted as described previously (5). To quantitate the phagocytosis of bacteria, COS-7 cells, PMA-stimulated THP-1 cells (PMA-THP-1 cells), or DCs (2×10^5 cells/ml) were incubated for 60 min at 37°C with FITC-labeled bacteria (3×10^6 cells/ml for COS-7 cells, and 6×10^5 cells/ml for PMA-THP-1 cells and DCs). Then cells were washed, detached with trypsin and treated with trypan blue for 10 min to quench the fluorescence of extracellular bacteria. The numbers of cells with intracellular FITC-labeled bacteria were quantified by EPICS Elite (Coulter, Hialeah, FL). In blocking experiments, cells were preincubated with lipoteichoic acid (LTA; 500 μg/ml), LPS (500 μg/ml), dextran sulfate (500 μg/ml), chondroitin sulfate (500 μg/ml), native LDL (200 μg/ml), OxLDL (200 μg/ml), $F(ab')_2$ of monoclonal anti-SR-PSOX neutralizing mAb 22-19-12 (20 μg/ml), $F(ab')_2$ of control IgG (20 μg/ml), or cytochalasin D (2 μM) for 30 min at 37°C. The data of bacterial phagocytosis represent the mean ± SD from at least three independent experiments, and statistical significance was calculated by Student's *t* tests.

Results

SR-PSOX/CXCL16 mediates bacterial adhesion and phagocytosis

Scavenger receptors such as SR-A, MARCO, lectin-like OxLDL receptor 1 (LOX-1), and *Drosophila* scavenger receptor CI (dSR-CI) are known to bind and uptake bacteria (2–5). Therefore, we examined whether SR-PSOX/CXCL16 could also mediate adhesion of bacteria. COS-7 cells were transfected with expression vectors for SR-PSOX as described previously (9). As shown in Fig. 1*A*, SR-PSOX-transfected COS-7 cells (COS-SR-PSOX cells), but not control COS-7 cells, were found to efficiently bind FITC-labeled Gram-negative *Escherichia coli* and Gram-positive *S. aureus*. We next examined phagocytosis of cell surface bound bacteria by COS-SR-PSOX cells under confocal microscopy. Phagocytosed *E. coli* (Fig. 1*B*) and *S. aureus* (data not shown) were observed in COS-SR-PSOX cells. As reported with other scavenger receptors, SR-PSOX did not mediate adhesion and phagocytosis of zymosan (data not shown) (3–5).

FIGURE 1. Adhesion and phagocytosis of *E. coli* and *S. aureus* mediated by SR-PSOX/CXCL16. *A*, COS-control and COS-SR-PSOX cells were incubated with FITC-labeled *E. coli* and *S. aureus* in the presence of 10% FCS for 1 h at 37°C. After washing, cells were observed under fluorescence microscopy. *B*, COS-SR-PSOX cells were incubated with FITC-labeled *E. coli* for 1 h at 37°C. After washing, cell surface labeling was performed with rhodamine-Con A at 4°C. After another wash, cells were observed under confocal microscopy. Arrows indicate internalized bacteria. *C*, COS-control cells, COS-SR-PSOX cells, COS-fractalkine cells, COS-SR-A cells, and COS-LOX-1 cells were incubated with FITC-labeled *E. coli* (■) or *S. aureus* (□) for 1 h at 37°C with or without cytochalasin D or in the medium without serum. Cells that internalized FITC-labeled bacteria were quantified by flow cytometry and expressed as a percentage of total COS-7 cells. *, $p < 0.01$.

To further quantitate cells phagocytosing bacteria, cells incubated with FITC-labeled bacteria were analyzed by flow cytometry after washing and quenching of surface fluorescence of extracellular bacteria with trypan blue. COS-SR-PSOX cells, but not COS-control or fractalkine-transfected COS-7 cells (COS-fractalkine cells), were indeed found to efficiently phagocytose both *E. coli* and *S. aureus* (Fig. 1*C*) in the condition that expression levels of the transfected SR-PSOX and fractalkine were almost the same (see Fig. 3, *B–D*). The level of bacterial phagocytosis by COS-SR-PSOX cells was almost comparable to that by COS-7 cells expressing other scavenger receptors such as SR-A and LOX-1 which were reported to have bacterial phagocytosis activity (2, 5). Furthermore, COS-SR-PSOX cells efficiently phagocytosed *E. coli* and *S. aureus* in serum-free medium as well as in serum-containing medium (Fig. 1*C*). Bacterial phagocytosis was effectively suppressed by an actin-depolymerizing agent, cytochalasin D (Fig. 1*C*). Collectively, these findings clearly demonstrate that serum factors are not required for SR-PSOX-mediated bacterial phagocytosis, and the actin cytoskeleton is necessary for SR-PSOX-mediated bacterial firm adhesion and/or phagocytosis.

Role of SR-PSOX/CXCL16 in bacterial adhesion and phagocytosis by professional APCs

We generated novel anti-human SR-PSOX mAbs, 22-19-12 and 28-12, which recognize the chemokine and mucin domain of SR-PSOX, respectively. To examine inhibitory activity of the mAbs for chemotactic activity of SR-PSOX/CXCL16, we generated soluble SR-PSOX as a fusion protein consisting of the extracellular domain of SR-PSOX (amino acids 1–206) fused at its C terminus with the secreted form of placental alkaline phosphatase (SEAP). SEAP was used for quantification of SR-PSOX-SEAP by ELISA with anti-SEAP mAb, and the fused SEAP was shown not to significantly affect the chemotactic activity of SR-PSOX (data not shown). mAb 22-19-12 was shown to inhibit chemotactic activity to CXCR6-expressing cells by soluble SR-PSOX, while mAb 28-12 did not show the inhibitory activity (Fig. 2*B*).

The phagocytosis of bacteria is a necessary step for the presentation of bacterial Ags by professional APCs (17, 18), which were reported to express SR-PSOX/CXCL16 (9–11). Therefore, we examined whether SR-PSOX plays a role in bacterial phagocytosis by macrophage-like cells and DCs. We confirmed the expression of SR-PSOX in PMA-THP-1 cells and monocyte-derived DCs by RT-PCR (data not shown) and flow cytometry (Fig. 2*A*). We then analyzed the effects of $F(ab')_2$ of anti-SR-PSOX mAb 22-19-12 on bacterial phagocytosis by SR-PSOX-expressing cells. Anti-SR-PSOX 22-19-12 $F(ab')_2$ was clearly shown to inhibit bacterial phagocytosis by COS-SR-PSOX cells (Fig. 2*C*). In PMA-THP-1 cells, 30–40% of the phagocytosis of both *E. coli* and *S. aureus* were specifically inhibited by $F(ab')_2$ of the mAb (Fig. 2*D*). In DCs, $F(ab')_2$ inhibited 60% of phagocytosis of *E. coli*, while it did not significantly inhibit phagocytosis of *S. aureus* (Fig. 2*E*). These results indicate that SR-PSOX/CXCL16 plays an important role in

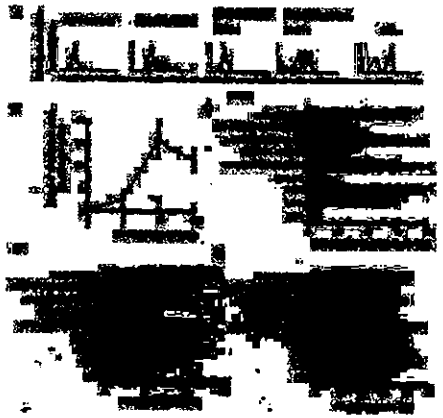

FIGURE 2. Role of SR-PSOX/CXCL16 in bacterial adhesion and phagocytosis by professional APCs. *A*, Surface expression of SR-PSOX on indicated cells was determined by flow cytometry after staining with anti-SR-PSOX mAb 22-19-12 (bold line) or control IgG (dotted line). *B*, Soluble SR-PSOX, which was generated as a fusion construct consisting of the extracellular domain of SR-PSOX (amino acids 1–206) fused at its C terminus with SEAP, was examined for its chemotactic activity against CXCR6-expressing L1.2 cells (L-CXCR6 cells) (●) and control L1.2 cells (■) by standard Transwell assays (21). Effects of 5 μg/ml anti-human SR-PSOX mAbs 22-19-12 (○) and 28-12 (□) were also analyzed. The number of cells that migrated into bottom wells was expressed as a percentage of input cells. The data shown represent the mean ± SD from at least three independent experiments. *C–E*, COS-SR-PSOX cells (*C*), PMA-THP-1 cells (*D*), and human peripheral monocyte-derived DCs (*E*) were incubated with FITC-labeled *E. coli* (■) or *S. aureus* (□) for 1 h at 37°C with or without various inhibitors as described in *Materials and Methods*. Levels of phagocytosis were quantified by flow cytometry. *, $p < 0.01$.

bacterial phagocytosis by professional APCs including DCs and activated macrophages, although other cell surface molecules must be also involved.

Effects of various scavenger receptor ligands on binding of SR-PSOX to bacteria

We further examined the effects of scavenger receptor ligands on phagocytosis of bacteria by COS-SR-PSOX cells (Fig. 2*C*). OxLDL and dextran sulfate were used as scavenger receptor ligands because they can inhibit uptake of 1,1′-dioctadecyl-3,3,3′3′-tetra-metyllindocarbocyanin perchlorate (DiI)-labeled OxLDL by SR-PSOX-expressing cells (9). Dextran sulfate and OxLDL inhibited bacterial phagocytosis by COS-SR-PSOX cells, while chondroitin sulfate and native LDL showed very weak or undetectable inhibitory effects. In the presence of LTA, the cell wall component of Gram-positive bacteria reported to be recognized by another scavenger receptor SR-A (2), the phagocytosis of *S. aureus* by COS-SR-PSOX cells, PMA-THP-1 cells, and DCs were clearly inhibited (Fig. 2, *C–E*). In contrast, LPS, the cell wall component of Gram-negative bacteria reported to be recognized by SR-A (19), slightly inhibited the phagocytosis of *E. coli* by PMA-THP-1 cells and did not inhibit it by COS-SR-PSOX cells and DCs (Fig. 2, *C–E*). Phagocytosis of both *E. coli* and *S. aureus* by PMA-THP-1 cells was specifically inhibited by 70–80% by dextran sulfate and OxLDL, while neither chondroitin sulfate nor native LDL inhibited it (Fig. 2*D*). In DCs, the inhibitory activities of phagocytosis of *E. coli* by dextran sulfate and OxLDL were lower, but significant, than those in PMA-THP-1 cells (Fig. 2*E*).

Domain analysis of SR-PSOX/CXCL16

In the extracellular domain of SR-PSOX/CXCL16 and fractalkine, there are two distinct domains, namely the chemokine domain and the mucin domain. Chemotaxis of CXCR6-expressing cells was induced by only the chemokine domain of SR-PSOX (data not shown). To clarify the binding domain of SR-PSOX for bacteria, we generated SR-PSOX/CXCL16-fractalkine hybrid molecules by shuffling the chemokine domains and mucin domains of SR-PSOX and fractalkine (Fig. 3*A*). COS-7 cells were transfected with expression vectors for hybrid molecules and similar levels of cell surface expression were confirmed among these hybrid proteins on the transfected COS-7 cells by flow cytometry using anti-human SR-PSOX/CXCL16 mAbs 49-36 (Fig. 3*B*) and 28-12 (Fig. 3*C*) that recognize the chemokine and mucin domains of SR-PSOX/CXCL16, respectively, or the anti-human fractalkine mAb (Fig. 3*D*) that recognizes the chemokine domain of fractalkine. COS-7 cells expressing a hybrid molecule with a chemokine domain of SR-PSOX/CXCL16 and a mucin domain of fractalkine showed significant bacterial phagocytosis (Fig. 3*E*), while COS-7 cells expressing a hybrid molecule with a chemokine domain of fractalkine and a mucin domain of SR-PSOX/CXCL16 did not show these activities. Interestingly, COS-7 cells expressing SR-PSOX without its mucin domain impaired the activity (Fig. 3*E*) although the cell surface expression was confirmed by flow cytometry (Fig. 3*B*). All the data indicate that the recognition specificity for CXCR6 and bacteria is determined by only the chemokine domain of SR-PSOX/CXCL16, while the mucin domain of SR-PSOX/CXCL16 is necessary for other activities of SR-PSOX, including efficient recognition and/or uptake of bacteria.

Discussion

SR-PSOX/CXCL16 is a recently identified molecule with distinct dual biological functions. We and others independently identified this molecule as a novel class of scavenger receptor capable of uptaking OxLDL (9) and as a transmembrane-type chemokine capable of recruiting cells expressing CXCR6 (10, 11), respectively. Importantly, we have demonstrated here for the first time that SR-PSOX/CXCL16 is capable of mediating bacterial phagocytosis. This activity of SR-PSOX/CXCL16 is shared with several other scavenger receptors but not with another transmembrane chemokine, fractalkine/CX_3CL1 (Fig. 1). Furthermore, we demonstrated that the recognition specificity for bacteria is determined by only the chemokine domain of SR-PSOX/CXCL16 (Fig. 3).

We have also shown that SR-PSOX/CXCL16, which is expressed on macrophages and DCs, plays an important role in bacterial phagocytosis by these APCs (Fig. 2). Thus, SR-PSOX/CXCL16 has unique characteristics as a transmembrane chemokine by providing another set of multiple functions for professional APCs, i.e., recruitment of CXCR6-expressing cells such as activated T and NKT cells and also uptake of bacteria for Ag presentation.

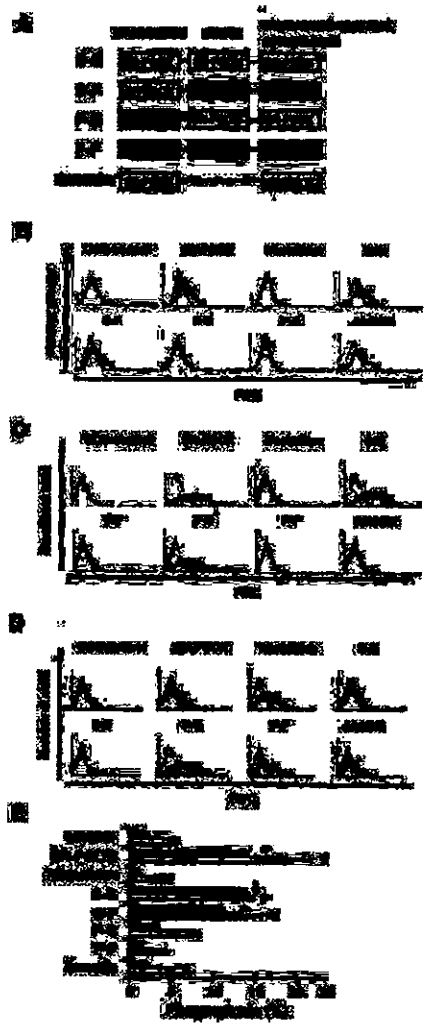

FIGURE 3. Domain analyses of SR-PSOX/CXCL16 to bind bacteria. *A*, Schematic illustration of SR-PSOX/CXCL16-fractalkine hybrid molecules. ΔMucin construct shows SR-PSOX without mucin domain. *B–D*, Flow cytometric analysis. COS-7 cells were transiently transfected with each SR-PSOX/CXCL16-fractalkine hybrid molecules schematically shown in *A*. Surface expression of human SR-PSOX-fractalkine hybrid molecules was analyzed by flow cytometry after staining with anti-human SR-PSOX mAb (*B*) 49-36 (bold line) which recognize chemokine domain or (*C*) 28-12 (bold line) which recognize the mucin domain of SR-PSOX or with anti-human fractalkine mAb, (*D*) 51637.11 (bold line) which recognize the chemokine domain of fractalkine or (*B–D*) control IgG (dotted line) and thereafter anti-mouse IgG-FITC. *E*, COS-7 cells transfected with the indicated SR-PSOX/CXCL16-fractalkine hybrid molecules were incubated with the indicated FITC-labeled *E. coli* (■) or *S. aureus* (□) for 1 h at 37°C. Cells internalizing FITC-labeled bacteria were enumerated by flow cytometry. *, $p < 0.01$.

Recently, some chemokines were reported to have killing activity against bacteria, which is similar to that of antimicrobial peptides such as β-defensin (20). We have confirmed not only direct binding of soluble SR-PSOX/CXCL16 to bacteria, but also its killing activity against bacteria (data not shown). However, higher concentrations of SR-PSOX/CXCL16 were necessary to kill bacteria than those of other antimicrobial chemokines previously reported (20). The previous report and our data suggest that innate immune activity as well as chemotactic activity may be evolutionary conserved in the chemokine superfamily, and some chemokines may be a new class of pattern recognition receptor for bacteria.

Gram-positive and Gram-negative bacteria have different cell wall components. LPS and LTA are the cell wall components of Gram-negative and Gram-positive bacteria, respectively. Because SR-PSOX/CXCL16 can recognize negative-charged molecules such as OxLDL and dextran sulfate, SR-PSOX/CXCL16 may recognize common and/or different negative-charged molecules on these bacterial cell walls. LTA with negative charge is a candidate on Gram-positive bacteria recognized by SR-PSOX/CXCL16, while that on Gram-negative bacteria remains to be identified (Fig. 2*C*).

DCs play an important role in providing a link between the innate and adaptive immune systems by phagocytosing pathogens, presenting Ag, and triggering T cell activation (21). Though scavenger receptor family members, such as mammalian SR-A, MARCO, and LOX-1 as well as *Drosophila* dSR-CI, were reported to be involved in phagocytosis of Gram-negative and Gram-positive bacteria by mammalian macrophages and endothelial cells as well as *Drosophila* macrophages (2–5), it remains to be determined which kinds of scavenger receptors on DCs are involved in the phagocytosis of bacteria. In this study, we showed that SR-PSOX/CXCL16 plays a role in the phagocytosis of bacteria in monocyte-derived DCs, while SR-A, LOX-1 and/or other scavenger receptors may be also involved in bacterial phagocytosis in other-type DCs. After phagocytosing bacteria, DCs possibly present bacterial peptide epitopes and glycolipids together with self histocompatibility Ags to T cells and NKT cells, respectively. In contrast, the soluble form of SR-PSOX/CXCL16, released by DCs, can recruit activated T cells and NKT cells expressing CXCR6 by its chemotactic activity in cooperation with other chemokines.

In conclusion, SR-PSOX/CXCL16, which is a unique class of transmembrane molecule with multiple biological activities as a scavenger receptor and chemokine through the same chemokine domain, is likely to play important roles in host defense by mediating innate and adaptive immunity. Future studies using SR-PSOX/CXCL16 gene-disrupted and CXCR6 gene-disrupted mice will no doubt clarify the physiological roles of SR-PSOX/CXCL16 in innate and acquired immunity.

Acknowledgments

We thank Drs. K. Sakamaki, K.-K. Lee, N. Fukumoto, K. Hieshima, K. Hori, R. Morita, M. Matsuoka, and E. Kodama for their generous help.

References

1. Steinbrecher, U. P. 1999. Receptors for oxidized low density lipoprotein. *Biochim. Biophys. Acta. 1436:279.*
2. Dunne, D. W., D. Resnick, J. Greenberg, M. Krieger, and K. A. Joiner. 1994. The type I macrophage scavenger receptor binds to Gram-positive bacteria and recognizes lipoteichoic acid. *Proc. Natl. Acad. Sci. USA 91:1863.*
3. Ekman, O., M. Kangas, C. Sahlberg, J. Tuukkanen, R. Sormunen, A. Liakka, I. Thesleff, G. Kraal, and K. Tryggvason. 1995. Cloning of a novel bacteria-binding

receptor structurally related to scavenger receptors and expressed in a subset of macrophages. *Cell 80:603.*
4. Ramet, M., A. Pearson, P. Manfruelli, X. Li, H. Koziel, V. Gobel, E. Chung, M. Krieger, and R. A. Ezekowitz. 2001. *Drosophila* scavenger receptor CI is a pattern recognition receptor for bacteria. *Immunity 15:1027.*
5. Shimaoka, T., N. Kume, M. Minami, K. Hayashida, T. Sawamura, T. Kita, and S. Yonehara. 2001. LOX-1 supports adhesion of Gram-positive and Gram-negative bacteria. *J. Immunol. 166:5108.*
6. Suzuki, H., Y. Kurihara, M. Takeya, N. Kamada, M. Kataoka, K. Jishage, O. Ueda, H. Sakaguchi, T. Higashi, T. Suzuki, et al. 1997. A role for macrophage scavenger receptors in atherosclerosis and susceptibility to infection. *Nature 386:292.*
7. Thomas, C. A., Y. Li, T. Kodama, H. Suzuki, S. C. Silverstein, and J. El Khoury. 2000. Protection from lethal Gram-positive infection by macrophage scavenger receptor-dependent phagocytosis. *J. Exp. Med. 191:147.*
8. Gough, P. J., and S. Gordon. 2000. The role of scavenger receptors in the innate immune system. *Microbes Infect. 2:305.*
9. Shimaoka, T., N. Kume, M. Minami, K. Hayashida, H. Kataoka, T. Kita, and S. Yonehara. 2000. Molecular cloning of a novel scavenger receptor for oxidized low density lipoprotein, SR-PSOX, on macrophages. *J. Biol. Chem. 275:40663.*
10. Matloubian, M., A. David, S. Engel, J. E. Ryan, and J. G. Cyster. 2000. A transmembrane CXC chemokine is a ligand for HIV-coreceptor Bonzo. *Nat. Immunol. 1:298.*
11. Wilbanks, A., S. C. Zondlo, K. Murphy, S. Mak, D. Soler, P. Langdon, D. P. Andrew, L. Wu, and M. Briskin. 2001. Expression cloning of the STRL33/BONZO/TYM-STRligand reveals elements of CC, CXC, and CX3C chemokines. *J. Immunol. 166:5145.*
12. Bazan, J. F., K. B. Bacon, G. Hardiman, W. Wang, K. Soo, D. Rossi, D. R. Greaves, A. Zlotnik, and T. J. Schall. 1997. A new class of membrane-bound chemokine with a CX3C motif. *Nature 385:640.*
13. Pan, Y., C. Lloyd, H. Zhou, S. Dolich, J. Deeds, J. A. Gonzalo, J. Vath, M. Gosselin, J. Ma, B. Dussault, et al. 1997. Neurotactin, a membrane-anchored chemokine upregulated in brain inflammation. *Nature 387:611.*
14. Kim, C. H., E. J. Kunkel, J. Boisvert, B. Johnston, J. J. Campbell, M. C. Genovese, H. B. Greenberg, and E. C. Butcher. 2001. Bonzo/CXCR6 expression defines type 1-polarized T-cell subsets with extralymphoid tissue homing potential. *J. Clin. Invest. 107:595.*
15. Nomiyama, H., K. Hieshima, T. Nakayama, T. Sakaguchi, R. Fujisawa, S. Tanase, H. Nishiura, K. Matsuno, H. Tokamori, Y. Tabira, et al. 2001. Human CC chemokine liver-expressed chemokine/CCL16 is a functional ligand for CCR1, CCR2 and CCR5, and constitutively expressed by hepatocytes. *Int. Immunol. 13:1021.*
16. Yonehara, S., A. Ishii, and M. Yonehara. 1989. A cell-killing monoclonal antibody (anti-Fas) to a cell surface antigen co-downregulated with the receptor of tumor necrosis factor. *J. Exp. Med. 169:1747.*
17. Corinti, S., D. Medaglini, A. Cavani, M. Rescigno, G. Pozzi, P. Ricciardi-Castagnoli, and G. Girolomoni. 1999. Human dendritic cells very efficiently present a heterologous antigen expressed on the surface of recombinant Gram-positive bacteria to $CD4^+$ T lymphocytes. *J. Immunol. 163:3029.*
18. Svensson, M., B. Stockinger, and M. J. Wick. 1997. Bone marrow-derived dendritic cells can process bacteria for MHC-I and MHC-II presentation to T cells. *J. Immunol. 158:4229.*
19. Hampton, R. Y., D. T. Golenbock, M. Penman, M. Krieger, and C. R. Raetz. 1991. Recognition and plasma clearance of endotoxin by scavenger receptors. *Nature 352:342.*
20. Durr, M., and A. Peschel. 2002. Chemokines meet defensins: the merging concepts of chemoattractants and antimicrobial peptides in host defense. *Infect. Immun. 70:6515.*
21. Rescigno, M., and P. Borrow. 2001. The host-pathogen interaction: new themes from dendritic cell biology. *Cell 106:267.*